A HIGH-RESOLUTION VIEW OF MEIOTIC RECOMBINATION INITIATION IN *SACCHAROMYCES CEREVISIAE*

A Dissertation

Presented to the Faculty of the Weill Cornell Graduate School

of Medical Sciences

In Partial Fulfillment of the Requirements for the Degree of

Doctor of Philosophy

by

Xuan Zhu

June 2015

A HIGH-RESOLUTION VIEW OF MEIOTIC RECOMBINATION INITIATION IN *SACCHAROMYCES CEREVISIAE*

Xuan Zhu, Ph.D.

Cornell University 2015

Meiotic recombination initiates with DNA double-strand breaks (DSBs) made by Spo11. In *Saccharomyces cerevisiae*, many DSBs occur in "hotspots" coinciding with nucleosome-depleted gene promoters. Transcription factors (TFs) stimulate DSB formation in some hotspots, but TF roles are complex and variable between locations. Until now, available data for TF effects on global DSB patterns were of low spatial resolution and confined to a single TF. Here, I examine at high resolution the contributions of two TFs to genome-wide DSB distributions: Bas1, which was known to regulate DSB activity at some loci, and Ino4, for which some binding sites were known to be within strong DSB hotspots. I examined fine-scale DSB distributions in TF mutant strains by deep sequencing oligonucleotides that remain covalently bound to Spo11 as a byproduct of DSB formation, mapped Bas1 and Ino4 binding sites in meiotic cells, and evaluated chromatin structure around DSB hotspots. Our findings definitively support the hypothesis that TF control of DSB numbers is context-dependent and frequently indirect. TFs often affected the fine-scale distributions of DSBs within hotspots, and when seen, these effects paralleled effects on local chromatin structure. In contrast, changes in DSB frequencies in hotspots showed no obvious correlation with quantitative measures of chromatin accessibility or of histone

H3 lysine 4 trimethylation levels. I also ruled out hotspot competition as a major source of indirect TF effects on DSB distributions. Thus, counter to prevailing models, roles of these TFs on DSB hotspot strength cannot be simply explained via chromatin "openness", histone modification, or compensatory interactions between adjacent hotspots.

In addition to TFs, meiotic DSB formation is regulated by factors involved in chromatin structure and modifications. The effect of some of these factors on DSB landscape has been examined by hybridizing DSB-associated DNAs on microarrays. However, the DSB maps generated by microarrays usually have relatively low resolution and high background. To overcome these limitations, I generated high-resolution meiotic DSB maps from mutants of *PCH2*, *SIR2* and *SET1*. Analysis of these maps further supports the view that the global DSB landscape is shaped by a hierarchical combination of factors.

BIOGRAPHICAL SKETCH

Xuan Zhu was born in Nanning, Guangxi Province, China in 1983. She attended elementary school at Minle Road School beginning in 1990 until 1996. Xuan attended Nanning No.14 Middle School from 1996 to 1999 and was voted to the list of Ten Best Middle/High School Students of Nanning. After that, she went to Nanning No.2 High School. During her second year in Nanning No.2 High School, she represented Guangxi Province to participate in China Biology Olympiad and won a silver medal. In the fall of 2003, Xuan matriculated at Yuanpei College, an elite liberal college of Peking University, Beijing, China where she majored in Biological Sciences. In her second year at Peking, she was granted a scholarship to study at the University of Hong Kong. Xuan started her graduate program at the Weill Graduate School of Medical Sciences, Cornell University in 2007. She joined Dr. Scott Keeney's laboratory where she conducted her doctoral research on the regulation of meiotic double-strand break formation in the budding yeast, *Saccharomyces cerevisiae*.

For my parents and my grandparents.

ACKNOWLEDGMENTS

I would like to express my deepest gratitude to my mentor, Dr. Scott Keeney, for his inspiring guidance throughout my journey to Ph.D. His experience and expertise in the field is unparalleled and was indispensible during the course of every research project. I sincerely appreciate him for being extraordinarily kind and patient to always support me to pursue my ideas, even after periods of frustration.

I would also like to extend my appreciation to my committee members: Dr. David C. Allis and Dr. Hironori Funabiki for their invaluable advice during my research.

I would like to thank current and former members of the Keeney lab, who provided a scientifically stimulating and fun working environment. My special thanks go to Dr. Hajime Murakami and Dr. Jing Pan, who were my mentors during the rotation. Not only did they teach me all they know without reservation about the technologies used in the lab, they also gave me a lot of insights into my projects through enthusiastic discussions. Also, thanks to Dr. Julian Lange and Jodi-Ann Sampson, for being such amazing bay mates. I would like to thank other lab members too. I had a lot of unforgettable memories with them in and outside the lab.

I thank Dr. Beate Schwer for assistance with RNA-seq experiments; Agnes Viale and the MSKCC Integrated Genomics Operation for DNA sequencing; Nick Socci and the MSKCC Bioinformatics Core Facility for assistance with data analysis; Dr. Stewart Shuman for gifts of T4 RNA ligase; Dr. Kunihiro Ohta, Dr. Mariko Sasaki and Dr. Drew Thacker for strains; and Isabel Lam and Dr. Scott Keeney for discussion and comments on the thesis.

Finally, I could not accomplish the graduate work without many of my wonderful friends and family. I am especially grateful to my parents, my grandparents, Peipei Guo, Ying Liu, Ray Zhicheng Qiu, Xiaonan Wang, Na Xu and Yong Yun, who always supported me. Thank you all.

TABLE OF CONTENTS

LIST OF FIGURES

Chapter 1

Chapter 2

Chapter 3

Chapter 4

Appendix

LIST OF TABLES

Methods

Chapter 1: Introduction

Meiotic recombination and its initiation

Meiosis is a specialized cell division, in which cells undergo one round of DNA replication followed by two successive rounds of cell division (**Figure 1.1**). Whereas mitosis produces diploid daughter cells from diploid cells, meiosis generates haploid gametes from diploid precursors.

In meiotic prophase, most sexually reproducing organisms induce homologous recombination. Homologous recombination occurs between DNA strands of similar or identical nucleotide sequences, which provides physical connections between homologs. This connection is essential for accurate homologous chromosome segregation (Gerton and Hawley 2005). Errors in meiotic recombination can result in aneuploidy or genome rearrangements among progeny, which in humans can lead to congenital miscarriage and genetic disorders such as Down's syndrome (Stankiewicz and Lupski 2010; Liu *et al.* 2012; Nagaoka *et al.* 2012; Sasaki *et al.* 2013). Recombination also disrupts the linkage of polymorphisms on the same chromosome, and thus promotes genome diversity and evolution (Kauppi *et al.* 2004).

Programmed DNA double-strand break (DSB) formation by Spo11 is a widely conserved feature of meiotic recombination initiation in fungi, plants, invertebrate and mammals (Keeney 2008). The number of Spo11-induced DSBs in meiotic cells is surprisingly high: approximately 150-200 breaks are formed per nucleus in *Saccharomyces cerevisiae* (Chen *et al.* 2008a; Mancera *et al.* 2008; Pan *et al.* 2011); on average, more than 200 DSBs per nucleus are formed in mice (Plug *et al.* 1996; Cole *et al.* 2012). For comparison, 1 Gy of ionizing radiation induces 20-40 DSBs and 2 Gy can lead to somatic cell death (Kauppi *et al.* 2013b).

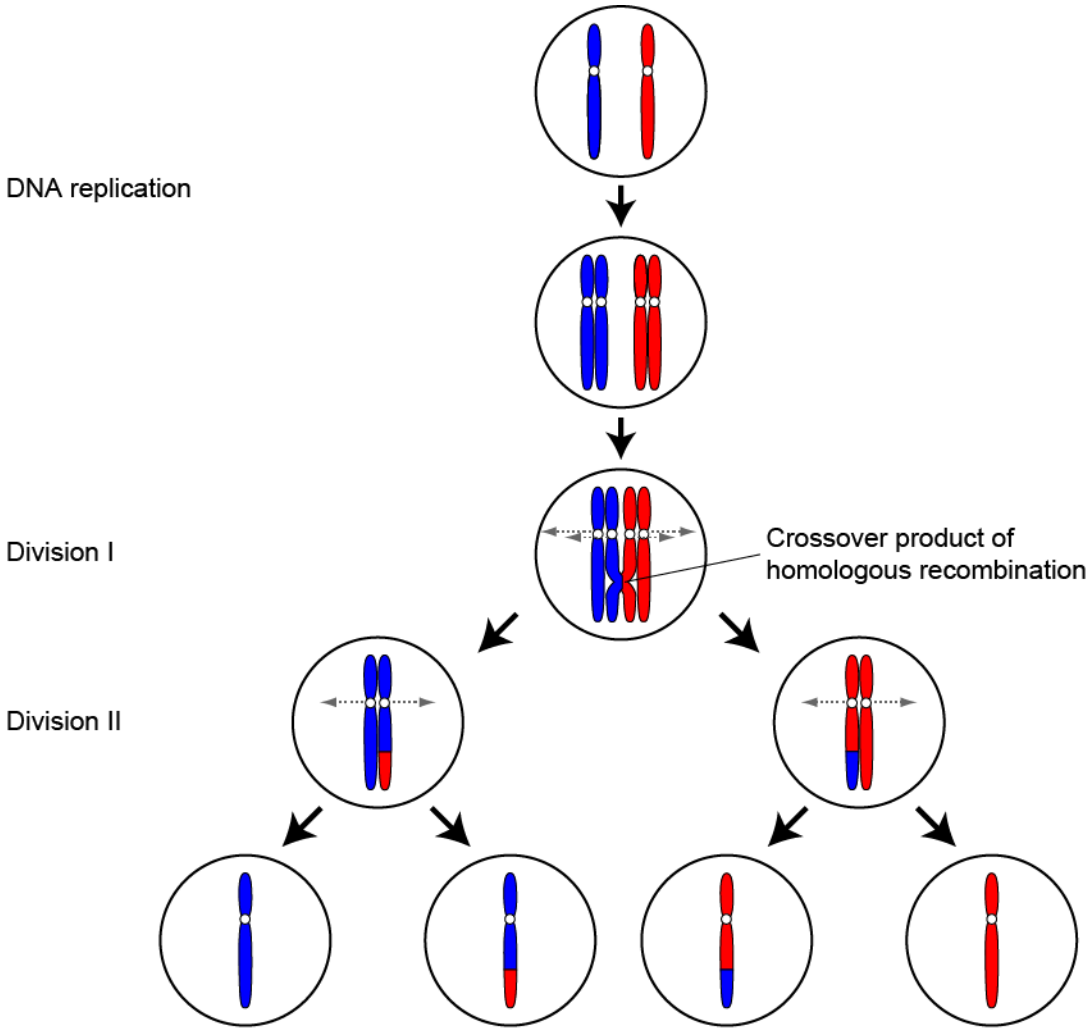

Figure 1.1 Overview of the events in meiosis. Meiosis initiates with one round of DNA replication, followed by two consecutive rounds of chromosome segregation. Homologous chromosomes are shown in red and blue. In meiosis I, homologous chromosomes exchange genetic information via recombination and are then segregated. Meiotic recombination provides a physical linkage between homologs, which along with sister chromatid cohesion helps orient a pair of sister kinetochores to opposite spindle poles. In meiosis II, sister chromatids separate. For simplicity, only one pair of homologous chromosomes is depicted. Figure adapted from Mariko Sasaki's thesis, Weill Cornell Graduate School of Medical Sciences.

Extensive studies using the budding yeast *S. cerevisiae* as model organism have elucidated the molecular mechanisms of meiotic recombination (Keeney 2008; De Massy 2013b; Lam and Keeney 2014). Spo11, a topoisomerase-like enzyme, catalyzes meiotic DSB formation (Bergerat *et al.* 1997; Keeney *et al.* 1997). Spo11 cleaves both strands of double-stranded DNA as a homodimer. After break formation, Spo11 remains covalently bound to the 5′ DNA termini (De Massy *et al.* 1995; Keeney and Kleckner 1995; Liu *et al.* 1995). Single-stranded nicks at sites 3′ to the break release Spo11 bound to a short oligonucleotide, which are referred to as Spo11-oligo complexes (**Figure 1.2**) (Neale *et al.* 2005). This endonucleolytic cleavage requires the Mre11-Rad50-Xrs2 complex and Sae2 protein. The cleaved strands further undergo 5′-to-3′ resection (Sun *et al.* 1991; Zakharyevich *et al.* 2010). Strand exchange proteins Rad51 and Dmc1 then bind to the 3′ single-stranded DNA (ssDNA) tails and catalyze strand invasion into the intact homologous duplex DNA (Chen *et al.* 2008b; San Filippo *et al.* 2008). Although some DSBs are repaired via the sister chromatid, most DSBs are subsequently repaired using the homolog as templates (Schwacha and Kleckner 1994; Goldfarb and Lichten 2010). Recombination produces reciprocal exchange of chromosome arms flanking the DSB site (crossovers) or no exchange (noncrossovers) (Hunter 2007; Serrentino and Borde 2012).

Many genes in the meiotic recombination pathway are conserved (Gerton and Hawley 2005). Mutations in any of these genes cause meiotic defects. For example, *S. cerevisiae spo11* mutants do not form DSBs, have decreased levels of recombination, and generate inviable spores due to aneuploidy (Klapholz *et al.* 1985; Wagstaff *et al.* 1985; Cao *et al.* 1990; Weiner and Kleckner 1994). Disruption of mouse Spo11 leads to the absence of DSBs, severe recombination defects and infertility (Baudat *et al.* 2000). Similar meiotic defects were also seen in *spo11* mutants of other organisms such as *Caenorhabditis elegans* (Dernburg *et al.* 1998) and *Drosophila melanogaster*

Figure 1.2 The meiotic double-strand break (DSB) formation and recombination pathway. Homologous chromosomes are shown in blue and red. Meiotic recombination initiates with programmed DSB formation. Meiotic DSBs are catalyzed by a Spo11 homodimer. After break formation, Spo11 remains covalently bound to the 5′ DNA termini. Single-stranded nicks at sites 3′ to the break release Spo11 bound to a short oligonucleotide referred to as Spo11-oligo complexes. The cleaved strands further undergo 5′-to-3′ resection and stand invasion, resulting in D-loop intermediates. D-loop intermediates are subsequently repaired via double-Holliday junction pathway or the synthesis-dependent strand annealing pathway, resulting in crossover or non-crossover (gene conversion). For simplicity, only one pair of homologous chromosomes is depicted.

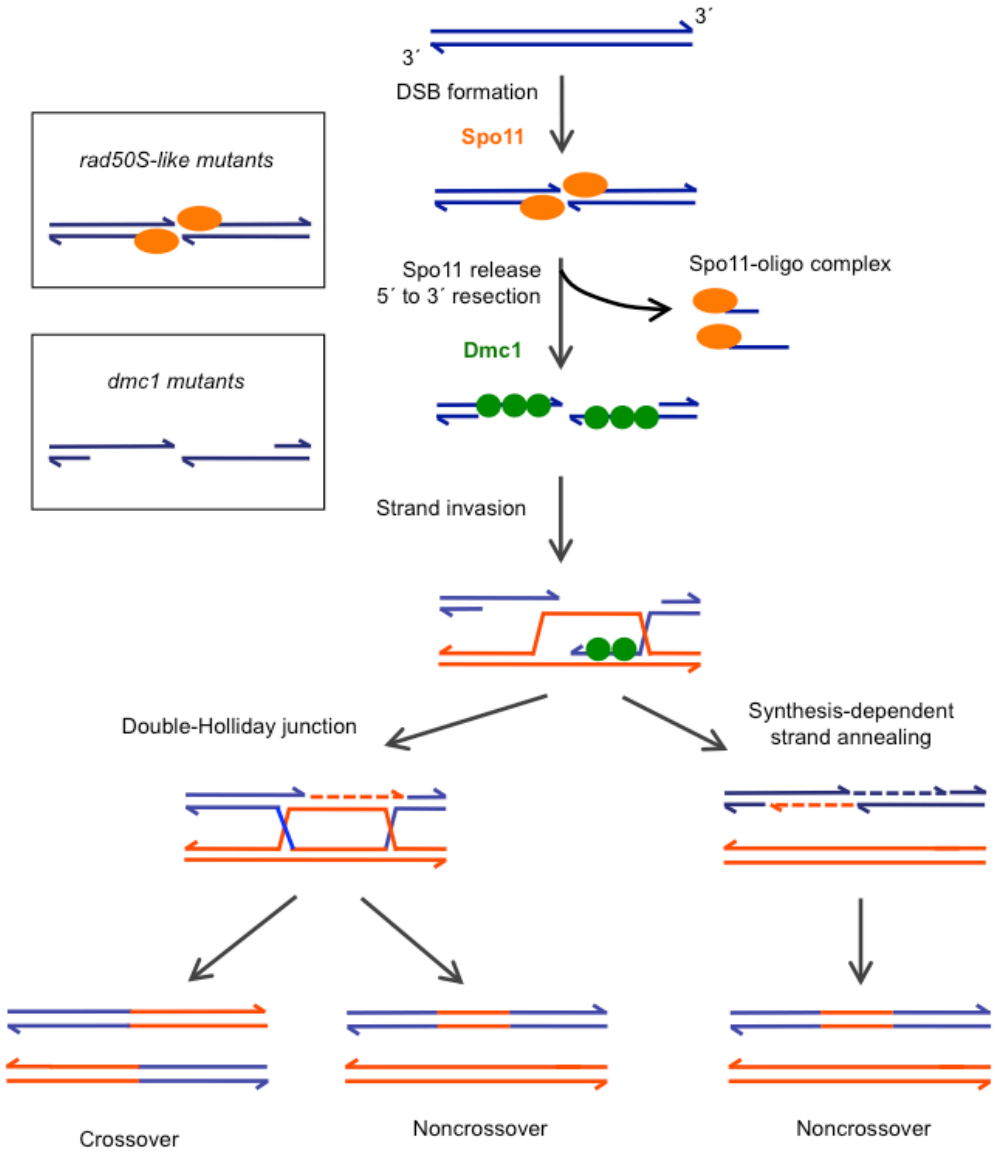
3′
3′
DSB formation
Spo11
rad50S-like mutants
Spo11 release
5′ to 3′ resection
Spo11-oligo complex
Dmc1
dmc1 mutants
Strand invasion
Double-Holliday junction
Synthesis-dependent
strand annealing
Crossover
Noncrossover
Noncrossover

(Mckim and Hayashi-Hagihara 1998). Thus, the meiotic recombination pathway elucidated in budding yeast provides great insights into meiotic recombination in other eukaryotes.

Mapping genome-wide meiotic DSB sites

Meiotic recombination does not occur randomly across the genome (Cherry *et al.* 1997; Chen *et al.* 2008a; Mancera *et al.* 2008). It is more likely to happen in some genomic regions than others, largely due to nonrandom DSB distribution (Baudat and Nicolas 1997; Gerton *et al.* 2000; Borde *et al.* 2004; Blitzblau *et al.* 2007; Buhler *et al.* 2007; Pan *et al.* 2011). Early studies using Southern blotting to physically detect DSBs revealed some factors affecting DSB patterns in *S. cerevisiae*. First, chromosome III is organized into large DSB-hot and -cold domains (tens of kilobases (kb)) (Baudat and Nicolas 1997). Second, within hot domains, DSBs preferentially form in short regions called DSB hotspots (typically several hundred base pairs (bp) wide), which tend to overlap gene promoters (Petes 2001; Lichten 2008). Binding of transcription factors has been implicated in influencing DSB formation (discussed in **Chapter 3**) (Schuchert *et al.* 1991; White *et al.* 1991; Kon *et al.* 1997; Steiner *et al.* 2002). To extend all the above findings from a limited number of hotspots to a global level, genome-wide DSB maps have been generated by several methods.

Chromatin immunoprecipitation (ChIP)- or ssDNA purification-based detection of meiotic DSB distribution. Gerton and colleagues were the first to use ChIP and microarrays to map global DSB distribution in yeast (Gerton *et al.* 2000). They hybridized Spo11-associated DSB fragments from a *rad50S*-like mutant (in which Spo11 is blocked from releasing from DSB sites and thus DSBs accumulate (Alani *et al.* 1990; Keeney *et al.* 1997)) to DNA microarrays containing all 6,200 *S.*

cerevisiae open reading frames. DNA sequences that were highly enriched in the immunoprecipitated fraction relative to total input DNA were defined as hotspots. Similar methodology has been used in subsequent microarray studies, all based on enrichment of Spo11-bound DNA in *rad50S*-like mutants (Borde *et al.* 2004; Mieczkowski *et al.* 2006; Mieczkowski *et al.* 2007; Robine *et al.* 2007). These maps reveal that spatial patterns for chromosome III can be extrapolated to other chromosomes: each chromosome can be divided into large domains with alternating DSB levels; DSBs are suppressed near the centromeres and telomeres. DSB distributions are also mapped in fission yeast *Schizosaccharomyces pombe* (Cromie *et al.* 2007). In this study, unlike *S. cerevisiae*, hotspots in *S. pombe* are usually widely separated (~50–100 kb apart) by genomic segments with little or no detectable DSBs.

These mapping efforts provided important new insights, but their mapping tool—*rad50S*-like mutants—were found to alter DSB distributions relative to wild type. Specifically, DSBs are reduced around centromeres and telomeres as well as in late-replicating regions in *rad50S*-like mutants (Baudat and Nicolas 1997; Borde *et al.* 2000; Blat *et al.* 2002). To overcome these limitations, ssDNA generated by DSB end resection (and enriched in *dmc1* mutants) was purified by chromatography on benzoylated naphthoylated DEAE-cellulose and hybridized to whole-genome microarrays (Blitzblau *et al.* 2007; Buhler *et al.* 2007). These *dmc1* maps detected substantial DSB formation in many regions where DSBs were absent or repressed in *rad50S*-like mutants. For example, DSB formation is still suppressed in pericentric and subtelomeric regions relative to wild type, but the highly suppressed zones are much smaller than previously thought (e.g., subtelomeric suppression is less than 20 kb from chromosome ends in *dmc1*, as opposed to ~50 kb in *rad50S*-like mutants). These maps represent more accurately the DSB distribution in wild-type cells, in that they agree better with the breaks detected by Southern blot analysis in wild type.

Genome-wide mapping of DSB distributions in mouse was performed by ChIP for the strand exchange proteins DMC1 and RAD51 from testis extracts, followed by DNA sequencing (Smagulova *et al.* 2011). To enrich the ssDNA intermediates, a *Hop2-/-* mutant was first used. *Hop2-/-* mutants lack a strand invasion accessory protein and accumulate DMC1- and RAD51-bound ssDNA intermediates (Petukhova *et al.* 2003). The protocol was further optimized and can also detect DMC1-bound sites in wild-type mice (Khil *et al.* 2012). Recently, this method was applied to map human DSB hotspots (Pratto *et al.* 2014). The meiotic DSB distribution in mouse and human will be discussed below.

These studies provided important insights but had relatively low spatial and quantitative resolution due to microarray design, non-linear range of hybridization signal, and the larger size of DSB-associated DNA used as probes or for sequencing. First, the resolution of these maps is relatively low (usually several kb) due to the limitations in DNA sample preparation and hybridization. In contrast, majority of DSB hotspots is 50–300 bp wide (Pan *et al.* 2011). Moreover, microarray probes were long (usually several hundreds bp at that time), and cross-hybridization of DNAs from other loci causes high background. Finally, these maps were generated in *rad50S* or *dmc1* mutant backgrounds to block DSB repair and enrich for intermediates as starting materials (Alani *et al.* 1990; Bishop *et al.* 1992; Keeney *et al.* 1997). However, some mutants may exhibit synthetic phenotypes when combined with *rad50S* or *dmc1*, such as *pch2Δ rad50S* mutants (see **Appendix**). Therefore, they can only reveal limited information about genomic features associated with DSB hotspots.

A quantitative, high-resolution map of meiotic DSBs by sequencing Spo11-oligos in yeast. We overcame these limitations by developing a novel method to map genome-wide DSB sites in budding yeast at nucleotide resolution (Pan *et al.* 2011).

After DSB formation, Spo11-oligo complexes are released from the DSB ends by an endonucleolytic reaction (Neale *et al.* 2005) (**Figure 1.2**). In *S. cerevisiae*, there are two discrete groups of Spo11-oligo complexes, comprising of Spo11 bound to oligonucleotides of ~21–37 nucleotides (nt) or of ≤12 nt. The amounts of long and short Spo11 oligos are approximately equal in a population of cells. Because each Spo11 oligo is a unique tag of a single DSB site, determining the 5′ end nucleotide of Spo11 oligos enables the accurate identification of Spo11 cleavage sites. By purifying and sequencing Spo11 oligos from synchronized meiotic cultures, high-resolution DSB maps have been generated in both budding yeast and fission yeast (Pan *et al.* 2011; Fowler *et al.* 2014; Thacker *et al.* 2014). These quantitative maps allow us to analyze the DSB patterns at various spatial resolutions, from whole chromosome to single nucleotide.

The landscape of meiotic recombination initiation

As mentioned earlier, meiotic DSBs and subsequent recombination are not randomly distributed (Baudat and Nicolas 1997; Cherry *et al.* 1997; Gerton *et al.* 2000; Borde *et al.* 2004; Blitzblau *et al.* 2007; Buhler *et al.* 2007; Chen *et al.* 2008a; Mancera *et al.* 2008; Pan *et al.* 2011). Their locations are important for genome integrity and are thus under tight control. For example, meiotic DSBs and recombination happen less frequently in repetitive elements, thereby reducing the probability of recombination between non-allelic DNA segments, which can cause genome rearrangements. The alteration of genome structure has been implicated in genomic disorders in human (Sasaki *et al.* 2010). Accurate meiotic DSB maps offer numerous insights into the mechanisms of meiotic DSB formation and repair, genome evolution, and for mammals, the predisposition to genomic disorders.

Meiotic DSB distribution in budding yeast. From the first detection of meiotic DSBs to the high-resolution genome-wide maps, many labs have contributed to the description of the DSB landscape in *S. cerevisiae* (Lichten and Goldman 1995; Petes 2001; Kauppi *et al.* 2004; Lichten and De Massy 2011; Pan *et al.* 2011; De Massy 2013a; Lam and Keeney 2014). At the chromosome level, DSBs form more frequently on chromosome arms and less frequently within ~5–10 kb around centromeres and ~20 kb from telomeres (two- to three-fold below the genome average) (Blitzblau *et al.* 2007; Buhler *et al.* 2007; Pan *et al.* 2011). Within these domains, DSBs are clustered in hotspots. 3,604 hotspots were identified in Spo11-oligo maps, by calling the regions where Spo11-oligo density was at least two-fold higher than the genome average (Pan *et al.* 2011). Hotspots are usually narrow regions (73.4% are 50–300 bp in size), and 88.2% overlap with intergenic promoters, indicating that some features unique to promoters favor DSB formation. Transcription is not required for robust DSB formation, in that deletion of TATA box (a AT-rich sequence bound by general transcription factors when transcription begins) abolished transcription but not DSB formation in the *HIS4* promoter (White *et al.* 1992).

Another feature of budding yeast promoters is the nucleosome-depleted region (NDR), which agrees with previous evidence for the importance of chromatin accessibility at DSB hotspots (Ohta *et al.* 1994; Wu and Lichten 1994; Berchowitz *et al.* 2009; Pan *et al.* 2011). Most DSB hotspots examined are nuclease-hypersensitive (Petes 2001; Lichten 2008). Thus, open chromatin is an important determinant of DSB formation. However, not all nucleosome-depleted sites are DSB hotspots, suggesting that open chromatin is necessary but not sufficient for robust DSB formation.

Another component, histone 3 lysine 4 trimethylation (H3K4me3), plays a major role in DSB formation. H3K4me3 is enriched at the 5′ end of genes and DSBs are enriched near H3K4me3. Set1 is a histone methyltransferase that methylates

H3K4. Depletion of H3K4Me3 in *set1Δ* reduces DSB activity in the majority of hotspots. Recent investigations have identified an H3K4me3 reader, Spp1, that links the histone modification and the DSB machinery, which will be discussed below (Acquaviva *et al.* 2013; Sommermeyer *et al.* 2013). In some cases, hotspots also depend on the binding of sequence-specific transcription factors (TFs), such as at the *HIS4* promoter (Schuchert *et al.* 1991; White *et al.* 1991; Kon *et al.* 1997; Steiner *et al.* 2002).

Meiotic DSB distribution in S. pombe. The distance between DSB hotspots in *S. pombe* is larger than in *S. cerevisiae*. Hotspots are usually 50–100 kb apart in *S. pombe* in comparison to an average of one hotspot per 3.4 kb in *S. cerevisiae*. Unlike in *S. cerevisiae*, hotspots in *S. pombe* do not correlate with transcription promoters but tend to localize in large intergenic regions (Cromie *et al.* 2007). These intergenic regions are often larger than 3 kb and include clusters of closely spaced NDRs (De Castro *et al.* 2012). However, DSBs are not strongly restricted to NDRs as in *S. cerevisiae* (Fowler *et al.* 2014). Moreover, some hotspots are dependent on transcription factor binding (e.g., *ade6-M26* hotspot bound by Atf1-Pcr1 transcription factors, which is discussed in **Chapter 3**), whereas others are independent of known transcription factors (Wahls and Smith 1994; Kon *et al.* 1997; Cromie *et al.* 2005; Hirota *et al.* 2007). In *S. pombe*, proteinaceous chromosome-associated structures known as linear elements form during meiotic prophase, and linear element components (Rec25, Rec27, and Mug20) are correlated with DSB hotspots (Fowler *et al.* 2013).

Meiotic DSB distribution in mammals. DSB hotspots have recently been mapped in mouse and human males. In human, up to 38,946 hotspots per individual

were identified, which is substantially more than the 15,000 to 20,000 hotspots identified in mouse (Brick *et al.* 2012; Pratto *et al.* 2014). Mouse and human hotspots do not correlate with transcription promoters and are located in both genic and intergenic regions (Mcvean *et al.* 2004; Myers *et al.* 2005; Arnheim *et al.* 2007; Frazer *et al.* 2007; Coop *et al.* 2008; Kong *et al.* 2010; Smagulova *et al.* 2011; Lu *et al.* 2012). Hotspot location in mice and humans is defined by specific alleles of the PRDM9 protein (Baudat *et al.* 2010; Myers *et al.* 2010; Parvanov *et al.* 2010; Grey *et al.* 2011; Brick *et al.* 2012). PRDM9 contains both a methyltransferase domain and a sequence-specific DNA-binding domain containing several C2H2 zinc fingers. DSBs form frequently around predicted PRDM9 binding sites. PRDM9 promotes H3K4me3 formation, and DSB hotspots overlap a subset of H3K4me3-enriched sites (Hayashi *et al.* 2005; Buard *et al.* 2009; Smagulova *et al.* 2011). Unlike budding yeast, this overlap does not generally include the strong H3K4me3-enriched regions around promoters. In human, factors other than PRDM9 modulate the DSB frequency, since less than half of the variation in hotspot intensity can be explained by sequence changes at PRDM9 binding sites (Pratto *et al.* 2014).

A hierarchical combination of factors shapes the landscape of meiotic DSBs

The spatial pattern of DSBs is not determined by a single factor but shaped by a combination of factors acting at different scales (**Figure 1.3**) (Lichten and Goldman 1995; Petes 2001; Kauppi *et al.* 2004; Lichten and De Massy 2011; Pan *et al.* 2011; De Massy 2013a; Lam and Keeney 2014). This is best understood in *S. cerevisiae,* but implicated in other organisms as well. For example, although PRDM9 is the key determinant of hotspot location in mouse, a distinct control operates in the pseudoautosomal region (PAR) on sex chromosomes. In the PAR, the location of DSB hotspots remains the same in strains with different *Prdm9* alleles or in strains that do

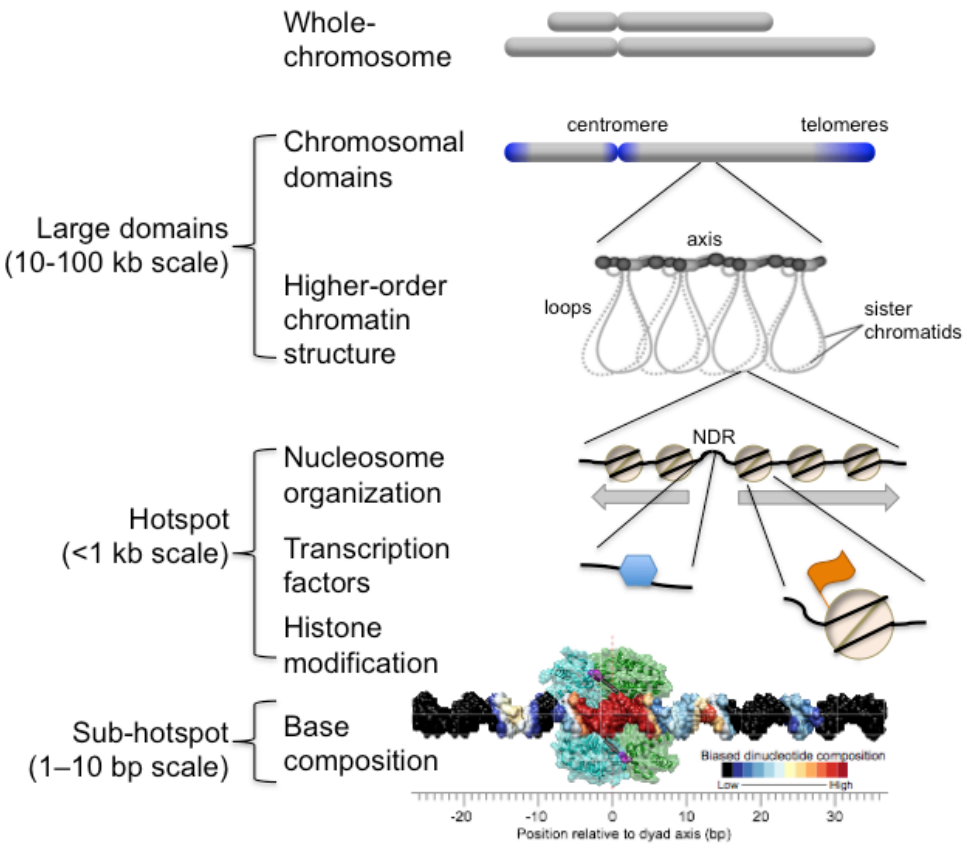

Figure 1.3 The DSB landscape in *S. cerevisiae* is shaped by a hierarchical combination of many factors. Important determinants includes whole chromosome variation, large subchromosomal domains, cohesins and other chromosome structure proteins, chromatin structure, transcription factors, histone modification and base composition. The level in hierarchy of these factors are generally proportional to scale. For example, DSBs are more frequent in chromatin loops than axes, which is hierarchical to the preference that DSBs are usually restricted to nucleosome-depleted regions (NDRs). Thus, even if two genomic loci are equally free of nucleosomes, they may have different hotspot activities depending on whether they are located on chromatin loops or axes. Figure adapted from Isabel Lam, MSKCC.

not express PRDM9 (Brick *et al.* 2012). Below, I will use *S. cerevisiae* as a model system to dissect the multiple regulatory layers controlling DSB distributions.

Whole chromosome variation. More than two decades ago, higher crossover densities were discovered on small chromosomes compared with longer chromosomes (also called "chromosome size effect") (Kaback *et al.* 1989; Mortimer *et al.* 1989; Kaback *et al.* 1992; Riles *et al.* 1993). This effect is largely due to the chromosome size-correlated variation in DSB frequencies (Pan *et al.* 2011). Similar to crossovers, more Spo11 oligos per kb were recovered from smaller chromosomes. In contrast, there is little difference between small and large chromosomes for the downstream steps of DSB formation, such as the crossover versus noncrossover decision and the choice of homolog versus sister chromatid as recombination partner. However, densities of Spo11 oligo hotspots are similar regardless of chromosome sizes, suggesting that the higher DSB density on small chromosomes is not because of the higher hotspot density. Zip3 (also known as Cst9) is required for the tendency of DSB density to vary with chromosome size (Thacker *et al.* 2014). Deletion of Zip3 causes the formation of excess DSBs due to the defect in homologous chromosome engagement. This implies a potential link between the chromosome size effect and Zip3-depedent DSB suppression. But the molecular mechanism is not yet clear.

Regulation in large subchrosomomal domains. DSBs are substantially suppressed near telomere, centromere and in ribosomal DNA (rDNA) (Baudat and Nicolas 1997; Gerton *et al.* 2000; Borde *et al.* 2004; Blitzblau *et al.* 2007; Buhler *et al.* 2007; Pan *et al.* 2011; Vader *et al.* 2011). DSBs are less frequent in the 20 kb closest to each telomere. This DSB repression is made more severe by deleting Sir2, which is a conserved NAD+ dependent histone deacetylase of the Sirtuin family and plays a

role in silencing at *HML*, *HMR*, telomeres and the rDNA locus (Rusche *et al.* 2003; Sauve *et al.* 2006; Mieczkowski *et al.* 2007).

DSBs are rare within 1-3 kb of centromeres and below genome average within ~5–10 kb on either side of centromeres (Pan *et al.* 2011). Hotspot density is lower than expected within 10 kb of centromeres, and hotspot activity within 5 kb appears to be weaker. DSBs near centromeres can lead to aneuploidy and spore inviability, in that DSB repair by recombination may disrupt pericentric cohesion and cause premature separation of sister chromatids at meiosis I (Rockmill *et al.* 2006).

The rDNA array is composed of 100-200 copies of a 9.1 kb repeat on chromosome XII. It is strongly repressed for meiotic DSB formation (75-fold below genome average) and recombination (Petes and Botstein 1977; Pan *et al.* 2011). This DSB prevention is partially through Sir2-dependent heterochromatin formation (Gottlieb and Esposito 1989; Mieczkowski *et al.* 2007). Furthermore, the edges of the rDNA array are exceptionally susceptible to meiotic DSBs and protected by the meiotic ATPase Pch2 and the origin recognition complex subunit Orc1 (Vader *et al.* 2011). Upon disruption of these factors, DSB formation and recombination increased specifically in the outermost rDNA repeats, leading to non-allelic homologous recombination (NAHR) and rDNA instability (Discussed in **Chapter 5**).

Cohesins and other chromosome axis-associated proteins. Many observations suggest that chromosome organization is involved in regulating various aspects of meiotic recombination, such as DSB repair template choice and crossover number control. Meiotic chromosomes are organized into a series of chromatin loops anchored to a proteinaceous axis (also called the lateral element at the beginning of meiotic prophase) (**Figure 1.3**) (Moens and Pearlman 1988; Page and Hawley 2004). DSB repair and recombination proteins are axially associated (Zickler and Kleckner 1999;

Blat *et al.* 2002; Kleckner 2006). Additionally, ChIP studies showed that axial sites are enriched for cohesin, Hop1, Red1, Mek1 and many of components of the DSB machinery (e.g., Rec114, Mei4 and Mer2) (Blat and Kleckner 1999; Blat *et al.* 2002; Glynn *et al.* 2004; Panizza *et al.* 2011). No DSBs form in the absence of these DSB machinery components. However, DSBs mostly occur within chromatin loops-associated DNA rather than axis-associated DNA (Blat *et al.* 2002; Glynn *et al.* 2004; Kugou *et al.* 2009; Pan *et al.* 2011; Panizza *et al.* 2011), suggesting DSB sites are tethered to the axis before or at the time of DSB formation (Blat *et al.* 2002; Kleckner 2006; Panizza *et al.* 2011).

Axis-associated proteins play a role in determining DSB frequencies and locations. Rec8 is a meiosis-specific subunit of cohesin, which is a complex that holds sister chromatids together. It substitutes the mitosis-specific Mcd1/Scc1 subunit at the beginning of meiosis (Klein *et al.* 1999; Watanabe and Nurse 1999). Cohesin preferentially binds to chromatin at regular intervals (~11-13 kb) in AT-rich sequences (Blat and Kleckner 1999; Blat *et al.* 2002; Glynn *et al.* 2004). Spo11 is initially colocalized with Rec8 on the axis and eventually relocates to loops during DSB formation (Kugou *et al.* 2009). Deletion of *REC8* influences the localization of Spo11 to centromeres and in some intervals of the chromosome arms. Thus, DSB formation was severely impaired at selective domains of many chromosomes other than chromosome III. Furthermore, DSBs are rare in regions within 0.8 kb of Rec8 binding sites probably due to the reduced histone H3K4me3 and inactivation of Spo11 activity on the axis (Ito *et al.* 2014).

Another axis-associated protein, Hop1, is a meiosis-specific HORMA (HOp1p, Rev7p and MAd2) domain-containing protein, which has been suggested to bind DNA and act as an adaptor to recruit other proteins (De Massy 2013a). Hop1 is recruited to chromosomes at the beginning of meiotic prophase, independent of DSB formation, in

complex with Red1. Hop1-enriched domains correlate with high-frequency DSB domains (Panizza *et al.* 2011). DSB proteins Rec114, Mei4 and Mer2 are also abundant in these domains. Deletion of Hop1 shows severe DSB reductions to only 5% to 10% of wild-type levels (Mao-Draayer *et al.* 1996; Woltering *et al.* 2000). Similarly, DSB levels are also reduced in mutants of other axis-bound proteins, such as *red1* and *mek1*, though the reduction is less severe (Rockmill and Roeder 1991; Blat *et al.* 2002).

Chromatin structure and histone modification. Of the few hotspots examined by direct physical assays, most are located predominantly within nuclease-hypersensitive sites in meiotic chromatin (Ohta *et al.* 1994; Wu and Lichten 1994). Genome-wide DSB maps show that the vast majority (88%) of DSBs occur in the NDR at gene promoters, and wider hotspots tend to have larger NDRs and higher DSB frequency (Pan *et al.* 2011). These findings suggest that a physically open chromatin is necessary for DSB machinery access to the DNA. However, open chromatin itself is not sufficient for hotspot activity. For example, NDRs are also prominent at the 3′ end of ORFs, but few hotspots are located at these loci unless they coincide with the promoter NDR of a downstream gene. Thus, open chromatin structure only provides a window of opportunity for Spo11-depedent DSB formation. An illustrating example is the DSB analysis on the *PHO5* promoter (Wu and Lichten 1994). When Pho5 is transcriptionally repressed, its promoter is occupied by a well-positioned nucleosome array and meiotic DSBs are detected as a narrow band by Southern blot. However, in the induced state, the nucleosomes are removed and the DSB band becomes dramatically wider across the whole nucleosome-depleted promoter.

Acetylation, ubiquitination, and methylation of histones are each implicated in meiotic recombination (Sollier *et al.* 2004; Yamashita *et al.* 2004; Mieczkowski *et al.* 2007; Borde *et al.* 2009; Acquaviva *et al.* 2013; Sommermeyer *et al.* 2013). In

particular, H3K4me3 influences DSB formation. H3K4me3 peaks at the start of transcriptionally active genes in exponentially growing cells and in meiosis (Pokholok *et al.* 2005; Zhang *et al.* 2011b). Recently, it has been discovered that an axis-associated component of DSB machinery, Mer2, interacts with Spp1, a protein containing a PHD (Plant Homeo *Domain*) finger. Spp1 binds H3K4me3 marks in chromatin loops, thereby tethering the chromatin loop to the axis and allowing DSB formation in NDRs in loops (Acquaviva *et al.* 2013; Sommermeyer *et al.* 2013). This discovery provides a feasible solution to the paradox of spatial discrepancy between the location of DSBs within loop DNA sequences and some components of the DSB machinery in the axis. In support of this, abolishing H3K4me3 by deleting the histone methyltransferase Set1 reduces DSB activity in most DSB active loci of the genome (Borde *et al.* 2009) (and see **Chapter 4**). However, it is not yet clear how much H3K4me3 is the minimal requirement for break formation at a single site. Furthermore, Spo11-oligo frequency (i.e. hotspot "heat") does not correlate with H3K4me3 levels (Tischfield and Keeney 2012), suggesting that although H3K4me3 targets DSBs in the chromatin loops, the level of H3K4me3 alone is not the major determinant of DSB frequencies. This histone modification is only one layer of the hierarchical control of the meiotic DSB landscape.

The binding of transcription factors (TFs). The influence of TFs on DSB formation was intensively studied at the *HIS4* promoter in *S. cerevisiae* by Petes and colleagues (Petes 2001). They have shown that the *HIS4* promoter displays strong hotspot activity and this activity requires the binding of TFs Bas1, Bas2 and Rap1 (White *et al.* 1991; Kon *et al.* 1997). This suggests that TFs stimulate meiotic recombination at their binding sites. However, local DSB stimulation at *HIS4* cannot be extrapolated to all genomic loci. Surprisingly, Bas1 can also repress DSBs around

its binding sites at some loci. Deletion of Bas1 caused hotspot activity elevation or suppression in a number of loci, suggesting Bas1 regulates DSB formation in a context-dependent manner (Mieczkowski *et al.* 2006).

Sequencing Spo11-oligos yields a single-nucleotide resolution map, allowing the alignment of DSB sites with TF binding sequences (typically 4-15 nt long). Spo11-oligos map frequently near 4233 binding sites of 77 TFs annotated based on ChIP and conservation (Pan *et al.* 2011). However, since TFs sites are enriched in promoters, it is unclear if those TFs are active in influencing hotspot activity or just bystanders. Furthermore, Spo11-oligo spatial patterns and counts varied widely among TFs. Thus, the role of TFs on DSB formation is still poorly defined, which I will discuss in detail in **Chapter 3**.

Local nucleotide composition. Spo11 has no or little DNA sequence specificity, but displays biases for which phosphodiester bonds to cut on DNA sequences. Spo11-oligo maps reveal some base composition preferences at or near the DSB sites (Pan *et al.* 2011). First, base composition was most strongly biased within the 10-12 bp centered on the predicted dyad axis of cleavage. This biased region is predicted to contact Spo11 based on the Top6A (the archaeal Spo11 homolog) structure (Nichols *et al.* 1999). It is AT enriched and the dinucleotide composition likely reflects relatively narrow, deep grooves on the side of the DNA contacting Spo11. Second, bias is also symmetrical at 10-16 bp to the right and left of the dyad axis. These regions are slightly GC enriched and probably reflect the footprint of a Spo11-associated protein or a Spo11 domain not modeled by the Top6A structure. Third, an asymmetric region is located ~ 25 nt from the dyad axis, which is consistent with bias for oligo 3′-end formation. These findings provide insights into the cleavage site selection of DSBs. Thus, bases of the same DNA fragment in a DSB hotspot do

not have equal opportunities for DSB formation, at least partially due to the base preferences and constraints from the intrinsic characteristics of Spo11 and its partners.

DSB feedback regulation. Several negative feedback loops that control DSB levels have been reported in *S. cerevisiae*. First, a DSB on one chromosome suppresses DSB formation on its sister chromatid or homologous chromosomes (Xu and Kleckner 1995; Rocco and Nicolas 1996; Fukuda *et al.* 2008; Zhang *et al.* 2011a). This *trans* inhibition constrains DSBs to one per four chromatids, even at a strong hotspot (Zhang *et al.* 2011a). Deletion of Tel1 or Mec1 (two proteins involved in checkpoint control in response to DNA damage) causes DSBs to occur often at the allelic position on two chromatids in the same cell, suggesting loss of *trans* inhibition (Zhang *et al.* 2011a). Second, a strong hotspot created by inserting an artificial hotspot-specifying DNA sequence or by fusing Spo11 to a sequence-specific DNA binding domain to target DSBs suppresses DSB formation in neighboring regions on the same chromatid (a phenomenon also known as "hotspot competition"), but the mechanism is not known (Wu and Lichten 1995; Xu and Kleckner 1995; Fan *et al.* 1997; Fukuda *et al.* 2008). Third, DSB formation is regulated via a feedback mechanism mediated by homolog engagement. Mutants lacking ZMM proteins (Zip1-4, Msh4-5, Mer3, Spo16 and Pph3) display defects in synaptonemal complex and recombination (Lynn *et al.* 2007). (The synaptonemal complex is a meiosis-specific structure comprising the proteinaceous axes of a pair of homologous chromosomes held together by transverse filaments; it serves as a scaffold stabilizing the juxtaposition of homologous chromosomes and promotes the completion of recombination (Zickler and Kleckner 1999).) ZMM mutants formed a substantially greater number of DSBs (Thacker *et al.* 2014). Negative feedback regulation has also been described in mice, flies, and worms (Bhagat *et al.* 2004; Henzel *et al.* 2011;

Joyce *et al.* 2011; Lange *et al.* 2011; Kauppi *et al.* 2013a). These feedback circuits function as part of the robust control system to prevent excessive DSBs in meiotic cells (Keeney *et al.* 2014).

An important implication is that the negative feedback processes influence DSB distribution. DSBs are more evenly spaced as a result of suppression via the local activity of Tel1 near DSBs or homolog engagement at sites of recombination (Bhagat *et al.* 2004; Thacker *et al.* 2014). For example, in *zip3* mutants, different chromosomal subdomains responded differently to the DSB increase, with domains of greater or lesser change alternating along chromosomes (Thacker *et al.* 2014). One possible explanation is that defective homolog engagement in *zip3* mutants relieves the DSB suppression that would normally occur near sites of recombination. If so, this further implies that ZMM-dependent DSB suppression in wild-type cells spreads along chromosomes from sites of homolog engagement, with the magnitude of suppression decreasing with the distance from the engagement site. Moreover, despite a 1.8-fold increase of total DSBs in *zip3* mutants, DSB frequencies in subtelomeric and pericentromeric regions were elevated less than genome average, and were unchanged or reduced near the rDNA (Thacker *et al.* 2014). Accordingly, ZMM-dependent DSB suppression is different from and subordinate to the DSB suppression mechanisms acting in these subdomains (Zhu and Keeney 2014) (also see the *Regulation in large subchrosomomal domains* section).

Coordination of DSBs with DNA replication. In yeast, DSBs usually form ~1–1.5 hour after premeiotic DNA replication (Borde *et al.* 2000; Cervantes *et al.* 2000; Murakami *et al.* 2003). In *S. cerevisiae*, deleting all active replication origins from the left arm of chromosome III causes a delay in local DSB formation in wild-type cells, indicating the mechanistic coupling of replication and DSB formation

(Borde *et al.* 2000). The coordination of timing between replication and DSB formation is at least partly carried out by recruitment of DDK (Cdc7-Dbf4 kinase, or Dbf4-dependent kinase) to the replication fork, thereby targeting Mer2 activity by phosphorylation in replicating regions (Murakami and Keeney 2008; Murakami and Keeney 2014). The origin-deleted left arm of chromosome III does not alter DSB positions and frequency in wild type, but shows a 4–5 and ~1.3 fold reduction of DSBs in *sae2* (a *rad50S*-like mutant) and *dmc1* background, respectively (Borde *et al.* 2000; Buhler *et al.* 2007). These findings suggest that delayed DSB formation causes a decrease in DSB formation at least in certain mutant backgrounds.

A possible related phenomenon was observed in *S. pombe* (Wu and Nurse 2014). More replication origins are utilized when cells are sporulated in nitrogen-rich media rather than in nitrogen-starving media. Correspondingly, regions with increased origins shift to earlier replication, and exhibit elevated DSBs. Thus, replication timing regulates DSB distribution presumably because of the coordination between replication and DSB formation.

Conclusions and aims of thesis

Recent work has clearly established that the meiotic DSB landscape is shaped by combinatorial action of many factors. Studies in budding yeast using high-resolution Spo11-oligo mapping technique have begun to illustrate the role of these factors that operate at different size scales. The goal of this thesis research is to advance our understanding of Spo11-induced DSB spatial distributions. In **Chapter 2**, I show some preliminary studies on validation of unusually broad hotspots, evaluation of DSB activity in tagged Spo11 strains, and raising anti-Spo11 polyclonal antibodies. In **Chapter 3**, I examine contributions of two TFs to genome-wide DSB distributions to shed light on the influence of TFs on DSB hotspots. In **Chapter 4**, I analyze

genome-wide, nucleotide-resolution DSB maps in the absence of H3K4me3 in *set1* mutants. In the **Appendix**, I focus on the subchromosomal domain-level DSB regulation revealed in *pch2* and *sir2* mutants. Detailed introductions about these mutants will be provided in following chapters.

Chapter 2: Initial studies

Summary

A genome-wide high-resolution approach to map meiotic DSBs was developed by purifying and sequencing Spo11 oligos, the byproduct of DSB formation. The first Spo11-oligo maps revealed that 73.4% hotspots are 50-300 bp wide, while 10.4% of hotspots were more than 500 bp wide. I verified anomalously wide hotspots at *YAT1*, *NAR1* as well as *WHI5*, and found that these hotspots are overlapped with ORFs. One caveat of previous Spo11-oligo mapping is using the *spo11-HA* strain, in which DSB level decreases to ~70% of that in wild-type strain. To overcome this limitation, I tested different tagged Spo11 strains and found that *Spo11-FLAG* and *Spo11-PrA* strains showed wild-type level of DSBs. Moreover, I raised anti-Spo11 polyclonal antibodies, which are validated tools to detect Spo11 in cell lysate and to immunoprecipitate Spo11-oligo complexes. These strains and reagents are now widely used in Spo11-oligo mapping.

Introduction

Jing Pan and Mariko Sasaki, former members of the Keeney lab, developed a method to purify and sequence Spo11 oligos from meiotic cultures of wild-type budding yeast cells (Pan *et al.* 2011). In these Spo11-oligo maps, 3,604 DSB hotspots were identified, with a median width of 189 bp (73.4% are 50-300 bp wide). 88.2% overlapped with promoters. These findings are consistent with stereotypical patterns inferred from direct detection of a small subset of hotspots by Southern blot. However, the genome-wide Spo11-oligo mapping revealed that 10.4% of hotspots were more than 500 bp wide. Particularly, nine of these "wide" hotspots were > 1.5 kb. Thus, it was important to verify these anomalous hotspots using independent assays.

The first Spo11-oligo maps were established using a *spo11-HA* strain, in which Spo11 is tagged at its C-terminus with three HA epitope tags and a hexahistidine sequence (Diaz *et al.* 2002). One caveat is that the DSB level in *spo11-HA* strain decreases to ~70% of that in wild-type strains (Martini *et al.* 2006). Moreover, *spo11-HA* can cause synthetic defects when combined with other mutants (such as *pch2Δ*) (Farmer *et al.* 2012). To overcome these limitations, I searched for other tagged Spo11 strains with normal levels of DSBs, and generated new anti-Spo11 polyclonal antibodies.

Results

Validation of unusually broad hotspots overlapping with open reading frames

To verify anomalously wide hotspots at *YAT1*, *NAR1* as well as *WHI5*, I performed Southern blot assays on these loci. Results from Southern blot agreed very well with Spo11-oligo maps. In contrast to typical hotspots within the NDR, these hotspots are more than 1.5 kb wide and overlapped with ORFs (**Figure 2.1**).

Spo11-FLAG strain shows wild-type level DSB activity

To overcome the limitations of *spo11-HA* strains, I tested differently tagged *SPO11* strains by Southern blot. High molecular weight chromosome DNA was purified 6 h after transfer to sporulation medium from meiotic *rad50S* cultures, and then separated by pulsed-field gel electrophoresis. Three chromosomes were probed and their DSB frequencies were calculated for comparison between different *SPO11* alleles. While *spo11-HA* has only 71% relative DSB activity of wild-type strains, both *SPO11-Flag* (97%) (Kugou *et al.* 2009) and *SPO11-PrA* (102%) (Thacker *et al.* 2014; Mohibullah, in preparation) alleles showed wild-type DSB levels on average (**Figure 2.2**). Therefore, DSB formation appears normal in *SPO11-Flag* and *SPO11-PrA*

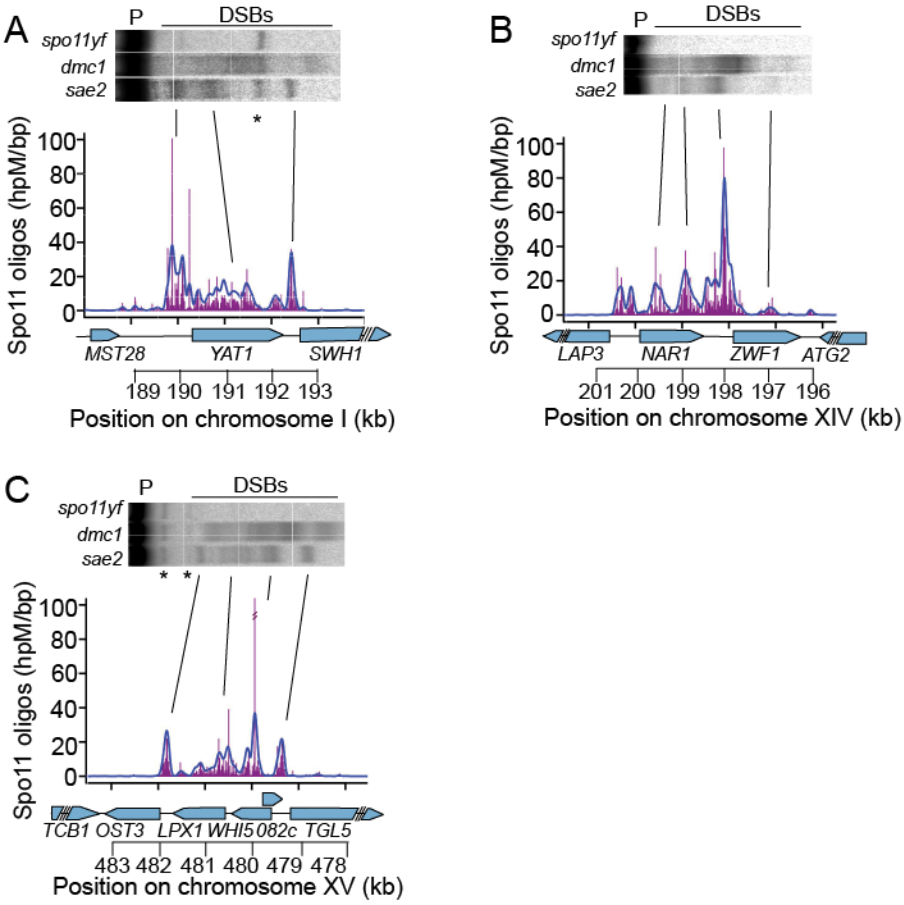

Figure 2.1 Verification of unusually broad hotspots within the gene open reading frames of *YAT1* (A), *NAR1* (B) and *WHI5* (C) by Southern blot of genomic DNA from *dmc1* and *sae2* mutants. DSB signals in *dmc1* spreads out due to hyperresection. *spo11yf* is the DSB-deficient mutant *spo11-Y135F*, which is used as control. P, parental band; asterisk, cross-hybridization. Spo11 oligos are shown in raw counts (magenta) or smoothed curve (with a 201 bp sliding Hann window, blue). Figure adapted from Pan *et al.* (2011).

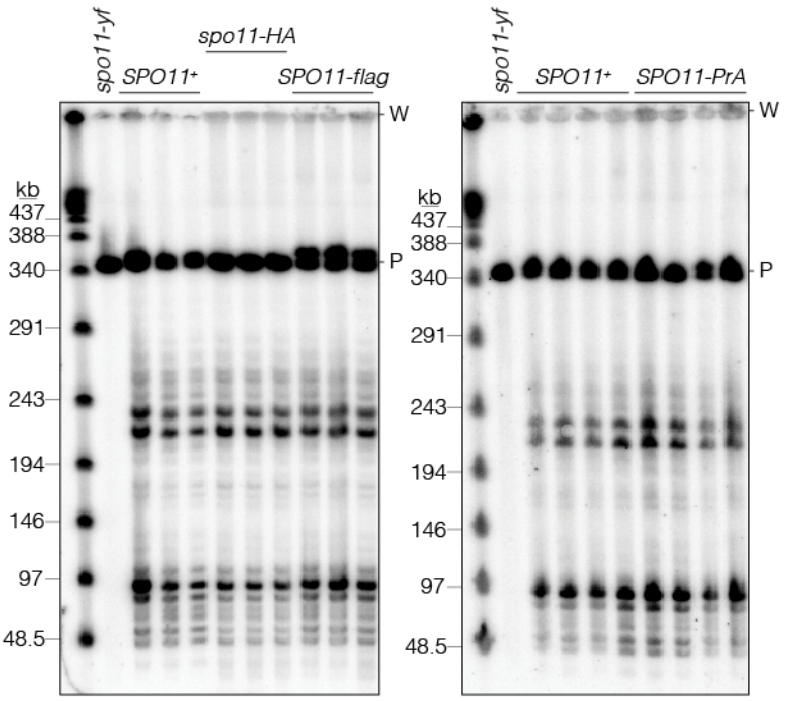

B

	DSB frequency, % of DNA in lane (% of *SPO11⁺*)				
	SPO11⁺	*spo11-HA*	*SPO11-flag*	*SPO11⁺*	*SPO11-PrA*
Chr III	56.3 ± 3.5 (100)	35.5 ± 1.7 (63)	52.3 ± 0.5 (93)	55.6 ± 4.0 (100)	56.5 ± 2.2 (102)
Chr VII	71.4 ± 2.9 (100)	55.1 ± 2.5 (77)	72.2 ± 1.9 (101)	72.2 ± 4.4 (100)	78.0 ± 1.7 (108)
Chr VIII	63.1 ± 1.9 (100)	45.5 ± 6.6 (72)	61.8 ± 1.8 (98)	59.6 ± 1.0 (100)	57.2 ± 5.4 (96)
Relative DSB frequency	100	71 ± 7	97 ± 4	100	102 ± 6

Figure 2.2 DSB formation appears normal in *SPO11-flag* and *SPO11-PrA* strains. (A) Southern blots probed for Chr III. High molecular weight chromosomal DNA was purified 6 hr after transfer to sporulation medium from meiotic *rad50S* cultures carrying the indicated *SPO11* alleles, then separated on pulsed-field electrophoresis gels. *spo11yf* is the DSB-deficient mutant *spo11-Y135F*, which is used as control. Samples from a *rad50S spo11-HA* strain are shown for comparison; HA-tagged Spo11 has reduced DSB frequency. Each lane represents an independent culture (*SPO11+* samples from the same cultures were run on both gels). P, parental-length DNA; W, wells. (B) Quantification of blots in panel a and separate blots (not shown) probed for Chr VII or VIII. Break frequencies are percent of DNA in lane (mean ± SD of 3–4 cultures). Numbers in parentheses indicate values from each tagged strain relative to *SPO11+* for the same chromosome. Relative DSB frequencies at the bottom are averages across the three chromosomes assayed. Figure adapted from Thacker *et al*. (2014).

strains. All the Spo11-oligo maps I generated in this thesis research were in *SPO11-Flag* background.

Generation and validation of anti-Spo11 polyclonal antibodies

Full-length Spo11 is insoluble, therefore I designed two peptides based on Spo11 protein sequence, and used the mixture of both peptides as antigens to inject into rabbits. One peptide was located on the N-terminus of Spo11, and the other was close to the C-terminus of Spo11 (**Figure 2.3A**). Both peptides overlapped with regions of high antigenic index and surface probability, indicating that they were good antigen candidates. Rabbit polyclonal antibodies were generated and purified (**Methods**).

To test these antibodies for western blot, cell lysates from wild-type (Spo11), *spo11Δ* and *Spo11-myc* (Prieler *et al.* 2005) strains were prepared, run on SDS-PAGE, and transferred onto the PVDF membrane. The blots were probed with different antibodies. Spo11-myc was recognized by anti-myc and anti-Spo11 antibodies (353 and 354) (**Figure 2.3B**, the band slightly lower than 100 kDa), while wild-type Spo11 was visualized near 50 kDa only by anti-Spo11 antibodies. Notably, several non-specific bands were observed with anti-Spo11 antibodies, and the patterns were not the same for anti-Spo11 antibodies 353 and 354. Therefore, anti-Spo11 antibodies can successfully detect wild-type or tagged Spo11 in cell lysates.

To test anti-Spo11 antibodies for purification of Spo11-oligo complexes, cell lysates were immunoprecipitated with anti-HA and anti-Spo11 antibodies. Purified Spo11-oligo complexes were detected by end-labeling of the oligos covalently bound to Spo11. Using anti-Spo11 antibodies, I was able to visualize Spo11-oligo complexes from wild-type (*SPO11*) and *spo11-HA* strains, but the yield was less than immunoprecipitates with anti-HA antibody from *spo11-HA* strains (**Figure 2.3C**).

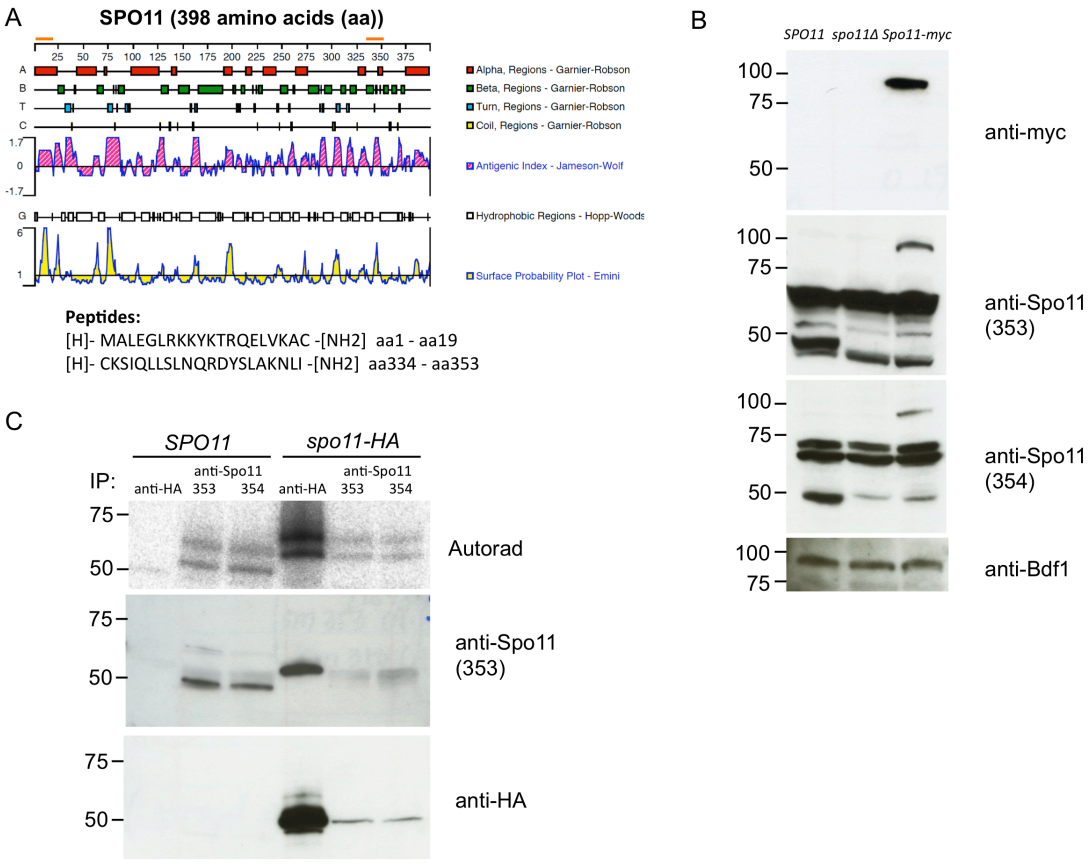

Figure 2.3 Generation and validation of anti-Spo11 polyclonal antibody. (A) Positions and sequences of peptides designed for raising anti-Spo11 polyclonal antibody. Orange bars indicate the positions on the full-length Spo11 protein. (B) Detection of Spo11 and Spo11-myc in cell lysates on Western blot using anti-Spo11 antibodies. Anti-Spo11 353 and 354 were purified from sera from two inoculated rabbits (Two rabbits were numbered as 353 and 354). Anti-myc and anti-Bdf1 antibodies are used as positive control and loading control, respectively. (C) Immunoprecipitation and detection of Spo11-oligo complexes from wild-type (*SPO11*) and *spo11-HA* strains. Radiolabelled Spo11-oligo complexes were detected by autoradiography (top) and total Spo11 was detected by anti-Spo11 (middle) or anti-HA (bottom) western blot. The main labelled species differ in oligo size. Nearly all of the western blot signal is Spo11 that has not made a DSB.

Thus, anti-Spo11 polyclonal antibodies are new alternative tools to detect Spo11 in cell lysate and to immunoprecipitate Spo11-oligo complexes. My application of these anti-Spo11 polyclonal antibodies to generate Spo11-oligo maps is beyond the scope of this thesis and was described elsewhere (Sam Globus, Ph.D. Dissertation, Weill Cornell Graduate School of Medical Sciences).

Discussion and conclusions

Chromatin structure is a primary determinant of hotspot width

Majority of hotspots are 50-300 bp wide and overlapped with gene promoters (Pan *et al.* 2011). However, some hotspots such as *YAT1*, *NAR1* and *WHI5* are unusually wide. The overall nucleosome occupancy was low, and nucleosomes appeared relatively disordered at these three loci, supporting that chromatin structure is a primary determinant of hotspot width (Pan *et al.* 2011).

Chapter 3: High-resolution analysis of context-specific direct and indirect influences of Bas1 and Ino4 transcription factors on meiotic DNA break distributions in *Saccharomyces cerevisiae*

Summary

In *Saccharomyces cerevisiae*, many DSBs occur in "hotspots" coinciding with nucleosome-depleted gene promoters. Transcription factors (TFs) stimulate DSB formation in some hotspots, but TF roles are complex and variable between locations. Until now, available data for TF effects on global DSB patterns were of low spatial resolution and confined to a single TF. Here, we examine at high resolution the contributions of two TFs to genome-wide DSB distributions: Bas1, which was known to regulate DSB activity at some loci, and Ino4, for which some binding sites were known to be within strong DSB hotspots. We examined fine-scale DSB distributions in TF mutant strains by deep sequencing oligonucleotides that remain covalently bound to Spo11 as a byproduct of DSB formation, mapped Bas1 and Ino4 binding sites in meiotic cells, and evaluated chromatin structure around DSB hotspots. Our findings definitively support the hypothesis that TF control of DSB numbers is context-dependent and frequently indirect. TFs often affected the fine-scale distributions of DSBs within hotspots, and when seen, these effects paralleled effects on local chromatin structure. In contrast, changes in DSB frequencies in hotspots showed no obvious correlation with quantitative measures of chromatin accessibility or of histone H3 lysine 4 trimethylation levels. We also ruled out hotspot competition as a major source of indirect TF effects on DSB distributions. Thus, counter to prevailing models, roles of these TFs on DSB hotspot strength cannot be simply explained via chromatin "openness", histone modification, or compensatory interactions between adjacent hotspots.

Introduction

The distribution of meiotic DSBs across the *S. cerevisiae* genome is highly non-random (Baudat and Nicolas 1997; Gerton *et al.* 2000; Borde *et al.* 2004; Blitzblau *et al.* 2007; Buhler *et al.* 2007; Pan *et al.* 2011). In some cases, DSB hotspot activity has been shown to depend on the binding of sequence-specific transcription factors (TFs), e.g., at the *HIS4* locus in *S. cerevisiae* and the *ade6-M26* allele in *Schizosaccharomyces pombe* (Schuchert *et al.* 1991; White *et al.* 1991; Kon *et al.* 1997; Steiner *et al.* 2002). However, the role of TFs in shaping genome-wide DSB patterns is complex and poorly defined. In certain *S. cerevisiae* strains, the *HIS4* promoter displays strong hotspot activity that requires the binding of TFs Bas1, Bas2 and Rap1 (White *et al.* 1991; Kon *et al.* 1997). A *bas1* null mutation reduces DSB activity at a number of other chromosomal sites, but it also causes increased DSB frequency at many other sites (Mieczkowski *et al.* 2006). Thus, the effect of Bas1 on DSB formation is context-dependent, and local DSB stimulation by this TF at *HIS4* cannot be simply extrapolated as a general feature to all genomic loci. Moreover, loci whose DSB activity changes in *bas1* mutants are poorly correlated with Bas1 binding sites defined by chromatin immunoprecipitation (ChIP), suggesting Bas1 has both direct and indirect roles in DSB regulation (Mieczkowski *et al.* 2006).

Even in those instances where DSB hotspot activity is clearly linked to TF binding, the nature of this link has remained elusive. Like most yeast promoters, the *HIS4* promoter exhibits hypersensitivity to DNase I digestion of chromatin, but it becomes nuclease resistant when it loses DSB hotspot activity in *bas1 bas2* double mutants (Fan and Petes 1996). Another example is the *PHO5* promoter, which is bound by the TF Pho4 (Wu and Lichten 1994). Deletion of Pho4 causes reduced NDR and thus more constrained DSB activity. Thus, TF binding can promote DSB formation nearby, possibly via establishing an open chromatin structure in the

surrounding area. However, *HIS4* and *PHO5* are the only TF-dependent hotspots for which the effect of TFs on meiotic DNA accessibility and DSBs has been examined in budding yeast. It is unknown whether TF binding can cause DNA accessibility change at DSB sites in all TF-affected hotspots.

Thus far, Bas1 is the only TF that has been studied genome-wide for its influence on meiotic DSB distribution. Bas1 is a Myb-related TF involved in the expression of genes acting in the adenine and histidine biosynthetic pathways (Arndt *et al.* 1987; Daignan-Fornier and Fink 1992; Denis *et al.* 1998). Bas1 binds to a site containing a GAGTCA motif found in the *ADE2* and *ADE5,7* promoters (Hovring *et al.* 1994). This motif is required for regulation of *ADE2* by Bas1 and another TF Bas2/Pho2 (Daignan-Fornier and Fink 1992). It has been proposed that formation of a complex between Bas1 and Bas2 unmasks an activator function of Bas1, but there may be other partners that can bind Bas1 as well (Denis and Daignan-Fornier 1998). Bas1 and Bas2 also regulate several genes involved in one-carbon metabolism, such as *GLN1*, *SHM2*, and *MTD1* (Denis and Daignan-Fornier 1998; Gelling *et al.* 2004).

Meiotic DSBs were previously mapped genome wide in a *bas1* mutant by microarray hybridization of Spo11-attached DNA from a *rad50S* mutant (Mieczkowski *et al.* 2006). One hundred fifty three open reading frames (ORFs) were identified as regions with different DSB frequency between wild type and *bas1*, but the spatial resolution (usually several kb) was not high enough to precisely locate DSB hotspots in these regions (Mieczkowski *et al.* 2006). Besides *bas1*, there are no genome-wide DSB maps of other TF mutants.

In this study, I wished to more precisely define the contributions of specific TFs to global DSB patterns. I examined a *bas1* mutant because, while it is known to affect DSBs, nucleotide-resolution information about changes in DSB patterns was lacking. To determine whether another TF affects break formation similarly to Bas1, I

also examined an *ino4* mutant. Ino4 motifs were previously found to be enriched in strong DSB hotspots (Pan *et al.* 2011), but it was unknown if Ino4 stimulates DSB activity in those hotspots. Ino4 controls genes involved in phospholipid synthesis and is required for derepression of inositol/choline-regulated genes such as *INO1*, *CHO1*, *CHO2* and *OPI3* (Santiago and Mamoun 2003). Ino4 forms a complex with Ino2 and binds the inositol-choline-responsive element through a basic helix-loop-helix domain (Schwank *et al.* 1995). Here, I compare DSB distributions in wild type, *bas1*, and *ino4* strains and explore how the binding of these TFs modulates local chromatin structure and DSB frequency.

Results

High-resolution maps of meiotic DSBs in *bas1* and *ino4* mutants

Each covalently bound Spo11 oligo is a unique tag from a DSB site, so sequencing Spo11 oligos generates quantitative, high-resolution DSB maps (**Figure 3.1A**) (Pan *et al.* 2011). Spo11-oligo maps from biological replicate cultures of wild type and *bas1* and *ino4* mutants agreed well with each other (Pearson's $r = 0.92–0.98$; **Figure 3.1B**) and thus were averaged (after normalization to millions of reads mapped, RPM) into consensus maps for further analysis.

The DSB landscape is shaped by a combination of many factors that operate at different scales. At large scales (tens of kb), *bas1* and *ino4* Spo11-oligo maps agreed with the wild-type map (**Figure 3.1C**, top). At small scales (< 1 kb), DSB hotspots are usually located in nucleosome-depleted promoters. This pattern was retained in *bas1* and *ino4* mutants, in that DSBs formed in the same hotspots (**Figure 3.1C**, bottom). The correlation of Spo11-oligo density in 5-kb bins was high across the genome

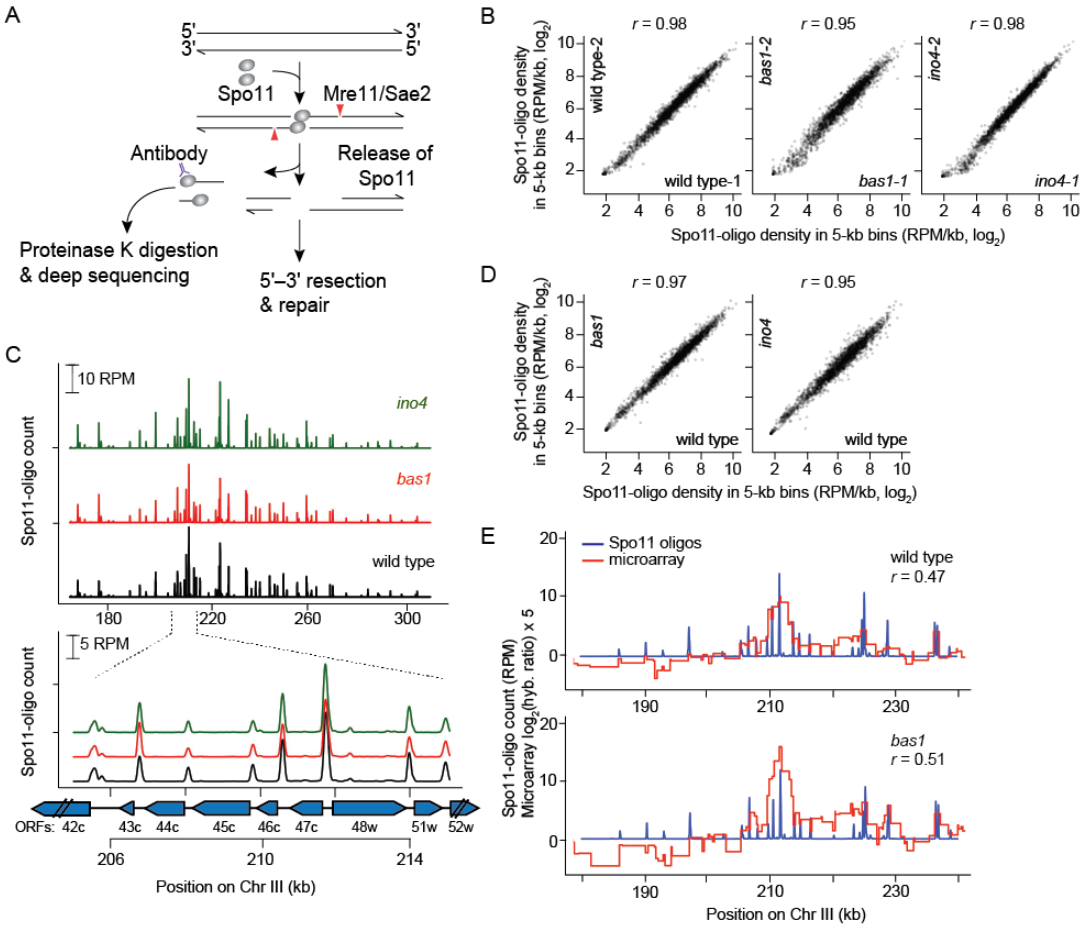

Figure 3.1 Spo11-oligo mapping in *bas1* and *ino4* mutants. (A) Formation and processing of meiotic DSBs (Spo11-oligo mapping method on left). (B) Quantitative reproducibility of Spo11-oligo maps. Comparisons are shown for individual wild type, *bas1* or *ino4* data sets. Spo11 oligos were summed in non-overlaping 5-kb bins and expressed as RPM per kb (plotted on a log scale). Correlation coefficients (Pearson's *r*) are shown on the top. (C) Top, *bas1* and *ino4* mutations do not cause widespread change in the large-scale patterns of the DSB landscape. Bottom, DSBs form at the same hotspots in *bas1* and *ino4* as in wild type. Positions of open reading frames are indicated by blue arrows. (D) Comparison between wild type and TF mutant data sets. For each genotype, Spo11-oligo maps were averaged from biological replicates. (E) The Spo11-oligo map agrees with previous *rad50S* Spo11 ChIP microarray analysis (32) but provides higher resolution. The correlation coefficient was calculated between the normalized microarray signal and the sum of Spo11-oligo counts within 2 kb on either side of each microarray probe.

(Pearson's r = 0.95-0.97) (**Figure 3.1D**). Thus, these TF mutants do not grossly alter the global DSB landscape.

To compile an unbiased list of hotspots to facilitate direct comparison of each mutant to wild type, I added the averaged wild-type map to the two averaged mutant maps, then called hotspots (clusters of Spo11 oligos) on this combined map using a previously described algorithm (Pan *et al.* 2011). I identified 3994 hotspots. Of these, 3524 (88.2%) overlapped the 3600 hotspots previously identified in wild type (Pan *et al.* 2011) (i.e., 97.9% of the previous hotspots were accounted for). The extra hotspots in the current study were generally weak hotspots, probably emerging from the greatly increased sequencing depth in the current study.

The wild-type and *bas1* Spo11-oligo maps agreed moderately well with the published microarray maps (Mieczkowski *et al.* 2006) (Pearson's r = 0.47–0.51) but had much higher spatial and quantitative resolution (**Figure 3.1E**). The high-resolution maps allowed us to analyze DSB activity at the individual hotspot level, which was not possible with the earlier data sets. First, I examined Spo11-oligo counts in mutants compared with wild type. Most hotspots were affected little if at all in the mutants (**Figure 3.2A and B**), but a small number was increased or decreased so I sought to identify all changed hotspots. To minimize impact of experimental variation on calculated fold change of weak hotspots, only hotspots with more than 100 RPM in at least one map were analyzed (100 RPM is equivalent to a DSB frequency of ~0.1% of total DNA, as estimated by comparing Southern blot data to Spo11-oligo counts (Pan *et al.* 2011)). After this filtering of weak hotspots, 2485 hotspots remained. I defined altered hotspots as having more than 20% change in Spo11-oligo counts with a p-value <0.1 (Student's t-test on biological replicates, without adjustment for multiple correction).

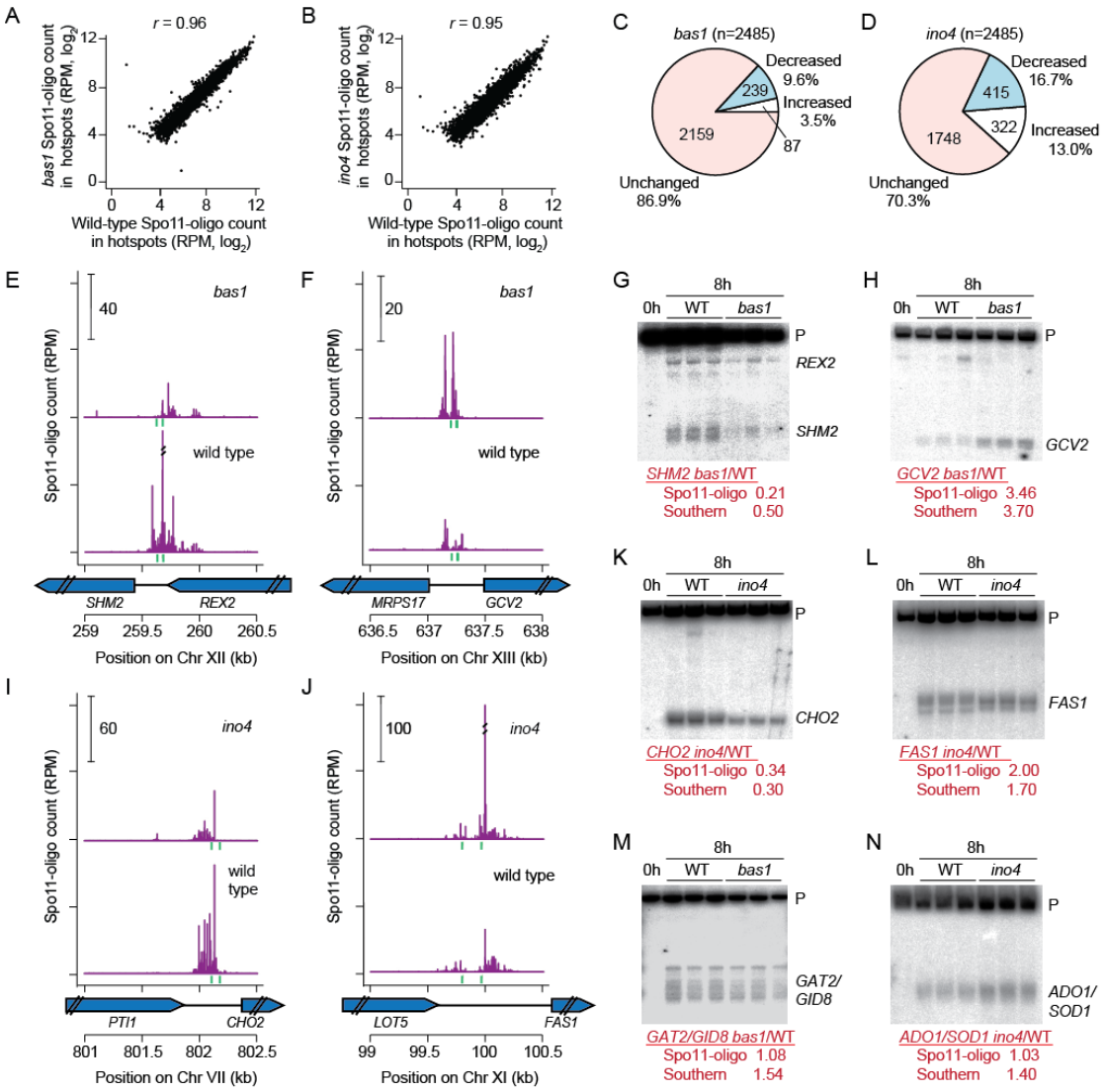

Figure 3.2 Effects of *bas1* and *ino4* mutations on DSB activity at individual hotspots. (A and B) Comparisons between wild type and TF mutants for all hotspots. (C and D) Proportion of hotspots that displayed at least a 20% change in Spo11-oligo counts relative to wild type. (E, F, I, J) Spo11 oligos in hotspots at the promoters of *SHM2* (E), *GCV2* (F), *CHO2* (I), and *FAS1* (J). Green vertical ticks indicate sequence matches to Bas1 (E, F) or Ino4 (I, J) binding motifs. (G, H, K, L, M, N) Physical analysis confirming the Spo11-oligo data for hotspots at the promoters of *SHM2* (G), *GCV2* (H), *CHO2* (K), *FAS1* (L), *GAT2/GID8* (M), and *ADO1/SOD1* (N). Genomic DNA was purified from three independent 8 hour *sae2Δ* cultures for each genotype and analyzed by Southern blotting and indirect end labeling. Fold change (mutant/wild type) for each hotspot is shown below the blots. P, parental.

Even with these very non-stringent criteria, only a small fraction of hotspots were detectably altered by the *bas1* mutation: 239 (9.6%) hotspots were decreased, and 87 (3.5%) were increased (**Figure 3.2C**). Of these, only 18 hotspots had changed by more than two fold (10 down and 8 up). The most decreased hotspot was in the *ADE17* promoter (17% of wild type) and the most increased was a relatively weak hotspot inside the *ADE4* open reading frame (6.1-fold higher than wild type; a stronger hotspot in the *ADE4* promoter was decreased 3.0-fold). Many of the altered hotspots are in regions where the prior microarray study by Mieczkowski et al. also detected changes in *bas1* (e.g., at *HIS4*, *SHM2* and *GCV2*; see below). Regions that did not show agreement between the studies are likely attributable to the differences in methodology and/or strains.

The *ino4* mutation affected more hotspots: 415 (16.7%) were decreased by >20% and 322 (13.0%) were increased (**Figure 3.2D**). Of these, 79 had changed by more than two fold (47 down and 32 up). The range of hotspot activity changes in *ino4* relative to wild type was 0.23 (*OPI3/MOG1* hotspot) to 4.4 (*INO1* hotspot). Thus, deletion of these TFs is capable of changing hotspot activity, but affects only a small portion of total hotspots.

To validate results from Spo11-oligo mapping, I analyzed meiotic DNA formation directly by standard Southern blot analysis for hotspots at the promoters of *SHM2*, *GAT2/GID8*, *GCV2*, *CHO2*, *ADO1/SOD1* and *FAS1* in the *rad50S*-like (DSB repair-deficient) mutant *sae2*. Consistent with Spo11-oligo maps, DSB activity was significantly reduced for *SHM2* and elevated for *GCV2* in the *bas1* mutant (**Figure 3.2E–H**), in agreement with previous results in a different strain background (Mieczkowski *et al.* 2006). In *ino4*, *CHO2* showed decreased DSB formation and *FAS1* showed increased DSB levels as well as altered spatial pattern (**Figure 3.2I–L**). *GAT2/GID8* and *ADO1/SOD1* were unchanged in TF-mutant Spo11-oligo maps, but

both hotspots were slightly increased by Southern blot analysis (**Figure 3.2M and N**). It is important to note that *sae2* mutants suppress late-forming DSBs (Borde *et al.* 2000). I cannot distinguish whether the discrepancies are from this *rad50S*-like mutant background or from measurement errors in either Spo11-oligo maps or physical assays. Comparable differences between these methods have been noted in the past for estimates of total DSB frequencies for some hotspots in *S. cerevisiae* and *S. pombe* (Pan *et al.* 2011; Fowler *et al.* 2014). Nevertheless, the Spo11-oligo maps in general showed excellent spatial and quantitative agreement with direct assays of DSBs.

Identification of Bas1 and Ino4 binding sites in meiotic cells

To evaluate whether hotspots altered in *bas1* or *ino4* mutants might be directly influenced by the TFs, I mapped Bas1 and Ino4 binding sites during meiosis by ChIP of Myc-tagged Bas1 and Ino4 followed by high-throughput sequencing. ChIP peaks were called as described (Murakami and Keeney 2014) (Methods), identifying 36 Bas1 binding peaks and 197 Ino4 binding peaks (**Figure 3.3A and B**). Most of these peaks (30 of the 36 Bas1 binding peaks and 176 of the 197 Ino4 binding peaks) were located in or near the promoter regions of genes. Specific enrichment of Bas1 at the promoters of *GCV2* and *GCV3* and of Ino4 at the *FAS2* promoter was also observed by ChIP followed by qPCR, validating results from ChIP-seq (**Figure 3.3C**).

I searched for likely TF recognition motifs in the 500 bp encompassing each ChIP-seq peak (Bailey *et al.* 2009). This analysis identified a motif containing the core sequence 5′-GAGTCA for Bas1 binding peaks (**Figure 3.3D**), in agreement with previous studies (Daignan-Fornier and Fink 1992; Mieczkowski *et al.* 2006; Zhu *et al.* 2009). More than half of the Bas1 ChIP-seq peak regions (21 of 36) contained one or more match to this motif. Peaks without a match to the motif may contain degenerate Bas1 binding sequences, may be targeted by Bas1 via interactions with other proteins,

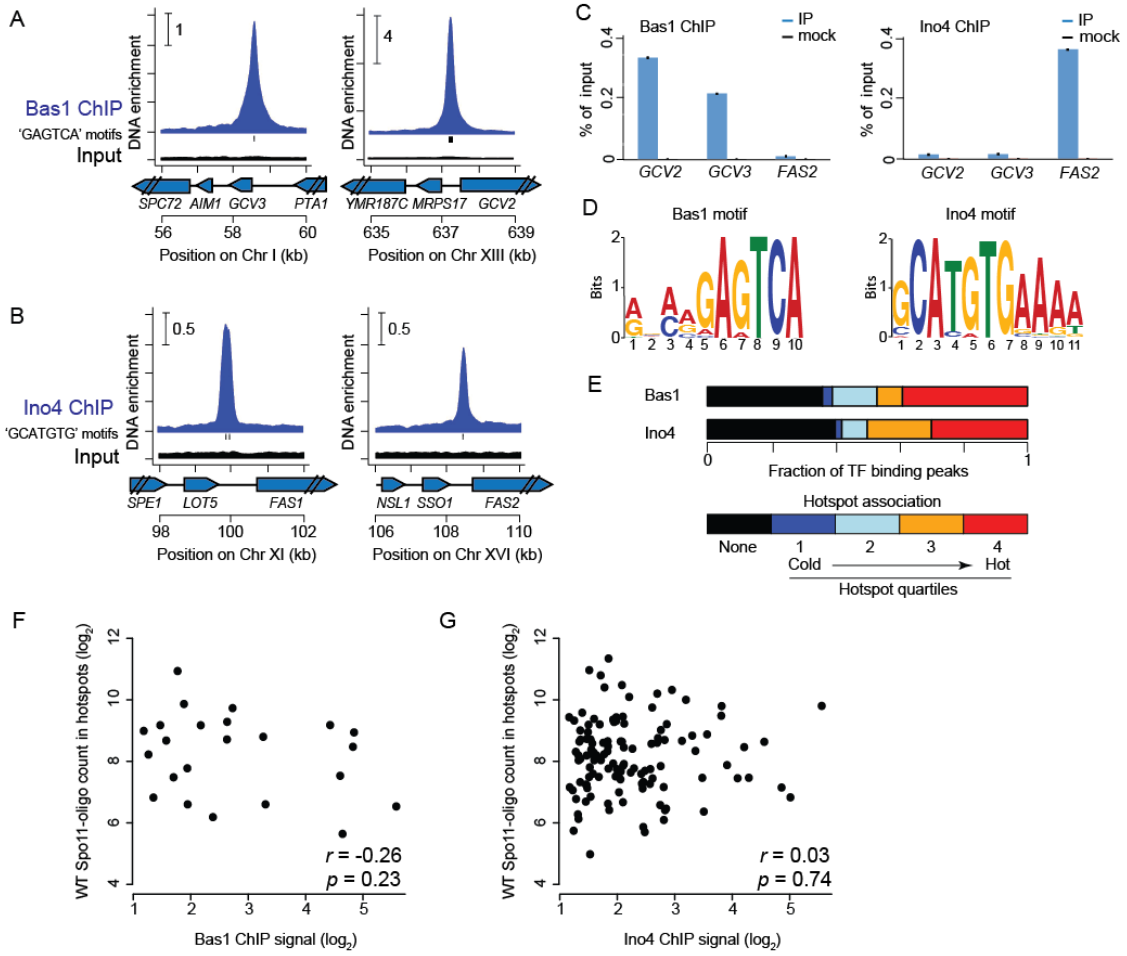

Figure 3.3 TF binding sites and their association with DSB hotspots in meiosis. (A and B) Examples of Bas1 (A) or Ino4 (B) ChIP-seq data. (C) ChIP-qPCR at *GCV2*, *GCV3* and *FAS2* promoters. (D) Consensus Bas1 and Ino4 motifs identified in meiotic ChIP-seq data sets. (E) Association of TF binding peaks with hotspots. Bars depict the fraction of ChIP-seq peaks not in DSB hotspots (black) and divide the remainder according to hotspot quartile. (F and G) For hotspots overlapping TF binding sites, no correlation between DSB hotspot activity in wild type (WT) and TF ChIP-seq signal (summed in a 401 bp window around the ChIP-seq midpoint).

or may be false positives from the ChIP-seq. The Bas1 ChIP-seq peaks accounted for most (27 of 37; 70% within 500 bp) of a previously annotated set of Bas1 binding sites (Macisaac *et al.* 2006).

Mieczkowski and colleagues identified 56 intergenic regions that were bound by Bas1 in meiotic cells (Mieczkowski *et al.* 2006). Twenty-one of these regions overlapped with our Bas1 ChIP-seq peaks. These overlapping Bas1 binding sites are in the promoters of many known Bas1-regulated genes involved in the adenine and histidine biosynthetic pathways (*ADE1*, *ADE2*, *ADE4*, *ADE6*, *ADE8*, *ADE17* and *HIS1*) and in one-carbon metabolism (*GCV1, GCV2, GCV3, MDT1* and *SHM2*) (Denis *et al.* 1998; Denis and Daignan-Fornier 1998; Gelling *et al.* 2004). However, *HIS4* and a few other known Bas1 targets were not identified in our data set. For *HIS4*, a very weak ChIP-seq signal was present below the peak-calling threshold (**Figure 3.4**), presumably reflecting a quantitative difference in Bas1 occupancy of the *HIS4* promoter between SK1 and the strain background used by Petes and colleagues (Stapleton and Petes 1991; Mieczkowski *et al.* 2006).

For Ino4, MEME identified the motif 5′-GCATGTGAAAA (**Figure 3.3D**), which matches well the upstream activation sequence recognized by Ino2/4 (UAS_{ino}, C/AATGTGAAAT) (Bachhawat *et al.* 1995). Most (162 of 197) Ino4 ChIP-seq peaks contained at least one match to the identified motif. Furthermore, Ino4 ChIP-seq peaks accounted for all but one of the small number of previously annotated Ino4 motifs (21 of 22; 95.5%) (Macisaac *et al.* 2006).

Hotspots containing Bas1 and Ino4 binding sites

In a prior study using a compilation of TF binding sites by MacIsaac et al. (Macisaac *et al.* 2006), I observed that 32 of 37 annotated Bas1 sites were contained within 18 hotspots, three-fourths of which were among the hottest 50% of all hotspots

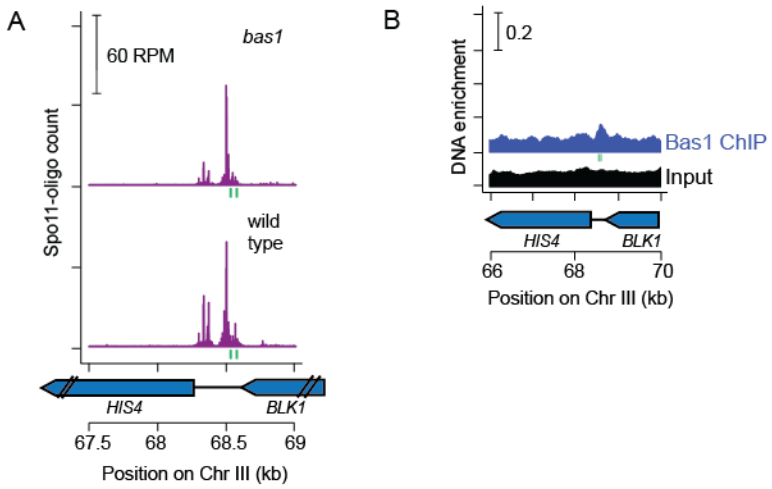

Figure 3.4 (A,B) Spo11 oligos (A) and Bas1 ChIP-seq signals (B) at the hotspot in the *HIS4* promoter. Green vertical ticks indicate matches to the Bas1 motif. *HIS4* is a modest hotspot in wild-type SK1 (870 RPM on average, equivalent to <2% of DNA broken) and Spo11-oligo counts decrease to 64% of wild type in the *bas1* mutant. A weak Bas1 ChIP-seq signal was discernible in the *HIS4* promoter, but was not sufficiently strong to pass our threshold for calling a Bas1 binding peak.

(Pan *et al.* 2011). For Ino4, all but 1 of the 22 annotated binding sites were inside 17 hotspots, nearly all of which were among the hottest 50% of all hotspots (Pan *et al.* 2011). These findings suggested that presence of a potential binding site(s) for Bas1 or especially Ino4 was a good predictor of strong local DSB activity. However, the available TF binding site data were incomplete and did not represent DNA binding in meiotic cells. Specifically, the sites compiled by MacIsaac et al. (2006) marked only a minority of the ChIP-seq peaks (38.9% of Bas1 peaks; 8.5% for Ino4). I therefore revisited comparisons between TF binding and DSBs with the new TF binding site data in hand.

I divided hotspots into quartiles according to Spo11-oligo counts and calculated the percentage of TF ChIP-seq peaks that overlapped hotspots in each quartile. Unexpectedly, approximately 40% of Bas1 ChIP-seq peaks and of Ino4 peaks were in loci that did not score as hotspots, even with our relatively non-stringent hotspot definition (**Figure 3.3E**). Thus, binding of neither Bas1 nor Ino4 is sufficient for high local DSB activity. Interestingly, however, those Ino4 sites that were in hotspots tended to be in relatively hot ones, similar to our prior findings (**Figure 3.3E**). TFs bind to their target sites with different fractional occupancies in vivo, and the range of ChIP-seq peak intensities was large, so I tested whether DSB hotspot activity correlates with TF binding strength (ChIP signal). No significant correlation was observed (**Figure 3.3F, G**). Therefore, counter to expectation from our prior study, the binding of these TFs has little or no predictive power for DSB activity.

Despite this lack of predictive power overall, I asked whether Bas1 or Ino4 influences the activity of the subset of hotspots that is directly bound by these TFs during meiosis. I used the same non-stringent criteria for defining hotspot changes as above ($p < 0.1$; >20% change from wild type; only hotspots with >100 RPM in at least one dataset). In *bas1* mutants, about half of the 23 hotspots overlapping Bas1 ChIP-

seq peaks had altered Spo11-oligo counts: 9 were decreased, 3 were increased (**Figure 3.5A**). This fraction is significantly higher than expected by chance (Fisher's exact test, $p < 9.9\times10^{-6}$; note that only ~13% of total hotspots were changed in the *bas1* mutant (**Figure 3.2C**)). In *ino4* mutants, only one third of the 119 hotspots overlapping Ino4 peaks were changed, similar to expectation from random ($p = 0.61$): 23 had decreased Spo11-oligo counts and 15 were increased (**Figure 3.5B**; compare to **Figure 3.2D**).

I further evaluated the effects of the TF mutations on local DSB activity by examining DSB changes in the TF mutants around all Ino4 and Bas1 binding peaks, regardless of whether these loci scored as DSB hotspots. I divided TF binding peaks into three groups according to their ChIP-seq signals, then measured the absolute fold change in local Spo11-oligo counts in the TF mutants (i.e., considering all changes equivalently, whether increasing or decreasing). Relative to control loci, Bas1 binding peaks tended to show greater change in local Spo11-oligo density in the *bas1* mutant, and this trend was statistically significant for the two-thirds of binding peaks with the highest ChIP-seq signal (**Figure 3.5C**). No such trend was observed for Ino4 (**Figure 3.5D**).

Taken together, these findings confirm and extend prior results implying that Bas1 often influences DSB formation nearby, but that the magnitude and direction (increasing or decreasing) of influence is context dependent (Mieczkowski *et al.* 2006). In contrast, even though *ino4* mutation has a larger net effect on DSB distribution genome wide, Ino4 modulates DSB formation near its binding sites only rarely and thus appears to exert more of its influence indirectly.

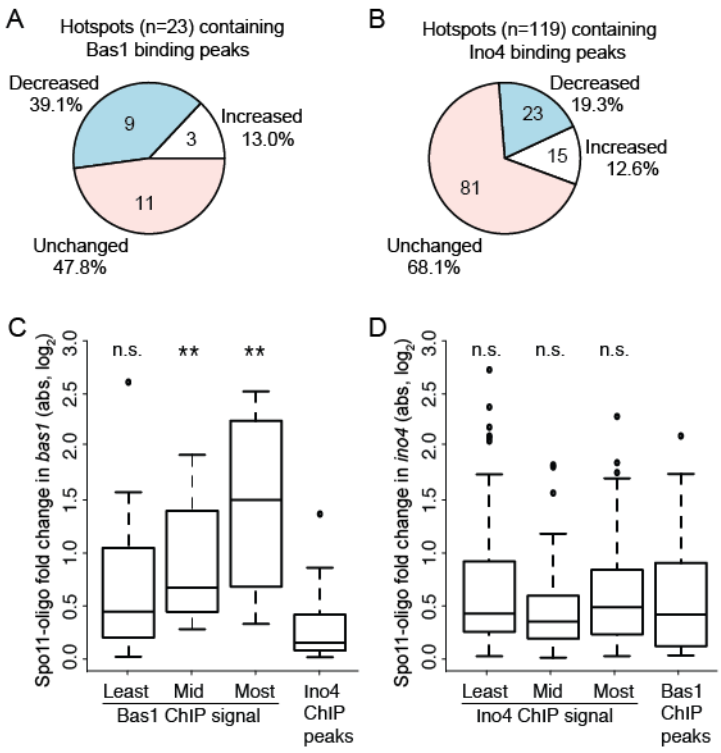

Figure 3.5 Context-dependent effects of *bas1* and *ino4* mutations around TF binding sites. (A,B) Proportion of hotspots overlapping TF ChIP-seq peaks that displayed at least 20% change in Spo11-oligo counts relative to wild type. (C,D) Changes in Spo11-oligo counts around all TF binding sites in the TF mutants. For each TF, all detected binding sites (regardless of whether the site was scored as a hotspot) were divided into three groups according to ChIP-seq signal, and Spo11-oligo counts were summed in 401-bp windows surrounding the peaks. Absolute log fold changes relative to wild type are plotted. Boxes indicate median and interquartile range; whiskers indicate the most extreme data points which are ≤1.5 times the interquartile range from the box; individual points are outliers. For the *bas1* mutant (C), 12 Ino4 ChIP-seq peaks were randomly chosen to serve as a negative control set. For the *ino4* mutant (D), all Bas1 ChIP-seq peaks were used as the negative control. Results are shown for Wilcoxon rank-sum tests comparing each TF binding site group to the respective negative control group (n.s., not significant; **, $p < 0.01$).

Chromatin structure in and near hotspots in *bas1* and *ino4* mutants

Open chromatin structure provides a window of opportunity for Spo11 (Ohta *et al.* 1994; Wu and Lichten 1994; Fan and Petes 1996; Keeney and Kleckner 1996; Berchowitz *et al.* 2009; Pan *et al.* 2011). Given the precedents of the *HIS4* and *PHO5* promoters (Introduction), a simple prediction might be that those hotspots whose DSB activity is affected in TF mutants would display correlated changes in chromatin structure at the DSB site: increased accessibility if TF removal increases DSBs, and decreased accessibility in hotspots with decreased DSBs. I tested this prediction by examining chromatin structure in the set of hotspots (both changed and unaffected) that were validated by Southern blotting (**Figure 3.2**). As described below, the relationship between chromatin and DSB changes is context-specific and more complex than the simplest model would predict.

Intact nuclei were prepared from meiotic cultures of wild-type and mutant cells and partially digested with MNase. DNA was then purified, digested with appropriate restriction enzymes, and analyzed by Southern blotting and indirect end labeling (**Figure 3.6**). Nucleosomal DNA is relatively resistant to MNase cleavage, while NDRs and linkers between nucleosomes appear as sites of preferred cleavage. MNase-digested naked DNA verified that banding patterns were chromatin-dependent. The positions of meiotic DSBs were shown by running MNase digests side by side with genomic DNA purified from meiotic cultures of *sae2* mutants.

In wild-type cells, the *SHM2* promoter (where *bas1* mutation reduces DSB formation (**Figure 3.2E, G**)) displayed a broad zone of MNase hypersensitivity (i.e., an NDR) encompassing the Bas1 binding motifs, and DSBs formed across a portion of this zone (**Figure 3.6A**). The distribution of DSBs did not match the fine-scale pattern of MNase cleavage, analogous to observations at *HIS4* (Fan *et al.* 1995). In the *bas1* mutant, the area containing the Bas1 motifs became strongly protected from MNase,

Figure 3.6 Chromatin structure in and around hotspots in wild type and TF mutants. MNase digestion patterns are shown for *SHM2* (A), *GCV2* (B), *CHO2* (C), *FAS1* (D), *GAT2/GID8* (E), and *ADO1/SOD1* (F). Intact meiotic nuclei were treated with zero or increasing amounts of MNase, then DNA was purified, digested with restriction enzymes, and analyzed by Southern blotting and indirect end-labeling. DSB positions are shown using DNA purified from *sae2* meiotic cultures. N, naked DNA (purified genomic DNA from vegetative cells, treated with MNase). Approximate positions of Bas1 or Ino4 motifs are indicated with green dots. The hybridization signals from the lanes with highest MNase concentration are plotted on the right of each panel, with interpretive cartoons illustrating regions of MNase resistance: darker brown ovals for regions that are relatively more MNase-resistant, lighter tan ovals for relatively less resistant, black lines for MNase-hypersensitive, and pink highlighting for regions with changed MNase digestion patterns. Note that the ovals do not necessarily correspond to positioned nucleosomes; some are smaller than nucleosome and may reflect footprints of transcription factors and/or sub-nucleosomal histone particles. + indicates enhanced contrast in the particular lanes in order to show the DSB postion better.

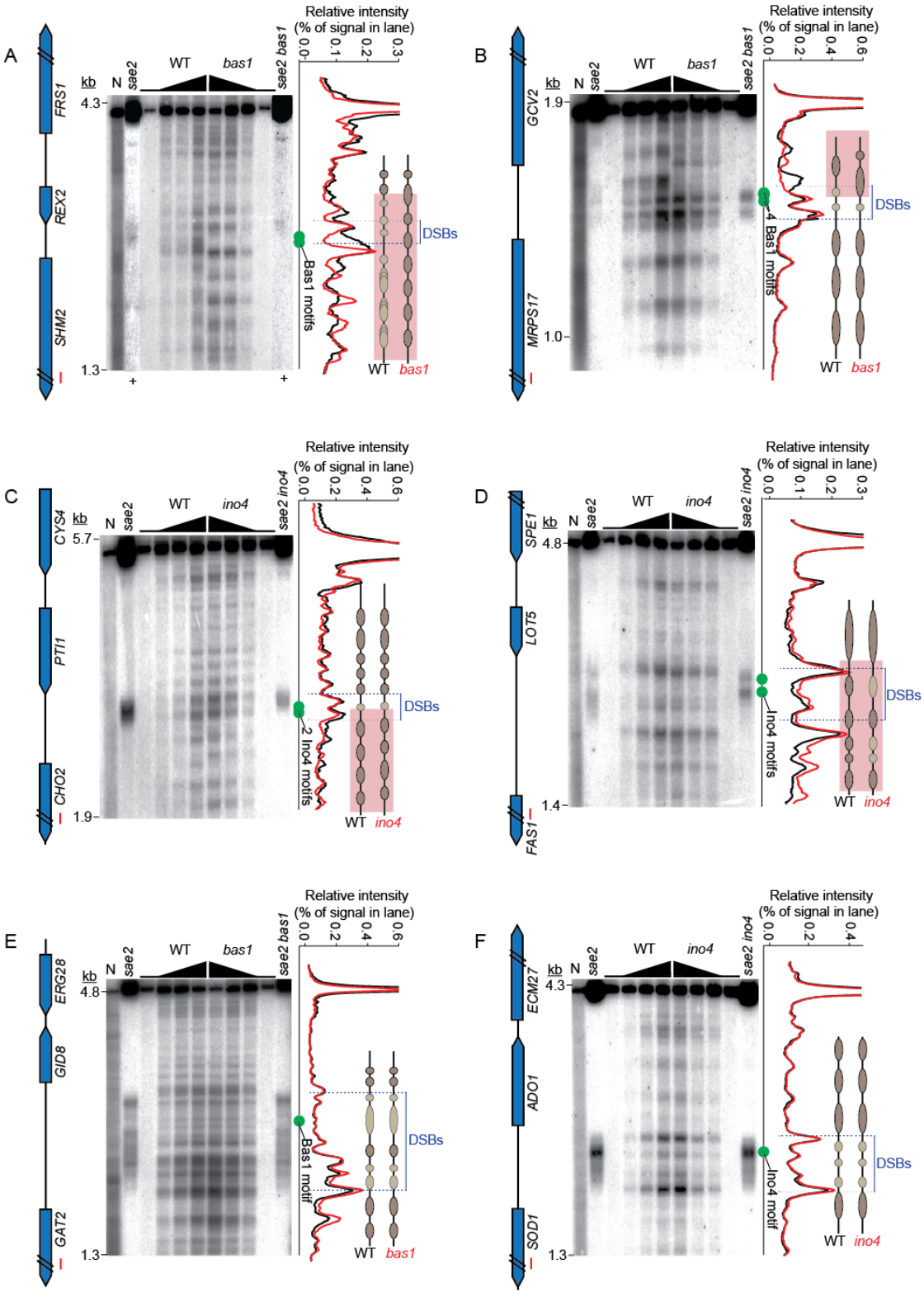
A
FRS1
REX2
SHM2
kb
4.3
1.3
N
sae2
WT
bas1
sae2 bas1
Relative intensity
(% of signal in lane)
0.0
0.1
0.2
0.3
DSBs
Bas1 motifs
WT
bas1
B
GCV2
MRPS17
1.9
1.0
0.0
0.2
0.4
0.6
4 Bas1 motifs
C
CYS4
PTI1
CHO2
5.7
1.9
ino4
sae2 ino4
2 Ino4 motifs
D
SPE1
LOT5
FAS1
4.8
1.4
Ino4 motifs
E
ERG28
GID8
GAT2
4.8
1.3
F
ECM27
ADO1
SOD1
4.3
1.3
Ino4 motif

indicating presence of a nucleosome. The remaining DSBs were now restricted to a smaller region corresponding to an MNase-hypersensitive site flanking the new positioned nucleosome (**Figure 3.6A**). Narrowing of the DSB zone was also seen in the Spo11-oligo map (**Figure 3.2E**). Previous studies showed that mutating the Bas1 motifs in the SHM2 promoter also diminishes DSB formation, even in strains expressing Bas1 (Mieczkowski *et al.* 2006), so the changes I observed in this analysis are likely to reflect direct effects of Bas1 on local chromatin structure.

In broad strokes, the parallel changes in chromatin structure and DSB formation near the Bas1 binding sites appeared similar to those reported for TF binding changes at *HIS4* and *PHO5*, and seemed consistent with the interpretation that reducing DNA accessibility via placement of a nucleosome may be sufficient by itself to reduce and spatially constrain DSB formation accordingly. However, the *bas1* mutant displayed substantial alteration in chromatin structure beyond just the immediate vicinity of the Bas1 motifs, corresponding to significantly reduced transcription of *SHM2* (based on RNA-seq results, which will be discussed in more detail in later sections). The *SHM2* transcription unit showed a nucleosomal ladder that was broad and shallow in wild type, indicating variable nucleosome positioning in the population. This ladder was more pronounced in *bas1*, indicating a more regularly positioned nucleosome array (**Figure 3.6A**). The neighboring gene (*REX2*) also displayed a more regular nucleosome array at its 3′ end when Bas1 was absent. (Little or no change occurred at the 5′ end of *REX2* and further upstream.) Furthermore, the *bas1* mutant retained just as much MNase hypersensitivity as wild type right where the DSBs occurred (**Figure 3.6A**), indicating that most cells still present a potential window of opportunity for Spo11 in the *SHM2* promoter. Because the *bas1* mutant still has accessible DNA that can be targeted for DSB formation, and because absence of Bas1 triggers a fairly wide-spread restructuring of chromatin for several kb around

this locus, our findings raise the possibility that the change in absolute DSB frequency is caused (at least in part) by other factors besides a quantitative change in nucleosome occupancy immediately at the positions where Spo11 cleaves (addressed further in Discussion).

Substantial chromatin changes were also observed in the *GCV2-MRPS17* intergenic region, which experiences more DSBs in *bas1*. Wild-type cells displayed a broad, strong MNase-hypersensitive site near the 5′ end of *GCV2* (**Figure 3.6B**). This site was flanked on the *GCV2*-proximal side by a zone of protection against MNase, presumably from a well-positioned, high-occupancy nucleosome overlapping the 5′ end of *GCV2*. On the *GCV2*-distal side, two more strong MNase-hypersensitive sites were seen, interdigitated with two areas of modest protection that were smaller than nucleosomes, presumably reflecting presence of other sequence-specific DNA binding proteins and/or subnucleosomal histone particles. One of the strong MNase sites overlapped the positions of four closely spaced Bas1 motifs. A nucleosomal ladder extended into the adjacent *MRPS17* gene, which encodes a protein of the small subunit of the mitochondrial ribosome; *MRPS17* is expressed during sporulation, and is not regulated by Bas1 (see later sections). DSBs occurred diffusely throughout a region encompassing the *MRPS17*-proximal MNase-hypersensitive sites and trailing weakly into the hypersensitive site that overlapped most of the Bas1 motifs. As at *SHM2*, DSBs showed little correlation with the fine-scale pattern of MNase cleavage (**Figure 3.6B**).

In *bas1*, the broad MNase-hypersensitive site nearest to *GCV2* disappeared, apparently because the nucleosome that should have overlapped the 5′ end of *GCV2* was now positioned over this region (**Figure 3.6B**). The nucleosome array over the *GCV2* transcription unit was also repositioned and became less distinct. In contrast, the nucleosome ladder within *MRPS17* and the MNase-hypersensitive sites closer to

MRPS17 — including the one overlapping the Bas1 motifs — were unaffected by absence of Bas1. Meiotic DSBs not only became more frequent, they were now more spatially restricted and more closely followed the pattern of MNase cleavage, including a more prominent peak of cleavage overlapping the Bas1 motifs (**Figure 3.2F, Figure 3.6B**).

A straightforward interpretation is that DSBs in wild type occur across a region encompassing portions of the adjacent promoters of *MRPS17* and *GCV2.* In the absence of Bas1, part of the *GCV2* promoter becomes occluded by a nucleosome that partially blocks Spo11 access. Nonetheless, the hotspot activity increases overall, with Spo11 now more constrained to cleave within a pair of MNase-hypersensitive sites closer to the *MRPS17* promoter. I note that, while this intergenic region became more MNase-resistant overall in the *bas1* mutant, the accessibility of the *MRPS17*-proximal MNase-hypersensitive sites themselves did not detectably change. Thus, the fine-scale distribution of DSBs within the hotspot appears to reflect DNA accessibility changes, but quantitative measures of accessibility to MNase are a poor predictor of total DSB levels at the hotspot (Pan *et al.* 2011).

The *CHO2* promoter contains two Ino4 motifs and experiences a decrease in DSB activity in the *ino4* mutant (**Figure 3.2I and K**). In wild type, a pair of strong MNase-hypersensitive sites bracketed a subnucleosomal-sized zone of modest protection that overlapped two Ino4 motifs (**Figure 3.6C**). Arrays of positioned nucleosomes were present across the *CHO2* transcription unit and the 3′ end of the adjacent gene (*PTI1*). DSBs were concentrated across the MNase-hypersensitive sites around the Ino4 motifs, including within the small zone that was protected from MNase and including the motifs themselves (**Figure 3.2I, Figure 3.6C**). In the *ino4* mutant, there was a very small decrease in MNase cleavage in the more *CHO2*-proximal of the pair of MNase-hypersensitive sites near the Ino4 motifs, but this

segment overall remained strongly MNase hypersensitive (**Figure 3.6C**). There was a pronounced change in the spacing of nucleosomes across the *CHO2* transcription unit, but no changes were seen upstream of the Ino4 motifs across *PTI1*. DSBs were distributed with similar spatial patterning as in wild type, consistent with the Spo11-oligo map (**Figure 3.2I, Figure 3.6C**). Thus, the essentially unchanged chromatin accessibility right at the DSB hotspot paralleled the relatively unchanged DSB distribution, whereas the chromatin structure in the adjacent transcription unit as well as the number of DSBs had changed substantially.

The *FAS1* promoter also contains two Ino4 motifs, but this region experiences an increase in DSB formation in *ino4* (**Figure 3.2J and L**). In wild type, two strong MNase-hypersensitive sites were located on either side of a more modest doublet of MNase sensitivity, with the Ino4 motifs positioned in one of the more MNase-resistant portions of this segment (**Figure 3.6D**). DSBs formed a diffuse pair of smears across the region containing the Ino4 motifs, and bore little similarity to the fine-scale pattern of MNase cleavage. In the *ino4* mutant, much of the intergenic region became modestly more sensitive to digestion, but the spatial array of bands was not detectably altered and the strong MNase-hypersensitive sites were largely unchanged (**Figure 3.6D**). DSBs were spread across a similar total area as in wild type, but redistributed so that segments containing the Ino4 motifs received a disproportionately higher fraction of total DSBs. In this case, the increased DSB frequency correlated with an increase in overall MNase hypersensitivity.

Finally, as controls I examined the *GAT2-GID8* and *SOD1-ADO1* intergenic regions, which contain single Bas1 or Ino4 motifs, respectively, and whose DSB levels were unchanged in the TF mutants (**Figure 3.2M and N**). The *GAT2-GID8* intergenic region displayed a complex MNase digestion pattern, with a large zone containing numerous MNase-hypersensitive sites upstream of the 5′ end of *GAT2* and a smaller

hypersensitive zone near the 5′ end of *GID8* (**Figure 3.6E**). DSBs were distributed diffusely across much of the intergenic region, and again the DSB spatial pattern correlated poorly with the fine-scale MNase pattern. In the absence of Bas1, there was little or no detectable change in the MNase cleavage pattern, even around the Bas1 motif, and there was likewise little change in the spatial pattern of DSBs (**Figure 3.6E**). Similarly, the *SOD1-ADO1* intergenic region displayed several MNase hypersensitive sites spanning the region where DSBs appeared as a diffuse smear, with no clear spatial correlation of DSBs with MNase cleavage (**Figure 3.6F**). I observed no change in either chromatin structure or the number or distribution of DSBs in the *ino4* mutant.

Taken together, these examples show that the relationships between TF binding, local chromatin structure, and DSB patterns are complex and context-specific. In three cases where removing the TF affected chromatin structure right where DSBs would normally form, I observed correlated changes in the fine-scale distribution of DSBs (**Figure 3.6A,B,D**). Conversely, no changes in fine-scale DSB patterns were observed at three loci that showed little or no change in MNase digestion right around the wild-type DSB positions (**Figure 3.6C,E,F**). Importantly, however, there was no clear correlation between quantitative changes in MNase sensitivity and changes in absolute DSB frequencies, ruling out effects on chromatin accessibility alone as a universal explanation for how TFs modulate DSB hotspot activity.

Changes in DSB frequency do not correlate with changes in histone H3 lysine 4 trimethylation around hotspots

In meiosis, sister chromatids form a linear protein axis (the axial element), with chromatin emanating out in loops; DSBs are more likely to occur in DNA sequences that are in loops, but many of the proteins needed for DSB formation are

enriched on the axis (Blat *et al.* 2002; Kumar *et al.* 2010; Panizza *et al.* 2011). This and other observations have led to a "tethered loop-axis complex" model in which DSBs are formed in loop segments captured by axis-associated DSB machinery (Blat *et al.* 2002; Panizza *et al.* 2011) (**Figure 3.7A**). Recently, it was discovered that the DSB-promoting protein Mer2 interacts with Spp1, a protein containing a PHD (Plant Homeo *Domain*) finger that binds H3K4me3 marks and thereby tethers the chromatin loop to the axis, promoting DSB formation in NDRs in loops (Acquaviva *et al.* 2013; Sommermeyer *et al.* 2013). Thus, one hypothesis to account for altered DSB frequencies could be that deletion of TFs alters the H3K4me3 modification status around certain promoters and thereby affects Spp1-dependent targeting efficiency.

To test this hypothesis, I performed ChIP-seq to measure H3K4me3 levels in wild type and TF mutants. Cells from 4 h meiotic cultures were crosslinked with formaldehyde and disrupted. Chromatin was digested into mononucleosomes with MNase, immunoprecipitated with anti-histone H3 and anti-H3K4me3 antibodies, and deep sequenced. Resulting maps showed the expected pattern of preferential H3K4me3 enrichment for nucleosomes near the 5′ ends of genes (**Figure 3.7B, C**) (Pokholok *et al.* 2005; Borde *et al.* 2009; Zhang *et al.* 2011b). However, counter to the hypothesis motivating this analysis, I observed no significant difference between the increased, decreased, and unchanged DSB hotspot groups when I examined the change in H3K4me3-to-H3 ratios caused by the *bas1* or *ino4* mutation (**Figure 3.7D, E**). Thus, changes in the level of this histone modification in TF mutants provide little or no predictive power for changes in DSB frequency. This finding fits with the observation that, even though H3K4me3 plays a critical role in targeting Spo11 activity to certain promoter regions (Borde *et al.* 2009; Acquaviva *et al.* 2013; Sommermeyer *et al.* 2013), quantitative measures of H3K4me3 correlate poorly if at all with DSB hotspot strength (Tischfield and Keeney 2012).

Figure 3.7 Tethered loop-axis model for DSB formation, and H3K4me3 levels in *bas1* and *ino4* mutants. (A) Tethered loop-axis model for DSB formation. Encircled numerals highlight potentially TF-dependent levels of the hierarchical combination of factors that shape the DSB distribution. 1) DSB-forming potential over regions of approximately 5 to 20 kb is established by the loop-axis structure of meiotic chromosomes and the axis-association of DSB-promoting proteins. 2) Within a loop, gene promoters are preferentially targeted for DSB formation, in part by interactions between the DSB machinery and promoter-proximal H3K4me3. 3) Within a hotspot, the fine-scale distribution of DSBs is shaped in part by accessibility of the DNA to Spo11, in competition with nucleosomes and other DNA binding proteins. (B) Snapshot of anti-H3K4me3 and anti-H3 ChIP-seq data from wild-type, bas1 and ino4 data sets. Sequence coverage values are normalized to genome average. (C) Average profiles of H3K4me3/H3 ratios relative to transcription start sites. (D and E) Log-fold change of H3K4me3/H3 ratios in groups of hotspots that responded as indicated to the *bas1* (D) or *ino4* (E) mutations. Hotspot groups are as indicated in Figure 2.2C,D. H3K3me4/H3 ratios were summed in 500 bp windows that begin 200 bp away on either side of hotspot midpoints.

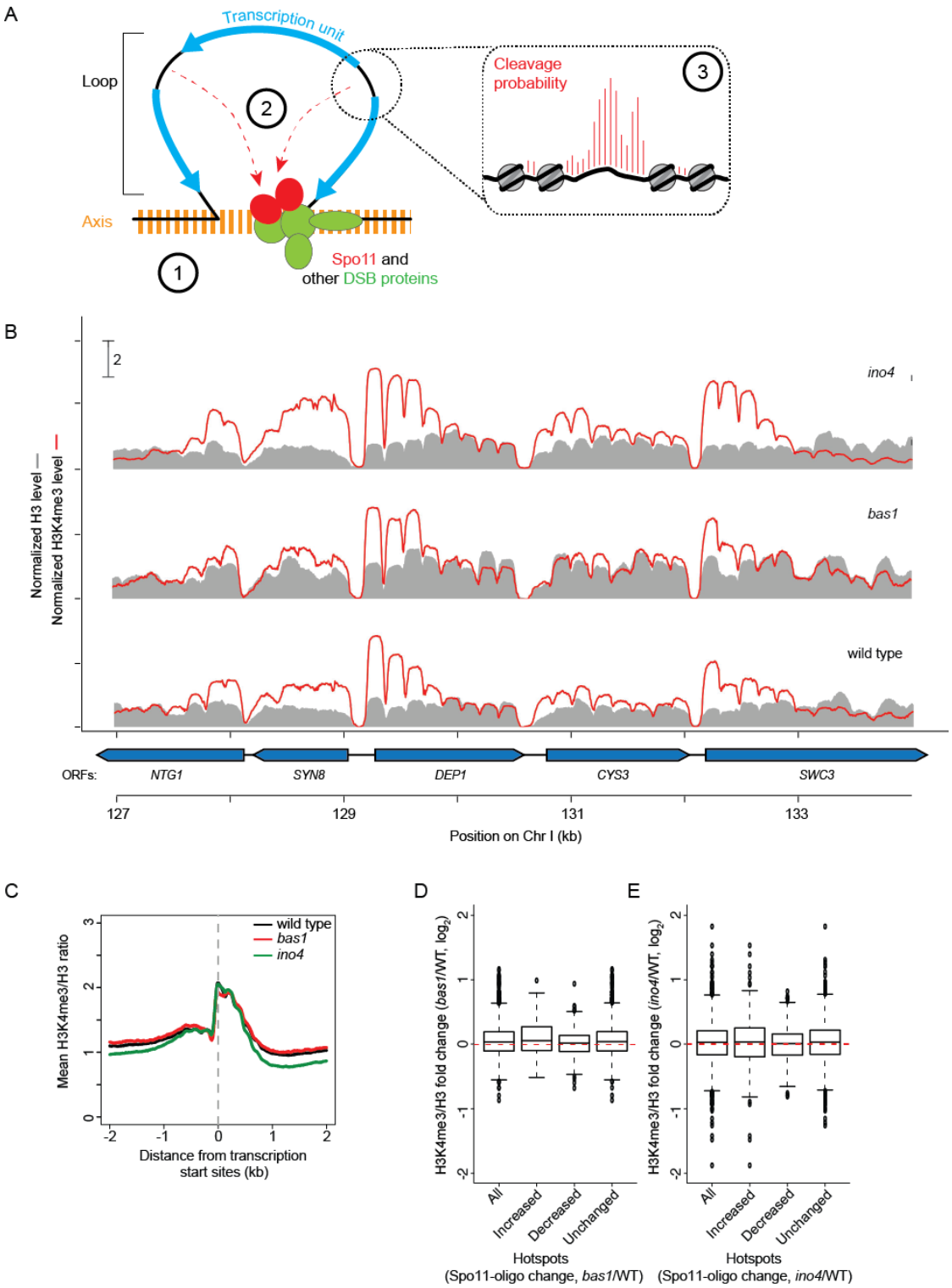
A
Transcription unit
Loop
2
Cleavage probability
3
Axis
1
Spo11 and other DSB proteins
B
2
ino4
bas1
wild type
Normalized H3 level
Normalized H3K4me3 level
ORFs:
NTG1
SYN8
DEP1
CYS3
SWC3
127
129
131
133
Position on Chr I (kb)
C
wild type
bas1
ino4
Mean H3K4me3/H3 ratio
Distance from transcription start sites (kb)
D
H3K4me3/H3 fold change (bas1/WT, log2)
All
Increased
Decreased
Unchanged
Hotspots
(Spo11-oligo change, bas1/WT)
E
H3K4me3/H3 fold change (ino4/WT, log2)
Hotspots
(Spo11-oligo change, ino4/WT)

Changes in DSB frequencies do not correlate with changes in gene expression

Since only a small portion of changed hotspots in *bas1* or *ino4* mutants contained Bas1 or Ino4 binding peaks, it raises the possibility that some changed hotspots are in the promoters of the genes that are Bas1 or Ino4 indirect targets (i.e. genes that is regulated by Bas1 or Ino4 without direct binding of Bas1 and Ino4 on the promoter). To identify these indirect targets, I measured mRNA levels during meiosis in wild-type, *bas1* and *ino4* strains (**Figure 3.8A and B)**. I identified 222 significantly up-regulated and 341 down-regulated genes in *bas1* mutants, as well as 27 up-regulated and 112 down-regulated genes in *ino4* mutants (**Figure 3.8C and D)**. Bas1-regulated genes were enriched for Gene Ontology (GO) terms: purine nucleotide metabolic process (31 out of 563 genes, 5.5%), phosphorus metabolic process (93 genes, 16.5%), carboxylic acid metabolic process (56 genes, 9.9%), and meiotic cell cycle process (68 genes, 12.1%). Ino4-regulated genes were enriched for GO terms: lipid biosynthetic process (13 out of 139 genes, 9.4%) and meiotic cell cycle process (25 genes, 18.0%). Thus, in addition to known Bas1- or Ino4-regulated pathways, some genes involved in meiosis were also differentially expressed in *bas1* and *ino4*. This may reflect altered transcription patterns in these TF mutants, or timing differences from culture-to-culture variation.

Next, I examined the gene expression patterns around the six hotspots we characterized in previous sections. All these hotspots contained Bas1 or Ino4 binding peaks, but deletion of Bas1 or Ino4 had different effects on gene expression. As expected, *SHM2* mRNA level was substantially reduced after deleting Bas1 (Denis and Daignan-Fornier 1998) (**Figure 3.8E**). However, mRNA levels of *GCV2/MRPS17* in *bas1* were similar to those in the wild type, even though DSB frequency in this divergent intergenic region was greatly increased in *bas1*. *GID8/GAT2* mRNA levels were also unchanged. For Ino4-bound hotspots, both *CHO2* and *FAS1* showed

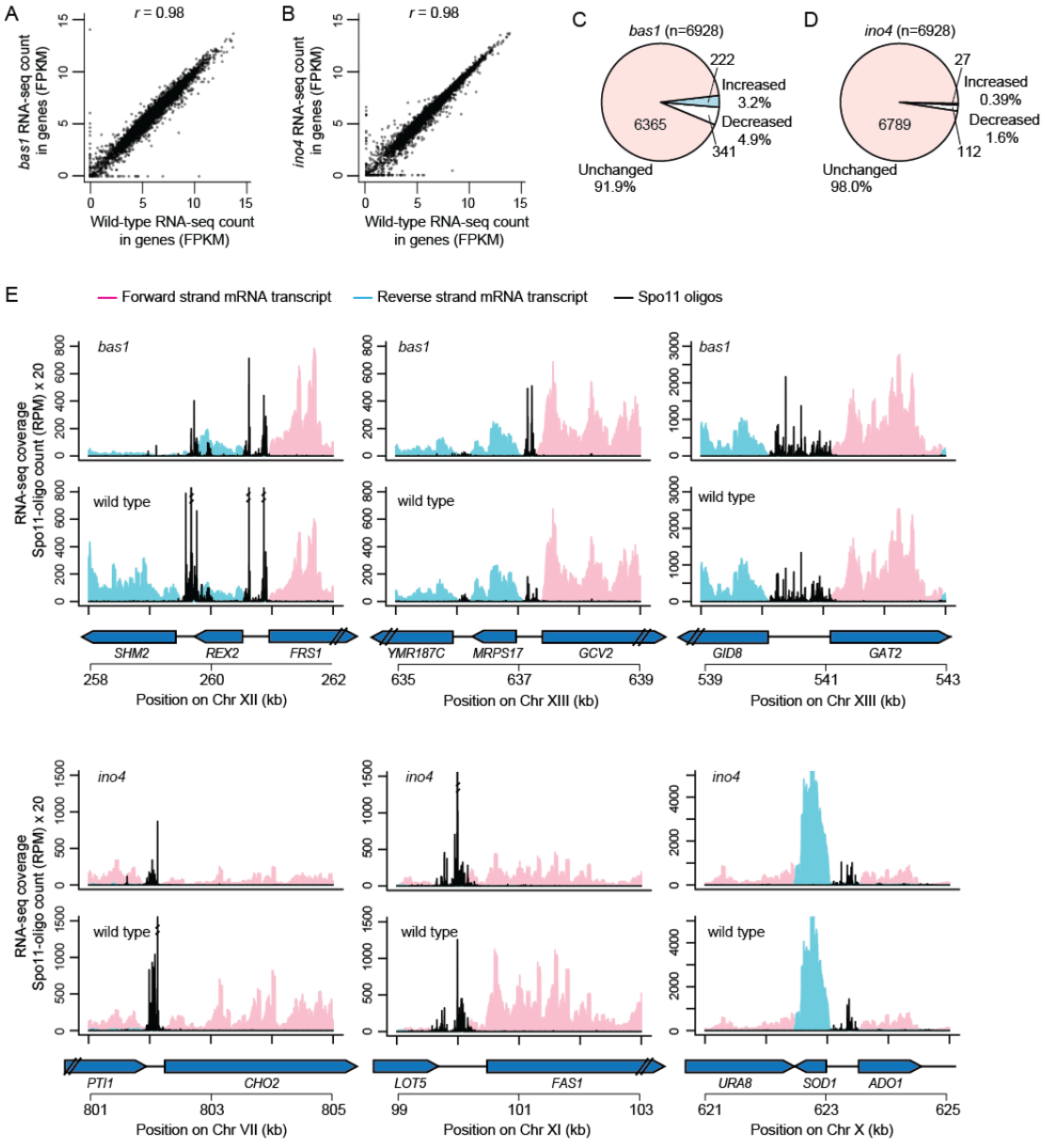

Figure 3.8 mRNA levels in *bas1* and *ino4* mutants. (A and B) Comparisons between wild type and TF mutants for all genes. (C and D) Proportion of genes that are significantly changed in RNA levels relative to wild type. (E) Snapshots of RNA-seq data around hotspots at the promoters of *SHM2*, *GCV2*, *GAT2/GID8*, *CHO2*, *FAS1*, and *ADO1/SOD1*.

similarly reduced mRNA levels in *ino4*, but had DSB levels that moved in the opposite directions (**Figure 3.8E**). *ADO1/SOD1* mRNA levels were similar in wild type and *ino4*. Taken together, these results reveal no simple correlation between the changes in Spo11-oligo counts and mRNA levels.

To extend this analysis to the whole genome, I plotted fold changes of Spo11-oligo counts in promoters against fold changes of mRNA levels for all non-dubious genes, and found that changes in the level of mRNAs in TF mutants provide little or no predictive power for changes in DSB frequency (**Figure 3.9**). Interestingly, several Bas1 and Ino4 direct targets (*SHM2, GCV1, ADE17, GCV3* for Bas1*; INO4* and *OPI3* for Ino4) exhibited some shared features: both the gene expression and hotspot activities were decreased in the respective TF mutant, which is similar to the case of *HIS4* hotspot in Mieczkowski's strains (Mieczkowski *et al.* 2006). However, this trend was not applicable for other Bas1 or Ino4 direct targets. For instance, *GCV2* showed increased DSB frequency in the promoter and unchanged RNA levels in *bas1*. Moreover, *INO1* transcription was substantially reduced but the DSB activity was slightly elevated. Therefore, our results fit the observation from previous study that no correlation has been found between DSB activity and transcript levels at *HIS4* hotspot (White *et al.* 1992).

Hotspot competition is unlikely be a significant source of the indirect effects of TF mutations on hotspot activity

In principle, indirect effects could also arise if hotspots that are direct TF targets influence neighboring hotspots via "hotspot competition". Insertion of very strong artificial hotspots can suppress the activity of nearby hotspots over distances up to tens of kb (Wu and Lichten 1995; Xu and Kleckner 1995; Fan *et al.* 1997; Ohta *et al.* 1999; Jessop *et al.* 2005). If a DSB hotspot becomes substantially hotter or colder

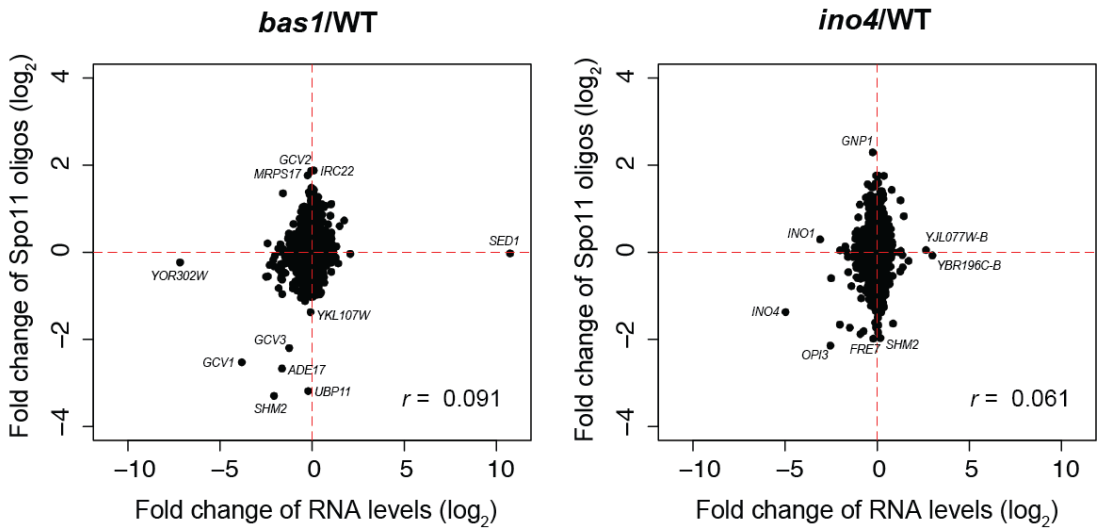

Figure 3.9 mRNA levels and DSB activity in *bas1* and *ino4* mutants. Fold changes of RNA levels do not correlate with fold changes of Spo1-oligo counts within 300bp windows upstream from gene open reading frames in *bas1* (left) and *ino4* (right) mutants.

in *bas1* or *ino4* mutants, competition could cause compensatory changes in DSB frequency in nearby hotspots. Such an effect predicts that change of a DSB hotspot in the TF mutants should be inversely correlated with changes of neighboring hotspots. However, I did not detect such a pattern in our data whether considering all hotspots relative to their neighbors or considering only the subset of direct TF targets that were most altered in the TF mutants (**Figure 3.10**). It is possible that hotspot competition is a property of artificial hotspots but not natural hotspots, but I favor instead the interpretation that the hotspots affected by *bas1* or *ino4* mutation are generally not strong enough to reveal hotspot competition in a cell population. The hottest hotspot that was directly bound by Bas1 or Ino4 and also showed at least a 2-fold change in activity had a Spo11-oligo count of only 1134 RPM, equivalent to a DSB frequency of less than 2.5% of DNA according to the regression relationship in (Pan *et al.* 2011), and most such hotspots had an inferred DSB frequency of <1%. For a hotspot with a DSB frequency of 2.5% of DNA, DSBs occur at this locus in ≤10% of the cell population (assuming one DSB per four chromatids in most cells (Zhang *et al.* 2011a)). Any potential suppression by this hotspot of its neighbors would likely be masked by the behavior of the majority of unaffected cells. These considerations indicate that hotspot competition is unlikely to be a significant source of the indirect effects of TF mutations on hotspot activity.

Discussion and Conclusions

Roles of sequence-specific DNA binding proteins in shaping the DSB landscape

DNA sequence-dependent targeting of meiotic recombination was first discovered more than two decades ago in two highly diverged organisms, fission yeast and budding yeast (Ponticelli *et al.* 1988; Schuchert *et al.* 1991; White *et al.* 1991).

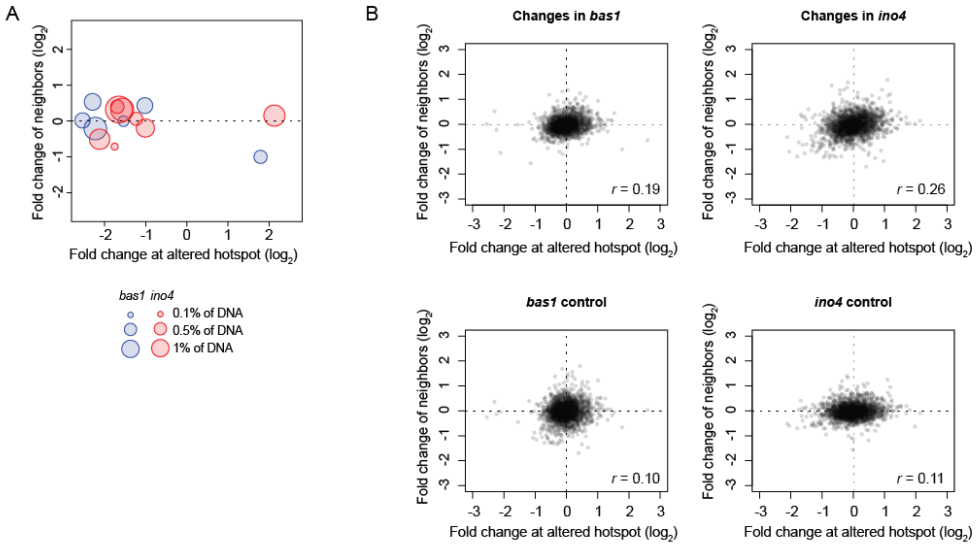

Figure 3.10 (A,B) Hotspot competition is not a major contributor to altered DSB distributions in TF mutants. It is known that a very strong artificial hotspot can inhibit DSB formation at natural DSB hotspots nearby (see Discussion and Conclusions). Such behavior predicts that a hotspot whose intrinsic activity is altered by a TF mutation should show compensatory changes in the opposite direction for its neighbors: hotspots that decrease activity should show increased activity among the neighbors, and vice versa. The bubble plot in panel A compares the log fold change in Spo11-oligo counts at specific hotspots in *bas1* (blue) or *ino4* (red) mutants with the total log fold change of Spo11-oligo counts within the neighbors of those hotspots (within 5 kb on either side). Only hotspots that overlap ChIP-seq peaks of the respective TF, have ≥100 RPM average in at least one genotype, and show ≥2-fold change of Spo11-oligo count within the hotspot are shown. The area of each point is proportional to the Spo11-oligo count (i.e., DSB strength) in either wild type or the TF mutant, whichever was higher. There was no significant correlation between the change in these hotspots and the change in their neighbors (p=0.313). Panel B is similar, but for all hotspots with ≥100 RPM average in at least one genotype. The top panels show fold changes in the *bas1* (left) or *ino4* (right) mutant. As controls for non-specific correlations, the bottom panels compare the fold change within each hotspot in one TF mutant with the fold change within the hotspot's neighbors in the other TF mutant. Only very weak positive correlations are seen, which is opposite the direction predicted for a hotspot competition effect. As discussed in the Main Text, it is likely that the lack of a signature of hotspot competition is because the hotspots whose activity changes have relatively low DSB frequencies, so their effects on their neighbors are too modest to be apparent when assayed in a cell population.

Additional regulatory DNA sites were identified subsequently in both yeasts (White *et al.* 1993; Fan *et al.* 1995; Steiner *et al.* 2009), and more recently it was found that mouse and human hotspots are defined by the histone methyltransferase PRDM9 binding to specific DNA sequences (Baudat *et al.* 2010; Myers *et al.* 2010; Grey *et al.* 2011; Brick *et al.* 2012; Pratto *et al.* 2014). These and other findings have focused attention on the roles of sequence-specific DNA binding proteins in shaping the DSB landscape, and have even led to proposals that one or a few such proteins and their binding sites are the principal architects of DSB hotspot location and activity across all of both yeasts' genomes (e.g., ref. Wahls and Davidson 2010).

However, although sequence-specific DNA binding by PRDM9 is clearly a primal determinant of hotspots in most mammalian species, the situation has been less clear for TFs in yeasts. Even those sequence motifs and their binding factors that are clearly capable of specifying strong DSB hotspot activity in some genomic contexts work poorly or not at all in other contexts (Ponticelli and Smith 1992; Mieczkowski *et al.* 2006) (this work). Moreover, presence of a sequence motif with DSB-targeting potential is by itself a poor predictor of local DSB frequency (Mieczkowski *et al.* 2006; Fowler *et al.* 2014).

An alternative to a DNA sequence-centric view is a model in which DSB distributions are shaped by combinatorial action of many chromosomal factors that work in a hierarchical and scale-dependent manner (Petes 2001; Mieczkowski *et al.* 2006; Lichten 2008; Lichten and De Massy 2011; Pan *et al.* 2011; De Massy 2013a). In this view, individual sequence-specific DNA binding proteins may contribute significantly to the DSB landscape, but in a circumscribed and highly context-dependent manner. Our findings in this study, in agreement with earlier work by Mieczkowski et al. (Mieczkowski *et al.* 2006), support the latter model.

Context-dependent direct and indirect influences of Bas1 and Ino4 TFs on DSB formation

Because the earlier genome-wide study of Bas1 used a low-resolution microarray and focused on information for probes corresponding to entire individual ORFs (Mieczkowski *et al.* 2006), it was difficult to assign the hybridization signal to individual DSB hotspots. Therefore, I wished to revisit this question with the higher resolution and greater dynamic range afforded by Spo11-oligo mapping. Mieczkowski et al. scored 153 ORFs as having statistically significantly different *rad50S* ChIP-chip signal in the *bas1* mutant (68 with decreased signal in *bas1*, and 85 with increased signal). I discerned a larger number of altered hotspots, at least in part because Spo11-oligo mapping resolves more total DSB hotspots. I also was able to more precisely localize changes in DSB formation, including fine-scale changes of local DSB distribution within hotspots themselves. Importantly, however, both studies support the same general conclusion: Bas1 effects on DSB formation are highly context dependent. Our results with Ino4 were similar in this regard, suggesting that context dependence is likely to be true for many if not all TFs that impinge on Spo11 activity.

Deletion of Bas1 affected DSB activity in about half of hotspots containing Bas1 binding sites, similar to frequencies observed previously (Mieczkowski *et al.* 2006). Deletion of Ino4 affected less than one third of the hotspots to which Ino4 binds directly during meiosis. Moreover, only a minority fraction of the hotspots that changed in the TF mutants were detectably bound by Bas1 or Ino4 protein during meiosis. This modest correspondence between TF binding and DSB activity is analogous to the relation of TFs to transcriptional regulation: numerous studies have documented that only a small fraction of genes whose promoters are bound by a given TF show expression changes when the TF is deleted, and only a small fraction of the genes that change expression are direct binding targets (reviewed in Macquarrie *et al.*

2011; Hughes and De Boer 2013) (and this study). Although it is possible that the ChIP-seq failed to detect direct Bas1 or Ino4 binding that does in fact occur, the results strongly indicate that a substantial portion of the DSB-modulating activity of these TFs is indirect. One possibility is that each TF mutant causes changes in cell physiology that, by crosstalk between transcriptional regulation networks, alter DSB activity at numerous gene promoters genome-wide via changes in local chromatin structure or loop-axis architecture. In this context, it is noteworthy that genome-wide DSB distributions can be altered by auxotrophies for certain amino acids or nucleobases, including auxotrophies caused by mutation of several of the genes whose expression is known to be Bas1-dependent such as *HIS4* and *ADE1* (Abdullah and Borts 2001; Cotton *et al.* 2009). Nevertheless, no correlation between DSB changes and gene expression changes was found in *bas1* and *ino4* mutants, indicating that most genes associated with indirectly changed hotspots are not regulated transcriptionally. However, the chromatin structure and DNA accessibility in and around these hotspots can still be affected indirectly (see below).

Tethered loop-axis model for DSB formation in *bas1* and *ino4* mutants

The context dependence for Bas1 effects on DSBs has previously been framed as reflecting locus-specific differences in the balance between chromatin "loosening" and "tightening" activities (Mieczkowski *et al.* 2006). However, for those sites I examined directly, there was no obvious correlation between changes in DSB frequency and changes in overall MNase hypersensitivity, suggesting that chromatin accessibility is not the principal link between TFs and DSB frequency at most hotspots. In contrast, if chromatin structure immediately within a DSB hotspot was altered by TF mutation, then the fine-scale DSB pattern was also generally altered. In particular, a shift of nucleosome position or appearance of a new nucleosome at *SHM2*

and *GCV2* appeared to result in local occlusion of Spo11 access to the DNA, consistent with inferences from genome-wide studies of DSBs relative to well-positioned nucleosomes (Pan *et al.* 2011). I interpret these results to mean that open chromatin provides windows of opportunity where Spo11 can cut, but it is not generally sufficient to determine overall break frequencies.

In the context of the tethered loop-axis complex model, I envision that regional factors (working on ~5–20 kb scales) shape loop-axis architecture and determine the DSB potential of a particular loop region (level 1 in **Figure 3.7A**). Within a loop, interactions between axis-bound DSB proteins and loop chromatin promote targeting of Spo11 activity to particular locations (i.e., hotspots). These interactions determine the relative likelihood that particular hotspots will fulfill the DSB-forming potential of the loop they reside in (level 2 in **Figure 3.7A**). Within a hotspot, fine-scale DSB patterns are shaped by geometry of the targeting mechanism plus competition of Spo11 with nucleosomes and other DNA-binding proteins (level 3 in **Figure 3.7A**). TFs can affect DSB formation at any (or all) of the levels shown; the context dependence presumably reflects differences in how a given TF influences each of these levels at various genomic regions. Thus, while there are common themes and general patterns, each hotspot tells its own story and TFs can play many and varied roles.

Chapter 4: High-resolution DSB mapping in *set1* mutants reveals H3K4me3-dependent and -independent DSB formation

Summary

In the "tethered loop-axis complex" model, DSBs are formed in loop segments captured by axis-associated DSB machinery. Spp1 reads and brings H3K4me3 regions in the loop segments to the chromatin axis to activate DSB formation in the nearby NDR regions. In the absence of H3K4me3 in *set1* mutants, DSB formation is strongly reduced, while several new DSB sites appear. However, previous genome-wide studies are limited by relatively low spatial resolution. Here, I re-mapped DSB distribution in *set1* mutants using Spo11-oligo mapping. With the accurate and nucleotide-resolution maps, I found that 70.8% of hotspots were decreased and 1.8% of hotspots were increased in *set1* mutants. Furthermore, I discovered that for those "new" DSB sites in previous study, DSBs occur on the same preferable bases as in wild type, but with increased frequencies. I also confirmed and extended the observation that these increased hotspots tend to be located in the promoters of genes with low H3K4me3 levels and closer to the chromatin axis. Thus, meiotic cells have a robust system to target Spo11 activity to chromatin loops: H3K4me3-dependent tethering is the predominant mechanism for DSB site selection, and abolition of H3K4me3 activates alternative DSB-promoting mechanisms.

Introduction

H3K4me3 plays an important role in spatial coordination of DSB formation with the loop and axis structure in *S. cerevisiae* (reviewed in **Chapter 1**). In meiosis, H3K4me3 is enriched on the first nucleosome (or the +1 nucleosome) within genes, in the proximity of DSB sites in NDR of promoters (Borde *et al.* 2009). Spp1 contains a

PHD finger, which binds H3K4me3 marks near DSB sites in the chromatin loop, and also interacts with DSB protein Mer2 located on the axis. Thus, Spp1 tethers the chromatin loop to the axis, allowing DSB formation in NDRs in loops (Acquaviva *et al.* 2013; Sommermeyer *et al.* 2013). Nevertheless, it is not yet clear how much H3K4me3 is the minimal requirement for break formation at a single site, and DSB strength does not correlate with H3K4me3 levels (Tischfield and Keeney 2012).

The Set1 lysine methyltransferase is responsible for all mono-, di- and trimethylation of H3K4 in *S. cerevisiae* (Briggs *et al.* 2001; Roguev *et al.* 2001; Shilatifard 2012). Genome-wide meiotic DSBs were previously mapped in a *set1* mutant by microarray hybridization of replication protein A (RPA)-bound ssDNA in a *dmc1Δ* background (Borde *et al.* 2009). In *dmc1Δ set1Δ* mutants, DSB formation is generally reduced with the exception of several new DSB sites. These results suggest that H3K4me3/Spp1/Mer2-mediated tethering of chromatin loops to axes is responsible for most DSB formation in NDR on chromatin loops. Moreover, appearance of new DSB sites in *set1* mutants reveals the existence of alternative DSB-promoting mechanism(s). DSBs likely still occur on the axes in the absence of H3K4me3-mediated tethering since DSB proteins (which are located on the axes) are still required (Sommermeyer *et al.* 2013). Furthermore, it has been suggested that these emerging DSB sites are associated with relatively low H3K4me3 in wild type, shorter distance to the axes and active transcription in *set1* (Borde *et al.* 2009; Sommermeyer *et al.* 2013). However, what targets H3K4me3-independent Spo11 activity is still unclear.

Moreover, the resolution of these maps is relatively low (usually several kb) due to the limitations in DNA sample preparation and hybridization. In contrast, the majority of DSB hotspots are 50–300 bp wide (Pan *et al.* 2011). The “hotspots” defined in the microarray study were actually relatively large domains that merged

overlapping hybridization signals from multiple nearby hotspots and cannot be assigned to individual DSB hotspots (Tischfield and Keeney 2012). Therefore, the comparison of "hotspots" with genome features (such as H3K4me3) is based on inaccurate definition of altered "hotspots". Furthermore, these maps were generated in *dmc1* mutant backgrounds to block DSB repair and enrich for ssDNA intermediates as starting materials (Bishop *et al.* 1992). Notably, the accumulation of unrepaired ssDNA triggers the DNA damage checkpoint response, causing cells to arrest in late prophase (Bishop *et al.* 1992; Lydall *et al.* 1996) and promoting DSB formation (Gray *et al.* 2013). Thus, the negative feedback control of DSB formation is affected in *dmc1*. Deletion of Dmc1 with *set1* mutants may cause synergistic effects on DSB frequency and locations.

Here, I re-mapped DSB distribution in *set1* mutants using Spo11-oligo mapping in a *DMC1* (wild-type) background. With the accurate and high-resolution maps, I assessed the contribution of H3K4me3 on DSB formation and the fine pattern of DSB changes. Furthermore, I discovered that DSBs occur on the same preferable bases as in wild type, with increased frequencies, in a small number of hotspots. I confirmed and extended the observations that these increased hotspots tend to be located in the promoters of genes with low H3K4me3 levels, and closer to the chromatin axis.

Results

Total meiotic DSBs are strongly reduced in the absence of Set1

Set1 is required for normal DSB formation in many hotspots, but the level of total DSB reduction is unknown. Moreover, previous measurement of DSBs was carried out in mutants with repair defects, which can cause synergistic effects (see Introduction). To assess DSBs globally and mitigate uncertainty from repair defects, I

examined Spo11-oligo complexes, by-products of DSB formation that can be used to measure DSB number. Extracts were prepared from cultures expressing phenotypically normal Flag-tagged Spo11 (Thacker *et al.* 2014) (Chapter 1). Spo11-oligo complexes were immunoprecipitated with anti-Flag antibodies, and then labelled with terminal transferase and [α^{32}P]dCTP. Labelled Spo11-oligo complexes were separated by SDS-polyacrylamide gel electrophoresis (SDS-PAGE) and detected by phosphorimager. Total Spo11 proteins were detected by western blotting. In wild type, Spo11-oligo complexes were detected at ~2 h, peaked at ~4 h, then declined (**Figure 4.1A and B**), which has similar timing with DSBs (Neale *et al.* 2005). In *set1* mutants, Spo11-oligo complexes appeared as late as ~3–4 h with lower levels than wild type, but continued to accumulate after 4h (**Figure 4.1A and B**). Spo11-oligo levels reached a maximum at ~6–7 h, which was only ~40% of the wild-type peak before they declined. The delayed Spo11-oligo complex formation is mostly likely due to the delayed meiotic entry in *set1* mutants (Sollier *et al.* 2004).

I next evaluated whether decreased DSBs could be tied to changes in Spo11 protein levels. Only a small fraction of Spo11 makes DSBs (Neale *et al.* 2005), so most Spo11 is not bound to oligos and free Spo11-Flag (migrating slightly lower than 50 KD) is predominantly detected in western blots. In wild type, Spo11 was induced as cells entered meiosis, as expected, and peaked around the peak of DSB formation, then decreased as the labelled Spo11-oligo complexes disappeared (**Figure 4.1A**). In contrast, Spo11 induction was delayed in *set1* mutants, as expected based on previous study (Borde *et al.* 2009). Free Spo11 was maintained at roughly constant levels even at late time points such as 9–10 h. Therefore, although Spo11 levels were slightly lower in *set1* than wild type around peak hours, it was not responsible for the reduction of labelled Spo11-oligo complexes because of the abundance of free Spo11 in *set1* mutants.

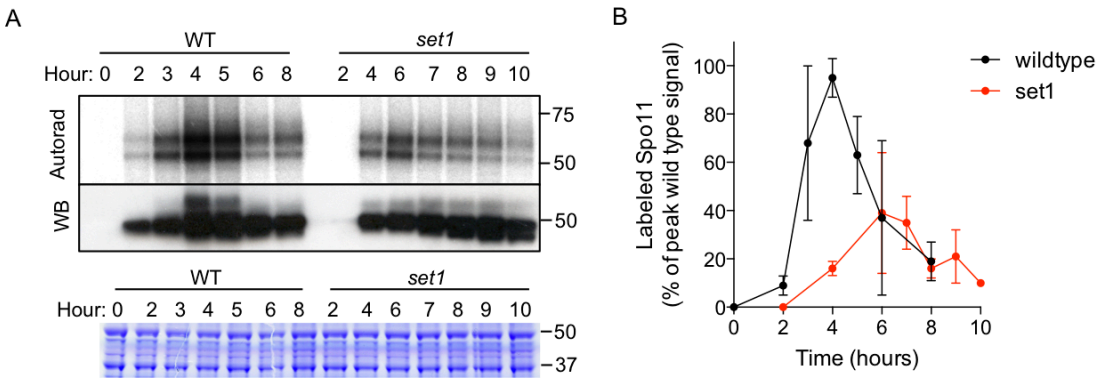

Figure 4.1 Fewer DSBs form in *set1* mutants. (A and B) Representative Spo11-oligo complex time courses are in (A) and quantification in (B) (mean ± s.d. for 3 cultures, except at 10h (1 culture)). Radiolabelled Spo11-oligo complexes were detected by autoradiography (top) and total Spo11 was detected by anti-Flag western blot (WB, middle). The main labelled species differ in oligo size. Nearly all of the western blot signal is Spo11 that has not made a DSB. Bottom, extract samples run separately and stained with Coomassie control for input to the immunoprecipitates.

More importantly, the relative level of total DSBs (the total DSB number in *set1* is ~40% of wild-type level, as estimated by comparing labelled Spo11-oligo complex peaks) serves as a normalization factor to scale the *set1* Spo11-oligo map related to the wild-type map.

Generating high-resolution DSB maps in *set1* mutants

Spo11-oligos were purified from meiotic cultures of wild-type (4 h) and *set1* mutants (7 h) and deep-sequenced with Illumina Hiseq. Reads were mapped to the *S. cerevisiae* genome. Each Spo11-oligo map was first normalized to the millions of reads mapped (RPM). At sub-kb scales, DSBs are clustered in hotspots, mostly in nucleosome-depleted promoters. This pattern was unaffected in *set1* mutants, in that DSBs formed in the same hotspots (**Figure 4.2**). However, *set1* mutants grossly changed the overall DSB landscape by changing the relative DSB frequencies (Pearson's $r = 0.62–0.72$) (**Figure 4.2 and 4.3**). Maps from biological replicate cultures of the same genotype agreed well with each other (Pearson's $r = 0.85–0.98$; **Figure 4.2 and 4.3**) and thus were averaged into consensus maps for further analysis. The fold change of Spo11-oligo counts (s*et1*/wild type) in non-overlapping 5 kb bins on all the chromosomes are shown in **Figure 4.4**. Altered DSB patterns are characterized in the following sections.

The majority of meiotic DSB hotspots exhibit decreased activity in *set1* mutants, while DSBs are elevated in a small number of hotspots

The wild-type and *set1* Spo11-oligo maps agreed moderately with published microarray maps (Borde *et al.* 2009) (Pearson's $r = 0.67–0.76$) but had much higher spatial and quantitative resolution (**Figure 4.5**). The high-resolution maps allowed us to analyze DSB activity at the individual hotspot level, which was not possible with

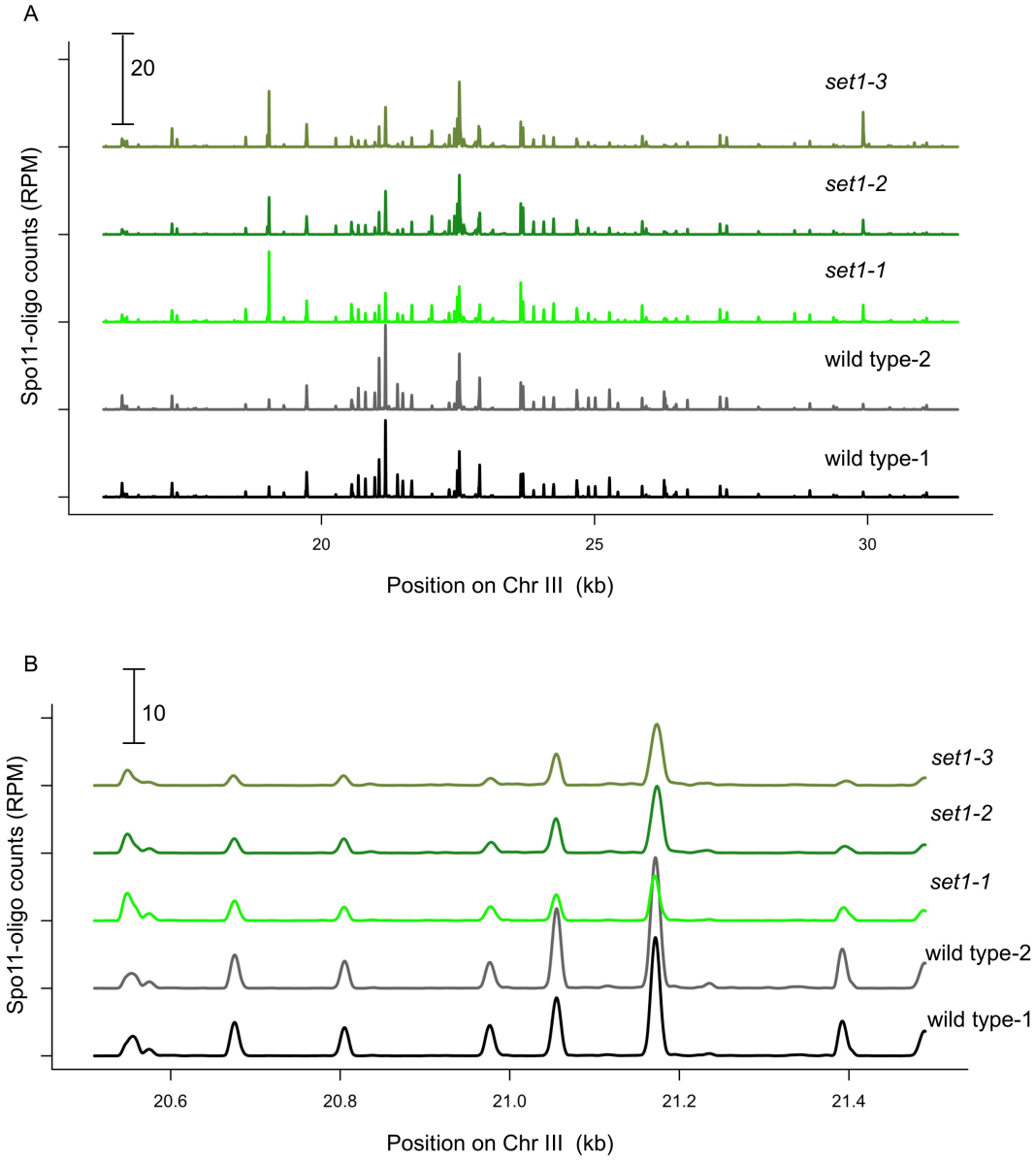

Figure 4.2 Spo11-oligo maps in wild type and *set1* mutants. (A) Reproducibility of Spo11-oligo maps. (B) DSBs form at the same hotspots in mutants as in wild type. Spo11 maps are normalized to reads per million (RPM) and smoothed with 201-bp Hann window.

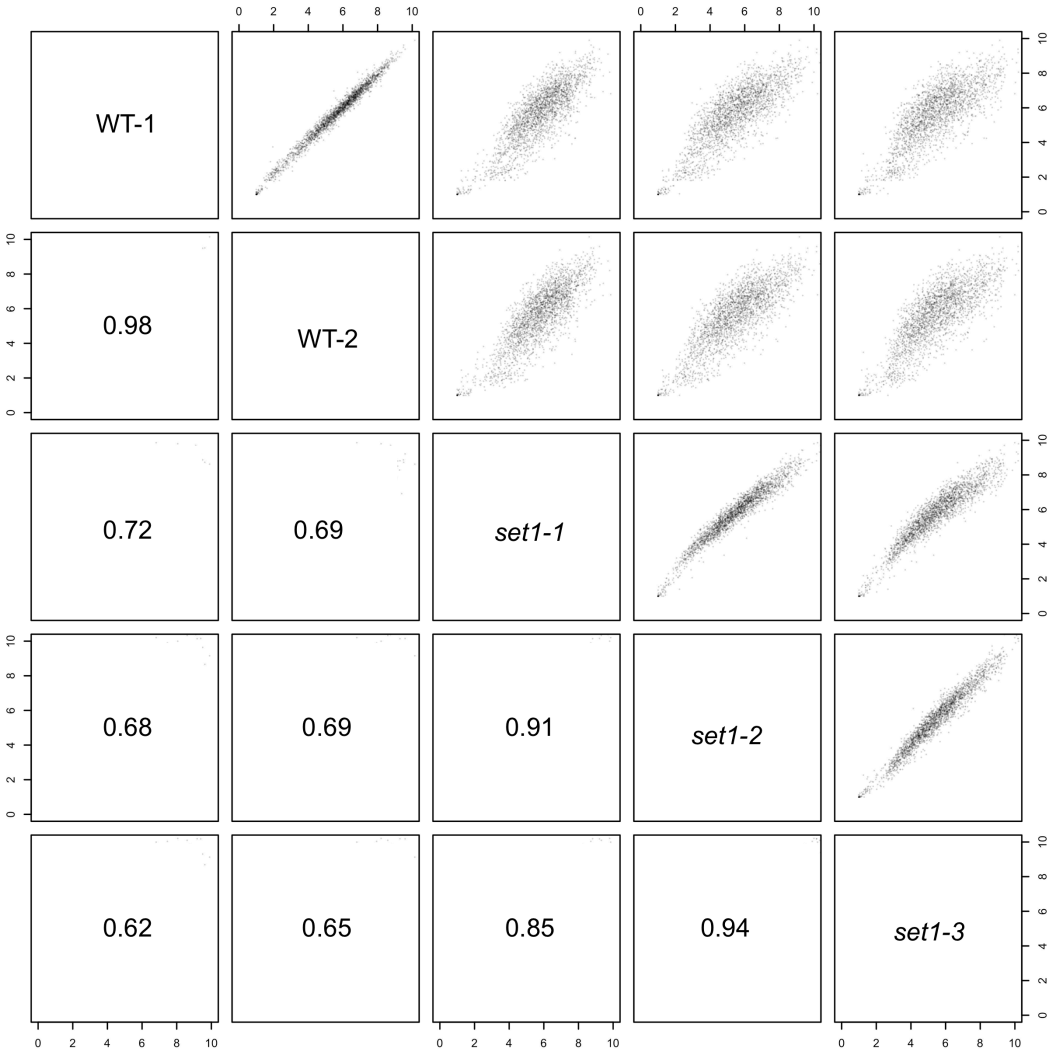

Figure 4.3 Quantitative reproducibility of Spo11-oligo maps. Comparisons are shown for individual wild type (WT) or *set1* datasets. Uniquely mapped Spo11 oligos were summed in non-overlapping 5-kb bins and expressed as reads per million (RPM) per kb (plotted on a log scale). Pairwise correlation coefficients are shown (Pearson's *r*).

Figure 4.4 *set1*/WT fold-change along 16 chromosomes. The total Spo11-oligo counts of *set1* map is scaled to 40% of wild-type map before taking the ratio. Red lines show *set1*/WT ratios, which are calculated in 5 kb bins and smoothed by Lowess fit. Cyan points indicate centromere positions; green box illustrate the rDNA region (represented by two rDNA repeats) on chromosome XII. Dashed lines mark values assumed as 2-fold change.

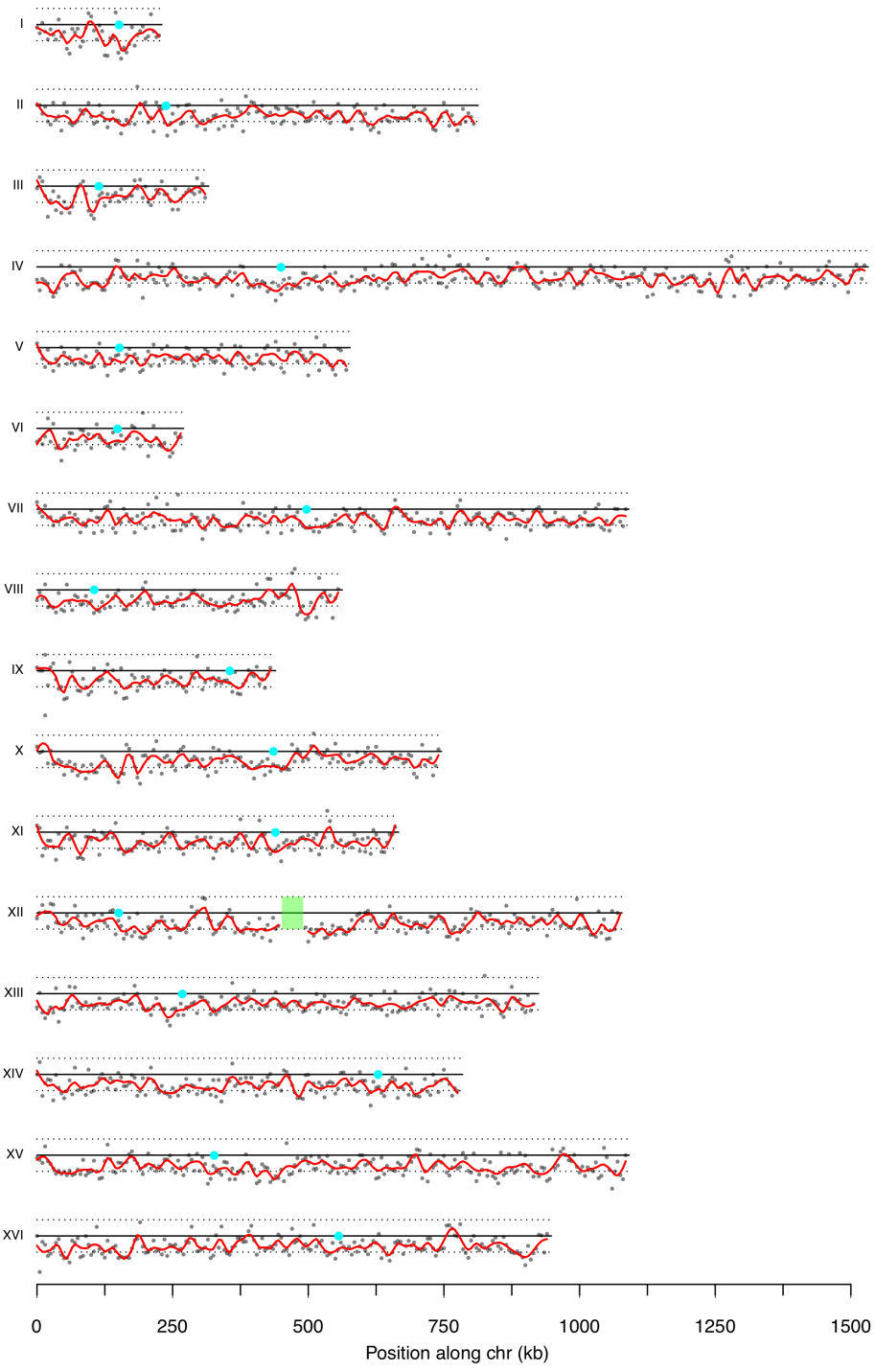
I
II
III
IV
V
VI
VII
VIII
IX
X
XI
XII
XIII
XIV
XV
XVI
0
250
500
750
1000
1250
1500
Position along chr (kb)

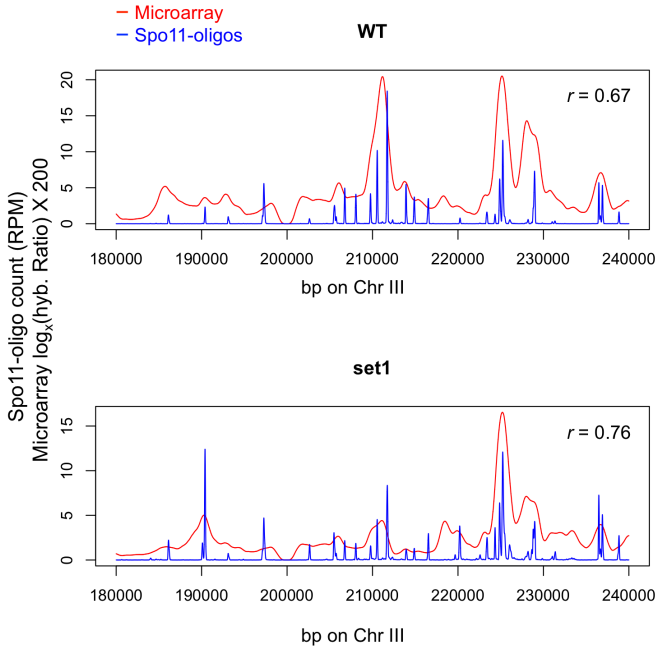

Figure 4.5 Comparison of wild-type and *set1* Spo11-oligo maps with published microarray maps. The Spo11-oligo map agrees with previous RPA ChIP microarray analysis (Borde et al., 2009) but provides higher resolution. Spo11 oligo maps are expressed as reads per million (RPM). The correlation coefficient is calculated between the normalized microarray signal and the sum of Spo11-oligo counts within 1.5 kb on either side of each microarray probe.

the earlier data sets. The total number of reads in the *set1* Spo11-oligo map was first scaled to 40% of the wild-type reads based on the results from Spo11-oligo complex labelling experiments (**Figure 4.1**). To avoid missing new hotspots in *set1* maps, I pooled averaged wild-type and averaged *set1* maps, then called hotspots on this combined map using a previously described algorithm (Pan *et al.* 2011). I identified 3934 hotspots and this number is close to the 3996 hotspots called in the combined wild-type and TF mutants (**Chapter 3**). In contrast, only 1085 "hotspots" were identified in both wild-type and *set1* microarray maps (Borde *et al.* 2009), indicating that many more hotspots are identified in the high resolution DSB maps compared to that in microarray maps (see Introduction). The fractions of Spo11-oligo counts in total hotspots were 88.9±0.5% and 84.4±2.7% for wild-type and *set1* maps, suggesting that slightly more DSBs were formed outside hotspots in *set1*. However, this difference is not statistically significant (Student's t-test, $p = 0.097$).

Next, I examined Spo11-oligo counts in hotspots in *set1* mutants compared with wild type. Most hotspots were decreased in the *set1* mutants, but several were increased (**Figure 4.6A**). I defined altered hotspots as p-value < 0.05 (Student's t-test on biological replicates, with Benjamini Hochberg adjustment for multiple correction). This criterion was quite stringent, in that I had a small number of replicates for each genotype (2 wild-type replicates and 3 *set1* replicates). Even so, a large fraction of hotspots were detectably altered by *set1* mutation: 2785 (70.8%) hotspots were decreased, and 70 (1.8%) were increased (**Figure 4.6B–C**). These quantified changes (72.6% decreased or increased hotspots) were comparable to what was detected in microarray maps, in which a total of 84% of the DSB peaks of the wild-type strain showed a greater than 1.5-fold reduction in the absence of Set1 (Borde *et al.* 2009). Within the remaining 1079 (27.4%) hotspots, I further divided them into unchanged hotspots (change is less than 1.5 fold) and hotspots whose changes were uncertain

Figure 4.6 Altered DSB hotspots in *set1* mutants. (A) Comparisons of Spo11-oligo counts in hotspots between wild type and *set1* mutant data sets. *set1* map is scaled to 40% of wild-type map in total reads. Red and cyan dashed lines indicate the diagonal line (fold change equals to 1) and genome average change (*set1*/wild type = 40%), respectively. (B) Proportion of changed hotspots in Spo11-oligo maps (*set1*/wild type) (see main text). (C) Fold change (*set1*/wild type) of Spo11-oligo counts in hotspots, grouped according to (B). (D) Comparison of *set1* fold change in Spo11-oligo maps with that measured by Southern blot. [a] data are from Borde et al., 2009. (E) Spo11 oligos in the hotspot at the promoter of *PES4*.

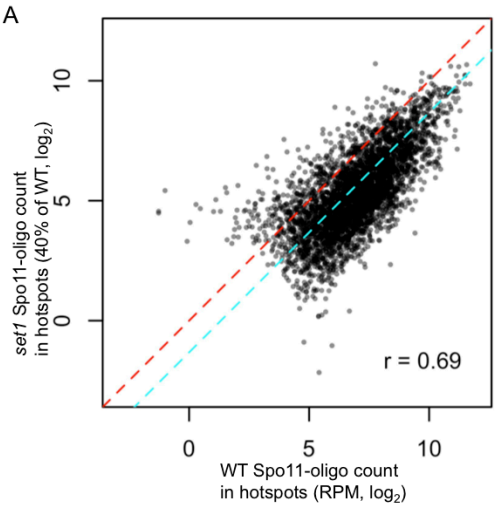

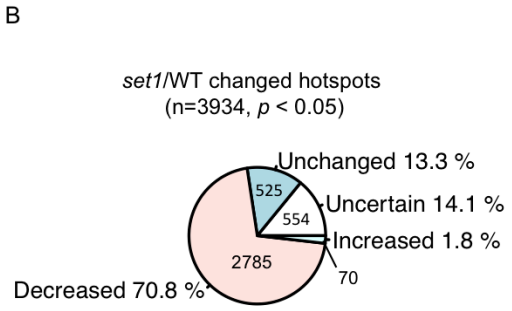

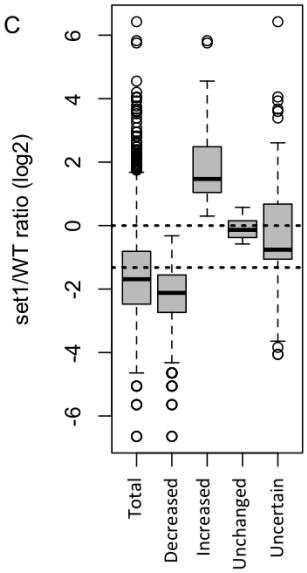

D

Hotspot	*set1* fold change in Spo11-oligo maps	*p* value in Spo11-oligo maps	*set1* fold change by Southern blot[a]
YCR047C	0.17	4.5×10^{-3}	0.28
FTR1	0.55	0.38	1.20
SET4	2.83	0.21	1.62
PES4	7.72	7.7×10^{-3}	14.0

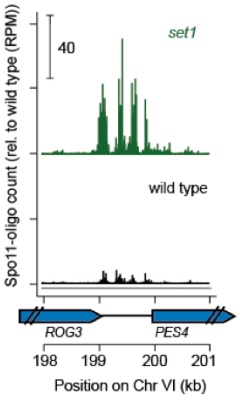

(change is greater than 1.5 fold but not statistically significant) (**Figure 4.6C**). The uncertain group of hotspots were a mixture of changed and unchanged hotspots, which I cannot discern in this study. Taken together, deletion of Set1 grossly affects DSB hotspot activity and thus the genome-wide DSB landscape.

To validate the changed hotspots, I compared the fold change in *set1* obtained from Spo11-oligo maps with that measured by independent physical assays. The direction of changes (increasing or decreasing) was consistent between this study and Southern blot analysis of hotspots (Borde *et al.* 2009), except the hotspot at the promoter of *FTR1*, which was decreased to 0.55-fold of wild-type level in Spo11-oligo maps but was 20% increased when measured by Southern blot (**Figure 4.6D**). However, there were discrepancies between the fold changes measured by these two different approaches. I cannot distinguish whether the discrepancies are from the *dmc1* mutant background (see Introduction) or from measurement errors in either Spo11-oligo maps or physical assays.

In contrast to the impression from low-sensitivity "hotspots" called in Borde *et al.* 2009, there were very few completely new hotspots in *set1*, and most of the increased hotspots in *set1* were weak DSB sites in wild type (**Figure 4.6A**). One example was the hotspot at the *PES4* promoter, which experienced more than 7-fold increase in *set1* mutants. Although the DSB frequencies were significantly different, the spatial patterns of Spo11-oligos were still similar in wild type and in *set1*, with four clusters of DSBs within this hotspot (**Figure 4.6E**). This suggests that there are very few *de novo* hotspots in *set1*. Moreover, *set1* does not affect the selection of DSB sites within hotspots, but changes the relative DSB frequencies among different hotspots. The selection of DSBs within hotspots are probably still constrained by DNA accessibility and local nucleotide composition (**Figure 1.3**, **Chapter 1**).

Regions near centromeres and rDNA are more decreased in *set1*

To test if the DSB reduction occurred evenly across the genome, I compared changes in Spo11-oligo counts in hotspots grouped by chromosomal context. Regions near centromeres and rDNA showed more reduction on average in *set1* (**Figure 4.4** and **Figure 4.7A**); thus, H3K4me3-dependent tethering of chromatin loops to the axis is likely to contribute more to the DSB formation in these regions in wild-type scenario. Additionally, the zone near telomeres showed slightly less decrease than the total hotspots (**Figure 4.4** and **Figure 4.7A**). Taken together, although these regions were all suppressed in wild type, they behaved differently in *set1*.

The increased hotspots are located in regions of low H3K4me3 in wild type

Although *set1* decreases DSB frequencies in 70.8% of the hotspots, 1.8% of hotspots are elevated. To investigate the reasons for these differences, I examined the wild-type H3K4me3 levels in three types of DSB hotspots: significantly reduced in *set1*, induced in *set1* and not affected by *set1* (**Figure 4.7B**). High levels of H3K4me3 were associated with decreased hotspots, whereas increased and unchanged hotspots were located in regions of low H3K4me3 (**Figure 4.7B**). In particular, increased hotspots showed extremely low H3K4me3 nearby in wild type, as suggested previously using imprecisely defined "hotspots" (Borde *et al.* 2009) (see Introduction). In summary, the absence of H3K4me3 in *set1* mutants most strongly impairs DSB formation at highly trimethylated sites but enhances DSBs in regions of low trimethylation in wild type.

The increased hotspots are closer to the chromatin axis

Spp1 tethers the chromatin loop (where DSBs occur) to the axis (where DSB machinery is located) (Acquaviva *et al.* 2013; Sommermeyer *et al.* 2013). In *set1*,

Figure 4.7 DSB patterns in *set1* mutants. (A) Change in Spo11-oligo counts in hotspots grouped by chromosomal context. Tel, within 20 kb of telomeres; Cen, within 10 kb of centromeres; rDNA, from 60 kb leftward to 30 kb rightward of rDNA; Interstitial, all others. Dashed lines mark values assumed as no change and average change (40% of WT). *, $p < 0.05$; **, $p < 0.01$ (Wilcoxon test) (B) Wild-type H3K4me3/H3 ratios in differently changed hotspots in *set1Δ*. H3K3me4/H3 ratios were summed in 500 bp windows that are 200 bp away on either side of hotspot midpoints. (C) Distance from the nearest Rec8 peak to the hotspots significantly reduced, increased, unchanged or uncertain hotspots in *set1*. (D) Genome average nucleosome occupancy and Spo11-oligo counts (in RPM, unscaled) around all annotated +1 nucleosomes. Dashed lines show the position of +1 nucleosomes. (E) Model for proposed DSB formation mechanism in the absence of H3K4me3 in *set1* mutants (see main text).

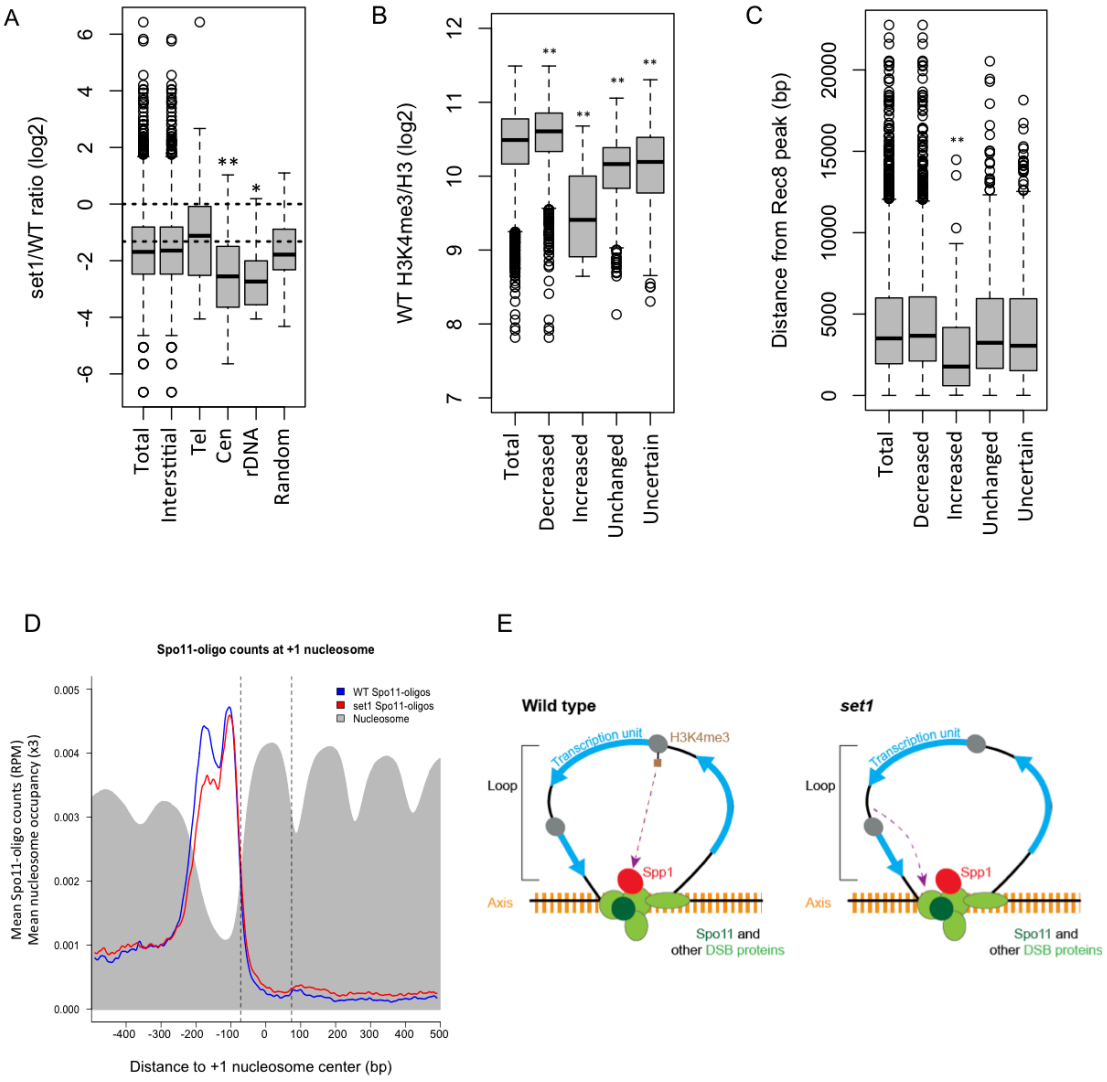
A
set1/WT ratio (log2)
Total
Interstitial
Tel
Cen
rDNA
Random
B
WT H3K4me3/H3 (log2)
Total
Decreased
Increased
Unchanged
Uncertain
C
Distance from Rec8 peak (bp)
Total
Decreased
Increased
Unchanged
Uncertain
D
Spo11-oligo counts at +1 nucleosome
WT Spo11-oligos
set1 Spo11-oligos
Nucleosome
Mean Spo11-oligo counts (RPM)
Mean nucleosome occupancy (x3)
Distance to +1 nucleosome center (bp)
E
Wild type
set1
Transcription unit
H3K4me3
Loop
Axis
Spp1
Spo11 and
other DSB proteins

since H3K4me3 is absent, Spp1 cannot bind the loop via H3K4me3 to promote DSB formation, suggesting that new or increased hotspots in *set1* are activated by alternative DSB-promoting mechanisms. One possibility is that these hotspots are located near the axis where DSBs are suppressed in wild type (Ito *et al.* 2014), but they are promoted to compensate for the global DSB reduction in *set1*. Indeed, I found that the increased hotspots were significantly closer to the axis (as defined by Rec8 ChIP peaks (Megan van Overbeek, et al. In preparation)), and the increased and unchanged hotspots were closer to the axis than decreased hotspots (**Figure 4.7C**). Similarly, Borde and colleagues showed that DSB sites that are strongly impaired by *set1* were significantly further from a Red1 association peak (another axis-associated protein) than DSBs that are more frequent in *set1* (Borde *et al.* 2009).

Deletion of Set1 alters the fine-scale DSB distribution near +1 nucleosomes

Finally, I reasoned that if Spp1 anchors +1, +2 and +3 nucleosomes where H3K4me3 is enriched onto the axis, DSBs in *set1* might be differentially distributed depending on their distance from these nucleosomes. To investigate fine-scale Spo11-oligo patterns, I extracted Spo11-oligo counts within 1 kb window around all annotated +1 nucleosomes in both wild type and *set1* mutants, scaled the counts to the total counts in the window for each nucleosome, and averaged the scaled counts (**Figure 4.7D**). In wild type, Spo11-oligos showed two peaks of similar heights in the NDR near the +1 nucleosome. In *set1,* the peak close to the +1 nucleosomes remained, but the peak distal to the +1 nucleosome was reduced, indicating the spatial change in DSB distributions (**Figure 4.7D**). Thus, although Spo11 is likely to cleave the same sites within promoters in the *set1* mutant (see previous sections), the relative DSB frequency at these sites was altered depending on their distances to the +1 nucleosome.

Discussion and Conclusions

The role of H3K4me3 on DSB formation

Here we provide the precise profiling of changes in DSB landscape in the absence of H3K4me3. The fact that the majority of hotspots experience reduced DSB activity in *set1* points to an important role of H3K4me3 in targeting Spo11 activity in these hotspots. Although H3K4me3 is a poor predictor of DSB frequency (Tischfield and Keeney 2012), these decreased hotspots are near H3K4me3-enriched regions (**Figure 4.7B**), supporting the tethered loop-axis model mediated by the interactions between H3K4me3, Spp1 and Mer2 (illustrated in the wild-type scenario in **Figure 4.7E**). However, similar to other factors that regulate DSB hotspots (such as organization of loop-axis chromatin structure, NDR and transcription factors), H3K4me3 is only one layer of the hierarchical control of DSB landscape. For example, two NDRs close to nucleosomes with the same H3K4me3 enrichment may have different DSB activities due to different DNA accessibility.

H3K4me3-independent strategies for Spo11 targeting

H3K4me3-dependent tethering is a general mechanism to target DSB formation in promoter NDRs (Borde *et al.* 2009; Acquaviva *et al.* 2013; Sommermeyer *et al.* 2013). Although DSB formation is reduced in most hotspots in the absence of Set1, 70 (1.8%) hotspots are significantly elevated and 525 (13.3%) hotspots are unaffected, suggesting the existence of alternative DSB-promoting mechanisms (**Figure 4.6B**). Indeed, these hotspots (especially the increased ones) are in the proximity of low level of H3K4me3 in wild-type cells (**Figure 4.7B**) (Borde et al., 2009). Furthermore, increased hotspots are located mostly in chromatin loop regions closer to the axis than decreased hotspots (**Figure 4.7C**) (Borde et al., 2009),

indicating that the H3K4me3-independent targeting mechanism works in a relatively short distance from the axis (**Figure 4.7E**).

It has been proposed that transcription plays a prominent role in selecting DSB sites in the absence of Set1 (Borde *et al.* 2009; Acquaviva *et al.* 2013; Sommermeyer *et al.* 2013). Five of the six most induced DSB hotspots in *set1* were found in the promoter of genes induced in *set1*. Transcription activation can shift mitotic cohesins from genes (Glynn *et al.* 2004; Lengronne *et al.* 2004). This raises the possibility that induced genes in *set1* shift Rec8 from the gene promoter to the end of the gene in *set1*, permitting DSBs to occur in the promoter, as observed in *PES4* promoter (Borde *et al.* 2009; Acquaviva *et al.* 2013; Sommermeyer *et al.* 2013). It will be interesting to map the genome-wide Rec8 localization in *set1* or *spp1* mutants to determine changes of Rec8 association and correlate them with DSB changes.

The feedback control of DSB numbers compensates for the DSB reduction in *set1* mutants

As potentially hazardous events, meiotic DSBs are tightly controlled in their timing, amount, and location. This is achieved by a complex network of regulatory circuits (Keeney *et al.* 2014). Although too many DSBs can cause repair problem for cells, a minimum amount of DSBs is required to support successful chromosome pairing and synapsis (Kauppi *et al.* 2013a). In *S. cerevisiae*, trimethylation of H3K4 by Set1 plays a key role in forming DSBs in NDR in promoters (Borde *et al.* 2009; Acquaviva *et al.* 2013; Sommermeyer *et al.* 2013). However, Set1 is dispensable for DSB formation per se, in that DSBs form in relatively normal numbers but at different locations in absence of Set1 (**Figure 4.1 and 4.6A–B**) (Borde et al., 2009). This can be explained in part by the cellular compensation for the reduction in DSB number. In

set1, the homeostatic responses of Spo11-regulating circuits will adjust, allowing DSB formation in places that are inhibited or not preferred in wild type.

A similar case was observed in *Prdm9*$^{-/-}$ mutant mice (Brick *et al.* 2012). PRDM9 is a histone 3 trimethylase as well as a key determinant of the preferred DSB and recombination hotspot location in mice (see **Chapter 1**). Surprisingly, *Prdm9*$^{-/-}$ mutant mice are still proficient in DSB formation but at new locations (promoters and near PRDM9-independent H3K4me3 loci), which are rarely targeted in wild-type mice (Brick *et al.* 2012). Hence, the feedback control of DSB numbers compensates for the DSB reduction in these mutants.

Chapter 5: Concluding discussion

Main conclusions

Genome-wide high-resolution mapping of meiotic DSBs by sequencing Spo11 oligos in different mutants provides a powerful tool to elucidate the roles of these factors on DSB formation.

In **Chapter 3**, my analysis of TF mutants *bas1* and *ino4* demonstrated that approximately 13% (*bas1*) and 30% (*ino4*) of hotspots showed detectable changes in DSB frequency using non-stringent criteria, but few hotspots had changed by more than two fold (0.7% and 3.1%, respectively). I also mapped Bas1 and Ino4 binding sites in meiotic cells. Absence of either TF altered DSB activity at many more genomic locations than were detectably bound by the protein during meiosis, confirming and extending prior results implying that TF roles in controlling DSBs are frequently indirect. For Bas1, direct binding during meiosis was a significant but imperfect predictor that DSB activity would change when the TF was missing, but direct binding by Ino4 was not predictive. For both TFs, DSBs increased at some binding sites and decreased at others when the TF gene was deleted, supporting the conclusion that, even at those sites where DSBs are most likely to be directly influenced by the TF, not only the magnitude but even the direction of TF influence is highly context dependent. Therefore, consistent with a previous report on *bas1* mutant (Mieczkowski *et al.* 2006), the effect of TF mutations on DSB activity is context-dependent and frequently indirect. However, it is still unclear what causes the changes in hotspot activity in TF mutants. To explore the potential mechanisms, I examined global histone H3 lysine 4 methylation patterns as well as local chromatin structure around individual DSB hotspots in wild type and the TF mutants. Counter to prevailing models, effects of these TFs on DSB hotspot strength cannot be simply

explained via chromatin "openness", histone modification, or compensatory interactions between adjacent hotspots.

H3K4me3 plays an important role in spatial coordination of DSB formation within the context of the loop and axis higher-order chromatin structure in *S. cerevisiae.* In the "tethered loop-axis complex" model, DSBs are formed in loop segments captured by axis-associated DSB machinery (Blat *et al.* 2002; Panizza *et al.* 2011). Spp1 reads and brings H3K4me3 regions to the chromatin axis to activate DSB formation in the nearby NDR regions (Acquaviva *et al.* 2013; Sommermeyer *et al.* 2013). In the absence of H3K4me3 in *set1* mutants, DSB formation is strongly reduced, while several new DSB sites appear (Borde *et al.* 2009). However, previous studies are limited by relatively low spatial resolution. In **Chapter 4**, I re-mapped DSB distribution in *set1* mutants using Spo11-oligo mapping. With the accurate and high-resolution maps, I revealed that 70.8% of hotspots were decreased and 1.8% of hotspots were increased in *set1* mutants. Furthermore, I discovered that for those "new" DSB sites in the previous study, DSBs occur on the same preferable bases as in wild type, with increased frequencies. I also confirmed and extended the previous observations that these increased hotspots tend to be located in the promoters of genes with low H3K4me3 levels and closer to the chromatin axis. Thus, meiotic cells have a robust system to target Spo11 activity to chromatin loops: H3K4me3-dependent tethering is the predominant mechanism for DSB site selection, and abolition of H3K4me3 activates alternative DSB-promoting mechanisms.

Lastly, DSBs are substantially suppressed near telomeres, centromeres and rDNA (Baudat and Nicolas 1997; Gerton *et al.* 2000; Borde *et al.* 2004; Blitzblau *et al.* 2007; Buhler *et al.* 2007; Pan *et al.* 2011; Vader *et al.* 2011). Sir2 and Pch2 have been shown to suppress DSB activity in and around rDNA (Mieczkowski *et al.* 2007; Vader *et al.* 2011). Consistent with previous studies, in the **Appendix**, my analysis of

Spo11-oligo maps in *pch2* and *sir2* mutants showed elevated DSB activities in the regions close to rDNA. In addition, *sir2* mutant exhibits more suppression of DSBs in regions beginning ~10–20 kb from the telomeres and extending ~120 kb toward the centromere. Interestingly, like Sir2, Pch2 is involved in shaping DSB landscape in subtelomeric regions, probably via the same pathway of Sir2. Moreover, average DSB frequency is increased in *pch2* within ~25–35 kb from centromeres, which was not observed in *sir2* and other mutants I analyzed. Thus, Pch2 regulates DSB distribution near centromeres. Pch2 and Sir2 seem to have both related and separate roles in controlling DSB formation. The impact of such derepression events is discussed below.

Scale-dependent features of DSB spatial patterns

DSBs predominantly occur in hotspots 50–250 bp wide (Baudat and Nicolas 1997; Pan *et al.* 2011). To understand how DSB distributions are shaped at the scale of hotspot level or smaller, the resolution of DSB maps must match or exceed sub-kb scale. Early studies mapped DSBs using Spo11-associated DNA at DSB sites that accumulate in *rad50S*-like mutants, or ssDNA generated by DSB resection as microarray probes (Gerton *et al.* 2000; Blitzblau *et al.* 2007; Buhler *et al.* 2007; Robine *et al.* 2007). The resolution of these studies was usually several kb due to microarray probe spacing and the large size of enriched DNA fragments hybridized to the arrays. With these low-resolution DSB maps, general trends could be seen by comparing DSBs in a large region to genome averages (Berchowitz *et al.* 2009; Borde *et al.* 2009), but sub-kb-scale features of the DSB landscape could not be well characterized. The "hotspots" were usually defined as peaks in hybridization signal, which were relatively large domains that merged overlapping hybridization signals from multiple nearby hotspots and cannot be assigned to individual DSB hotspots

(**Figure 3.1E** and **Figure 4.5**) (Pan *et al.* 2011). As a result, early microarray studies of *rad50S*-like mutants were only able to identify ~200–600 discrete hotspots, with only partial agreement between these studies (Gerton *et al.* 2000; Borde *et al.* 2004; Mieczkowski *et al.* 2006; Mieczkowski *et al.* 2007; Robine *et al.* 2007). Later studies using *dmc1* mutants greatly improved the picture by identifying ~1000–2000 hotspots (Blitzblau *et al.* 2007; Buhler *et al.* 2007; Borde *et al.* 2009). However, this was only approximately half of the number of hotspots accurately identified in the Spo11-oligo maps (Pan *et al.* 2011). Furthermore, it is difficult to associate low-resolution DSB sites with chromosomal features, such as promoters, transcription start sites, nucleosomes and their modification. Developing high-resolution maps is necessary to solve this issue. For example, to investigate if fine patterns of DSBs are changed in *set1* within hotspots, Spo11-oligo mapping data allow the alignment of DSB sites with +1 nucleosomes to explore changes in the fine-scale pattern (**Figure 4.7D**).

Consequences of DSB mis-regulation in subchrosomomal domains

The rDNA contains ~100–200 tandem repeats of a 9-kb sequence that encodes ribosomal RNA genes, and comprises almost 10% of the genome (Eickbush and Eickbush 2007). Repair of DSBs inside or near rDNA can cause non-allelic homologous recombination between rDNA repeats, resulting in an increase or decrease in rDNA copy number. When the copy number is reduced by spontaneous recombination in mitosis, cells amplify the rDNA repeat to make up for the missing copies (Kobayashi 2011). It has been proposed that this compensatory mechanism helps maintain the level of protein synthesis. Nevertheless, only half of the rDNA copies are actively transcribed, raising the question about the biological significance of maintaining such a high copy number (Kobayashi 2011). Further study revealed that when the rDNA copy number was reduced to ~20 copies, cells showed normal

growth but an increased sensitivity to DNA damaging agents such as ultraviolet light and methyl methanesulfonate (Ide *et al.* 2010). Thus, the high copy number of rDNA may contribute to genome stability with unknown mechanisms (Kobayashi 2011). Therefore, meiotic DSBs in or near rDNA can change rDNA copy number, which may not affect spore viability but sensitize cells to endogenous and exogenous DNA damages.

Subtelomeric regions are abundant with low-copy repeats such as highly repetitive subtelomeric repeat families and multigene families. Thus, formation of DSBs in these regions can induce non-allelic homologous recombination, which may result in exchanges of chromosome ends (Louis and Haber, 1992). The existence of these repeated genes and elements is evidence of ancient non-allelic exchanges of chromosome ends (Cohn *et al.* 2005). Furthermore, previous studies suggested frequent exchanges of chromosome ends in both mitotic and meiotic cells (Horowitz *et al.* 1984; Louis and Haber 1992; Louis *et al.* 1994), indicating that such recombination may not be that detrimental. Subtelomeric regions contain few essential genes, but they are enriched with duplicated genes involved in secondary metabolism, toxin resistance and cell-to-cell interaction (Cohn *et al.* 2005). Thus, subtelomeric recombination may promote cellular fitness in stressful environments.

Meiotic DSBs near centromeric regions can affect chromosome segregation due to premature dissociation of cohesion near the centromeres. Cohesion is mediated by cohesin complexes, which has been proposed to form a ring structure that encircles sister chromatids (Losada and Hirano 2005; Nasmyth and Haering 2005). In meiosis, cohesion on chromosome arms is released at anaphase I when homologous chromosomes begin to segregate. Cohesion near the centromere remains until anaphase II when sister chromatids separate and segregate (Lee *et al.* 2005; Nasmyth and Haering 2005; Watanabe 2005). The repair of pericentric DSBs by recombination

may disrupt pericentric cohesion and cause premature separation of sister chromatids at meiosis I (Rockmill *et al.* 2006). Therefore, DSBs near centromeres can lead to aneuploidy and spore inviability.

Understanding mechanisms that shape the meiotic DSB landscape

The spatial pattern of DSBs is not determined by a single factor but is instead shaped by a combination of factors acting at different scales (**Figure 1.3**) (Lichten and Goldman 1995; Petes 2001; Kauppi *et al.* 2004; Lichten and De Massy 2011; Pan *et al.* 2011; De Massy 2013a; Lam and Keeney 2014). For instance, as one layer of DSB control, DSBs are substantially suppressed in regions near telomere, centromere and rDNA (Baudat and Nicolas 1997; Gerton *et al.* 2000; Borde *et al.* 2004; Blitzblau *et al.* 2007; Buhler *et al.* 2007; Pan *et al.* 2011; Vader *et al.* 2011). Analysis of *pch2* and *sir2* mutants revealed the genetic requirements for this suppression (Mieczkowski *et al.* 2007; Vader *et al.* 2011) (and this study). Thus, Pch2 and Sir2 act in specific large subchromosomal domains (working on 10–100 kb scale). Within these domains, Spo11 is still likely to cut NDRs, which is not affected by deleting Pch2 or Sir2, indicating another layer of DSB control (working on sub-kb scale). Furthermore, different layers of DSB controls can interact with each other. For example, H3K4me3 is read and bound by Spp1, which brings the NDR in chromatin loops to axes, targeting Spo11 activity in NDR (Acquaviva *et al.* 2013; Sommermeyer *et al.* 2013). NDR itself is not sufficient for DSB formation, and DSB activity requires the interaction between NDRs and chromatin axes. Moreover, some factors can affect more than one layer of DSB control, which makes it difficult to interpret the phenotype in the mutants. TFs can alter DSB activity presumably by influencing several layers of control: loop-axis architecture, interactions between axis-bound DSB proteins and loop chromatin, and DNA accessibility in NDR. To further dissect the

complexity of mechanisms that shape the DSB landscape, it will be useful to map DSB distributions in other relevant mutants and double mutants.

Methods

Yeast strains and culture methods

Strains used in this study are of the SK1 background and are listed in **Table M1**. The *bas1*, *ino4*, *pch2*, *sir2* and *set1* deletions were made by replacing the coding sequence with the hygromycin B phosphotransferase gene (*hphMX4*). The *sae2* deletion was made by replacing the coding sequence with the ClonNAT resistance gene (*natMX*). Gene disruption was verified by PCR and Southern blotting. The *SPO11-FLAG* construct was provided by Kunihiro Ohta (Kugou *et al.* 2009). All mutants analyzed were moved into the desired tester strain backgrounds by crossing and tetrad dissection. Synchronous meiotic cultures were prepared as described (Alani *et al.* 1990; Padmore *et al.* 1991). Briefly, cells were grown in YPA (1% yeast extract, 2% Bacto Peptone, 1% potassium acetate) for 13.5–14 hr at 30ºC, harvested, resuspended in 2% potassium acetate, and sporulated at 30ºC.

Generation and purification of anti-Spo11 polyclonal antibodies

Two peptides ([H]- MALEGLRKKYKTRQELVKAC -[NH2] and [H]-CKSIQLLSLNQRDYSLAKNLI -[NH2]) were synthesized by Covance. The mixture of both peptides was used as antigens. Antibodies were raised by Covance's Polyclonal Antibody Production – 2 Rabbits, 84-day protocol. Two rabbits were numbered as 353 and 354 by the company. Sera from these rabbits were further purified by SulfoLink Immobilization Trial Kit (Thermo Scientific) (for both 353 and 354) or Affinity Purification – Up to 110 mL of pooled sera service (Covance) (only for 353). Purified antibodies were stored in -80ºC.

Table M1
Yeast strains

Strain number	Genotype
SKY41	*MATa/MATα; ho::LYS2/"; lys2/"; ura3/"; leu2::hisG/"; his4X::LEU2/"; arg4-Nsp/"; nuc1D::LEU2/"*
SKY971	*MATa/MATα; ho::LYS2/'; lys2/'; leu2::hisG/"; trp1::hisG/"; arg4-Nsp/arg4-Bgl; spo11Δ::hisG-URA3-hisG/"*
SKY1510	*MATa/MATα; ho::LYS2/"; lys2/"; ura3/"; leu2::hisG/"; his4X::LEU2/"; arg4-Nspl"; nuc1Δ::LEU2/"; SPO11-HA3-His6::kanMX4 /"; sae2Δ::kanMX6/"*
SKY1629	*MATa/MATα; ho::LYS2/"; lys2/"; ura3/"; leu2::hisG/"; his4X::LEU2/"; arg4-Nspl"; nuc1Δ::LEU2/"; SPO11-HA3-His6::kanMX4 /"; dmc1Δ::LEU2/"*
SKY2024	*MATa/MATα; ho::LYS2/"; lys2/"; ura3/"; leu2/"; arg4-Nsp/ARG4; nuc1Δ::LEU2/"; rad50-KI81::URA3/"*
SKY2025	*MATa/MATα; ho::LYS2/"; lys2/"; ura3/"; leu2/"; nuc1Δ::LEU2/"; spo11-Y135F-HA3His6::kanMX/"; rad50-KI81::URA3/"*
SKY2222	*MATa/MATα; ho::LYS2/"; lys2/"; ura3/"; leu2::hisG/"; his4X::LEU2/"; arg4-Nspl"; nuc1Δ::LEU2/"; spo11Y135F-HA3-His6::kanMX4 /"*
SKY3367	*MATa/MATα; ho::LYS2/"; ura3/"; his4B::LEU2-Mlu1/"; SPO11-Myc18::TRP1/"*
SKY3459	*MATa/MATα; ho::LYS2/"; lys2/"; ura3/"; leu2/"; nuc1Δ::LEU2/"; spo11-HA3His6::kanMX/"; rad50-KI81::URA3/"*
SKY3472	*MATa/MATα; ho::LYS2/"; lys2/"; ura3/"; leu2/"; nuc1Δ::LEU2/"; SPO11-His6-flag3-loxP-kanMX-loxP/"; rad50-KI81::URA3/"*
SKY3821	*MATa/MATα; ho::LYS2/"; lys2/"; ura3/"; leu2/"; arg4-Bgll"; nuc1Δ::LEU2/"; SPO11-His6-flag3-loxP-kanMX-loxP/"*
SKY3860	*MATa/MATα; ho::LYS2/"; lys2/"; ura3/"; leu2/"; arg4-Bgll"; nuc1Δ::LEU2/"; SPO11-His6-flag3-loxP-kanMX-loxP/"; bas1Δ::hphMX/"; sae2Δ::NatMX/"*
SKY3880	*MATa/MATα; ho::LYS2/"; lys2/"; ura3/"; leu2/"; arg4-Bgll"; nuc1Δ::LEU2/"; SPO11-His6-flag3-loxP-kanMX-loxP/"; sae2Δ::NatMX/"*
SKY4019	*MATa/MATα; ho::LYS2/"; lys2/"; ura3/"; leu2/"; arg4-Bgll"; nuc1Δ::LEU2/"; SPO11-His6-flag3-loxP-kanMX-loxP/"; bas1Δ::hphMX/"*
SKY4209	*MATa/MATα; ho::LYS2/"; lys2/"; ura3/"; leu2/"; arg4-Bgll"; nuc1Δ::LEU2/"; SPO11-His6-flag3-loxP-kanMX-loxP/"; set1Δ::hphMX/"*
SKY4256	*MATa/MATα; ho::LYS2/"; lys2/"; ura3/"; leu2/"; arg4-Bgll"; nuc1Δ::LEU2/"; SPO11-His6-flag3-loxP-kanMX-loxP/"; sir2Δ::hphMX/"*
SKY4264	*MATa/MATα; ho::LYS2/"; lys2/"; ura3/"; leu2/"; arg4l"; nuc1Δ::LEU2/"; SPO11-His6-flag3-loxP-kanMX-loxP/"; pch2Δ::hphMX/"*
SKY4574	*MATa/MATα; ho::LYS2/"; lys2/"; ura3/"; leu2/"; his3::hisG/"; nuc1Δ::LEU2/"; SPO11-ProteinA::HIS5/"; rad50-KI81::URA3/"*
SKY4603	*MATa/MATα; ho::LYS2/"; lys2/"; ura3/"; leu2/"; arg4-Nspl"; nuc1Δ::LEU2/"; BAS1-myc13-KanMX/"*
SKY4680	*MATa/MATα; ho::LYS2/"; lys2/"; ura3/"; leu2/"; arg4-Bgll"; nuc1Δ::LEU2/"; SPO11-His6-flag3-loxP-kanMX-loxP/"; ino4Δ::hphMX/"*
SKY4696	*MATa/MATα; ho::LYS2/"; lys2/"; ura3/"; leu2/"; arg4l"; nuc1Δ::LEU2/"; INO4-myc13-KanMX/"*
SKY4846	*MATa/MATα; ho::LYS2/"; lys2/"; ura3/"; leu2/"; arg4/"; nuc1Δ::LEU2/"; SPO11-His6-flag3-loxP-kanMX-loxP/"; ino4Δ::hphMX/"; sae2Δ::NatMX/"*

Spo11-oligo mapping

Diploid strains with *SPO11-FLAG* were patched from a frozen stock onto a YP-glycerol plate and grown at 30°C overnight to select for respiration competence. Cells were streaked for single colonies on YPD plates and grown for 48 hr at 30°C. A single colony was inoculated into 20 ml liquid YPD medium and grown overnight at 30°C. The saturated YPD culture was used to inoculate 1 L YPA culture (plus 0.001% antifoam 204) in a 2.8 L baffled Fernbach flask to OD_{600} 0.2 and grown for 13.5–14 hr at 30°C. Cells were harvested by centrifugation, washed once in deionized water, resuspended in 1 L 2% potassium acetate and incubated in 2.8 L baffled flasks at 30°C for 4 hr (7 hr for *set1* mutants), which is the approximate time of peak Spo11-oligo levels.

Cell lysates were prepared by grinding frozen cell paste in a bead mill, similar to methods described (Thacker *et al.* 2014). The lysate was then diluted with an equal volume of 2× immunoprecipitation (IP) buffer (2% Triton X-100, 30 mM Tris-HCl, pH 8.0, 300 mM NaCl, 2 mM EDTA) and incubated with protein G agarose beads (Roche) for mock IP (4 hr at 4°C mixing end-over-end, 400 µl beads per 50 ml extract). Supernatant was removed into fresh tubes and the mock IP beads were stored on ice. The supernatant was incubated with 80 µl anti-FLAG antibody (Sigma) and 400 µl protein G agarose beads per 50 ml of extract for 4 hr at 4°C mixing end-over-end, then beads were recovered. Mock and IP beads were washed 3× with cold 1× IP buffer. Protein was eluted from mock or IP beads with 400 µl 2× NuPAGE LDS buffer (Invitrogen) by boiling for 5 min, followed by a second elution with 400 µl 0.5× NuPAGE LDS buffer. The eluates were combined and diluted with 800 µl of 2× IP buffer, then incubated with 125 µl fresh protein G agarose beads (mock) or 25 µl anti-FLAG antibody plus 125 µl protein G agarose beads (IP), 4°C overnight with end-over-end rotation.

The beads were recovered and resuspended in 400 μl proteinase K buffer (100 mM Tris-HCl, pH 7.4, 1 mM EDTA, 0.5% SDS, 1 mM $CaCl_2$) and 100 μg purified proteinase K, and incubated overnight at 50°C with end-over-end rotation. The supernatant was collected using a SPIN-X tube (Corning) and ethanol precipitated with 0.3 volume of 9 M ammonium acetate, 10 µg of DNA-free glycogen and 2.5 volumes of 100% ethanol. Spo11 oligos were then quantified and used for library preparation as described (Thacker *et al*. 2014). Sequencing was performed using Illumina HiSeq in the MSKCC Integrated Genomics Operation core facility.

Statistical analyses were performed using R version 3.0.1 (http://www.r-project.org/). Clipping of library adapters and mapping of reads to the sacCer2 genome assembly was performed using a custom pipeline as described (Pan *et al*. 2011; Thacker *et al*. 2014). After mapping, the reads were separated into unique and multiple mapping sets, but only uniquely mapping reads were analyzed in this study (multiple mapping reads constituted a small minority of the total). Each map was normalized to the total number of uniquely mapped reads (RPM or reads per million; excluding reads mapping to mitochondrial DNA or the 2µ plasmid), then maps for biological replicates were averaged. Hotspot calling was performed as described (Pan *et al*. 2011). In analyses evaluating the fold change in TF mutants, we assumed genome-wide numbers of DSBs are approximately the same in wild type and in the TF mutants, which agreed with direct DSB measurement by Southern blotting. The *bas1-2*, *bas1-3*, *bas1-4*, *ino4-1* and *ino4-2* data sets contained a small number of spurious reads (<0.3% of total in *bas1-2*, <0.04% of total in the other data sets) at positions 244,583 bp and 244,584 bp on chromosome V as well as 152,223 bp on chromosome III, likely from contamination of the Spo11-oligo sequencing libraries with PCR primers from those loci. These reads were deleted from the maps.

Detection of meiotic DSBs by Southern blot

Genomic DNA was prepared in agarose plugs as described (Borde *et al*. 2000; Murakami *et al*. 2009). DSB analyses for whole chromosomes and at individual hotspots were performed as described (Murakami *et al*. 2009; Pan *et al*. 2011; Thacker *et al*. 2014). For plots from pulse-field gel electrophoresis, DNA was probed with part of the *CHA1* open reading frame (SGD coordinates 15838 to 16857), *SKI8* (coordinates 90062 to 91228), *YHL042w* (coordinates 15671 to 16112), or *POT1* (coordinates 40223 to 40728). Restriction enzymes and primer sequences for amplification of probes for individual hotspots were as follows: *YAT1* hotspot, Xba I, *SWH1* probe (5'-CCAACTTCGCTCAAGGCTAC, 5'-TTGCAGCAATTCGTTCAAAG); *NAR1* hotspot, Afl II, *ATG2* probe (5'-GTGCACGAAA
ATATTGA, 5'-CGCCTTTGAAAGAAGCTTTG); *WHI5* hotspot, Stu I, *DIA2* probe (5'-TGAATTGGAGATACTGCAGACTTGTCCTCTG, 5'-CACTTATCGATGTCCCCATTAGATCC); *GCV2*/*MRPS17* hotspot, StuI, *MRPS17* probe (5′-TCCATCATGACGTGCTTTCT, 5′-AGCCCAAAAGGCAAAAGAAT); *GAT2*/*GID8* hotspot, XbaI, *PSO2* probe (5′-GCTTTCGTCCCACATGTCAT, 5′-TCGAAGCAACGCCAAAATGA); *SHM2* hotspot, NcoI-HF, *SHM2* probe (5′-GAGAATCGGTACCGTTGGAA, 5′-CAGGTGTCATCCCATCTCCT); *CHO2* hotspot, XbaI, *CYS4* probe (5′-CTGGTGGGACTATTAGCGGT, 5′-AAGAGTCAAAACGGGCCAAC); *ADO1*/*SOD1* hotspot, XbaI, *YPS25* probe (5′-AATAGAGCAAGCTTTCGGGC, 5′-ACCCGTCAACCCAATTCTTT); *FAS1* hotspot, XbaI, *ASH1* probe (5′-CGCTTAGAGGAGTAGAGGCC, 5′-GCTTGGAGTGTATGCCTTGG). Blots were quantified by phosphoimager.

ChIP to define Bas1 and Ino4 binding sites

Bas1 and Ino4 were C-terminally tagged with eight copies of the Myc epitope (*BAS1-Myc* and *INO4-Myc*). ChIP was performed as described (Murakami and Keeney 2014). ChIP efficiencies (percent of input) were measure by qPCR. DNA from ChIP and input samples collected from the tagged strains were sequenced (50-bp paired-end reads) on the HiSeq platform (Illumina). Reads were mapped to the *S. cerevisiae* sacCer2 genome assembly using BWA mem (version 0.7.5a-r405) to generate coverage maps for each data set. To remove regions with spurious mapping, the map from the input sample of the *BAS1-Myc* strain was used to define "mask regions" where the coverage was out of a fixed range (>1.5 SD from mean coverage). These regions were censored from further analysis. Coverage was normalized to the mean coverage calculated from the masked map. The normalized ChIP-seq coverage maps were smoothed using a 501-bp Parzen (triangular) sliding window. Using the smoothed coverage maps, peaks were called using as a threshold 2.0 × mean genome coverage. *De novo* motif discovery on sequences corresponding to windowed peaks was performed using MEME (Machanick and Bailey 2011).

Micrococcal nuclease (MNase) digestion of chromatin

Nuclei isolation, MNase digestion of chromatin, and proteinase K treatment were performed as described (Keeney and Kleckner 1996; Sasaki *et al*. 2013). After proteinase K treatment, reactions were precipitated with an equal volume of isopropanol and dissolved in 50 μl TE buffer. *SHM2* and *GCV2* hotspots were analyzed using the same restriction enzymes and probes as in direct DSB measurement above. Additional restriction enzymes and primer sequences for amplification of probes were as follows: *GAT2*/*GID8* hotspot, XhoI, *GAT2* probe (5′-CGCGCCTCTTCAAAAGTTAC, 5′-TGGTCCCTTTCTCCATTCTG); *CHO2*

hotspot, BmgBI (isoschizomer of BtrI), *CHO2* probe (5′-TTGATGAAAGCAAGAACTCCAA, 5′-CTCCAATGACCACCTGATCC); *ADO1*/*SOD1* hotspot, HpaI, *URA8* probe (5′-ACCACGTTCCCTTATTGCTG, 5′-TCCACCAGGAACCAAAATTC); *FAS1* hotspot, SalI-HF, *FAS1* probe (5′-TGGTGCGAAGAATCTAGTCG, 5′-CTCGGAAATGGAACCTGAAA).

ChIP-seq of histone H3 lysine 4 trimethylation (H3K4me3)

Approximately 250 OD units of cells were collected for each sample. Cells were crosslinked with 1% formaldehyde for 15 minutes and quenched with 125 mM glycine for 5 minutes at room temperature. Cells were collected and disrupted by bead beating in 200 μl lysis buffer (50 mM HEPES-NaOH, pH 7.5, 150 mM NaCl, 2 mM EDTA, 1% Triton X-100, 0.1% Na-deoxycholate). Chromatin was prepared and washed with MNase reaction buffer (10 mM Tris-HCl, pH 7.5, 50 mM NaCl, 5 mM $MgCl_2$, 1 mM $CaCl_2$, 1 mM β-mercaptoethanol, 0.1% Igepal) and digested to predominantly mono-nucleosomes with 2 units MNase at 37°C for 30 minutes. ChIP-seq was then performed on nucleosomes with anti-H3 (Abcam, ab1791) or anti-H3K4me3 (Abcam, ab8580) as described (Zhang *et al*. 2011b; Murakami and Keeney 2014). Reads were mapped to the sacCer2 genome assembly using BWA mem (version 0.7.5a-r405). The midpoint position of each paired-end read was extracted. The coordinate of the midpoints was shifted 73 bp towards both the 5′ and 3′ ends to generate nucleosome coverage maps. Each H3 or H3K4me3 map was normalized to the mean coverage. H3K4me3 enrichment was measured by taking the ratio of H3K4me3 ChIP signal to H3 ChIP signal. To prevent dividing by zero and to minimize variability of ratios caused by small changes in denominators, we added a small constant to the numerator and denominator before taking the ratio.

RNA-seq

15 OD units of cells were collected for each sample from meiosis 4 hr. Cells were resuspended in 500 µl Complete Buffer A (50 mM NaAc pH 5.2, 10 mM EDTA, 1% SDS). 750 µl equilibrated RNA phenol was added. Cells were disrupted by incubating at 65°C for 5 minutes with vortex for 10 seconds every minute and a half and placing on ice for 3 minutes. After spinning in a mini centrifuge at 13,000 rpm for 6 min, the bottom layer was removed. Phenol incubation and vortex were repeated, but the top layer was transfer to a new 1.5 ml tube this time. RNA was purified by two rounds of phenol/chloroform extraction, one round of chloroform extraction and ethanol precipitation. After ethanol precipitation, the pellets were resuspended in 100 µl TE (10 mM Tris-HCl pH 6.8, 1 mM EDTA). mRNA was enriched by poly-A selection and sequenced using Illumina HiSeq in the Genomics Resources Core Facility of Weill Cornell Medical College. Reads were mapped to the *S. cerevisiae* sacCer2 genome assembly using the Spliced Transcripts Alignment to a Reference (STAR) software (Dobin *et al*. 2013). Transcriptome assembly and differential expression analysis were performed using the Cufflinks software (Trapnell *et al*. 2010).

End-labeling of Spo11-oligo complexes and western blot analysis

Yeast lysates were prepared as previously described (Neale and Keeney 2009). Immunoprecipitation of Spo11-oligo complexes was performed using 5 µg of mouse monoclonal anti-flag M2 antibody (Sigma). Precipitated Spo11-oligo complexes were end-labeled in NEBuffer 4 (New England Biolabs) containing 5 µCi of [α-^{32}P]dCTP and terminal deoxynucleotidyl transferase (TdT) (Neale and Keeney 2009). 25 µl of reaction mixture was added to the beads, mixed, and incubated at 37ºC for 1–2 hr. Spo11-oligo complexes were eluted by adding 25 µl of NUPAGE® loading buffer

(diluted to 2× and supplemented with 83.3 mM dithiothreitol) (Invitrogen) and boiling for 5 min. End-labeled Spo11-oligo complexes were separated on a Novex® 4–12% gradient denaturing polyacrylamide gel (Invitrogen) then transferred onto PVDF membrane using the iBlot protocol (Invitrogen) and visualized by phosphorimager. For Western blotting, blots were probed with mouse monoclonal anti-flag M2 conjugated to horseradish peroxidase (Sigma). Chemiluminescent detection was performed according to the manufacturer's instructions (ECL+ or ECL Prime, Amersham). Protein quantity was estimated by separating 1 µl of extract on a Novex® 4–12% gradient denaturing polyacrylamide gel and staining with Coomassie Brilliant Blue.

APPENDIX

Analysis of meiotic DSB landscapes in *pch2* and *sir2* mutants

Introduction of Pch2 and Sir2. Pch2 is a widely conserved meiosis-specific ATPase, which has been identified in yeasts, fruit flies, worms and mammals. Mutational analyses in these organisms revealed the role of Pch2 in meiosis (San-Segundo and Roeder 1999; Bhalla and Dernburg 2005; Li and Schimenti 2007; Joyce and Mckim 2009; Wojtasz *et al.* 2009; Joyce and Mckim 2010; Roig *et al.* 2010). Pch2 was first identified as a meiotic checkpoint factor (San-Segundo and Roeder 1999). It interacts with DNA damage response proteins to promote checkpoint signaling triggered by unprocessed DSBs (Ho and Burgess 2011). *pch2Δ* can bypass the cell cycle arrest caused by *rad50S*-like mutants, "*zip*" mutants and *dmc1Δ* (San-Segundo and Roeder 1999; San-Segundo and Roeder 2000; Hochwagen *et al.* 2005; Wu and Burgess 2006; Zanders *et al.* 2011).

Recent studies showed that Pch2 regulates CO outcomes. Meiotic recombination occurs preferentially between non-sister homologous chromosomes. Formation of COs suppresses nearby COs, which allows a more even distribution of COs along the chromosome (i.e., a phenomenon called CO interference). *pch2Δ* mutants are defective in suppressing intersister repair (Ho and Burgess 2011; Zanders *et al.* 2011), and display elevated CO levels as well as defects in CO interference (Joshi *et al.* 2009; Zanders and Alani 2009).

Furthermore, *Pch2* is involved in DSB control. DSB formation decreases prominently in *pch2Δ rad50S* or *pch2Δ spo11-HA* mutants, whereas the impact remains mild in *pch2Δ dmc1Δ* or *pch2Δ rad51Δ dmc1Δ* mutants (Hochwagen *et al.* 2005; Wu and Burgess 2006; Vader *et al.* 2011; Zanders *et al.* 2011; Farmer *et al.* 2012). The DSB reduction in *pch2Δ rad50S* or *pch2Δ spo11-HA* mutants is highly

variable among chromosomes, with minimal impact on small chromosomes VI and III (Farmer *et al.* 2012). Finally, Pch2 suppresses meiotic DSB formation and recombination at the rDNA border (San-Segundo and Roeder 1999; Vader *et al.* 2011). The edges of the rDNA array are exceptionally susceptible to meiotic DSBs, and are protected by Pch2 and the origin recognition complex subunit Orc1. Upon disruption of these factors, DSB formation and recombination increased specifically in the outermost rDNA repeats and the region next to the rDNA, leading to non-allelic homologous recombination and rDNA instability (Vader *et al.* 2011).

In addition, Pch2 is required for the normal distribution of Hop1 along SCs in *S. cerevisiae* (Borner *et al.* 2008), probably by direct remodeling Hop1 protein structure (Chen *et al.* 2014). Taken together, Pch2 has multiple roles in meiotic checkpoints, CO control, DSB regulation and distribution of axis-associated protein Hop1.

Sir2 is a widely conserved NAD^+-dependent histone deacetylase, one of whose substrates is histone H4 lysine 16 acetylation (H4K16ac) (Sauve *et al.* 2006). This marker is found on transcriptionally active chromatin in most species and marks early firing origins in yeast and flies (Kimura *et al.* 2002; Suka *et al.* 2002; Schwaiger *et al.* 2010). Deacetylation of H4K16ac by Sir2 results in tighter packaging of chromatin and a reduction in transcription at targeted gene loci. Sir2 is involved in silencing telomeric genes, the silent mating type loci, and genes inserted in rDNA (Rusche *et al.* 2003). Furthermore, Sir2 suppresses meiotic recombination in rDNA (Gottlieb and Esposito 1989; San-Segundo and Roeder 1999). Deletion of Sir2 affects the DSB frequency of ~12% of genes (significantly elevating DSBs for 5% of the genes and reducing DSBs for 7% of the genes), most of which are located at subtelomeric regions or near the rDNA region (Mieczkowski *et al.* 2007).

Previous microarray-based mapping of DSBs in *pch2* and *sir2* mutants revealed some roles of these factors in DSB formation and distribution (Mieczkowski *et al.* 2007; Vader *et al.* 2011). However, the resolution of these maps is relatively low (usually several kb) due to the limitations in DNA sample preparation and hybridization. Therefore, I remapped genome-wide DSBs in *pch2* and *sir2* mutants using Spo11-oligo mapping technique.

Generating high-resolution DSB maps in pch2 and sir2 mutants. Spo11-oligos were purified from meiotic cultures of WT, *pch2* and *sir2* mutants, in which Spo11 was tagged at its C-terminus with a Flag epitope tag. Unlike *spo11-HA* strains, which exhibit a reduction of DSBs to ~70–80% of that in an untagged *SPO11* strain, *SPO11-Flag* strains show normal levels of DSBs, as measured by Southern blot (**Figure 2.1**). Furthermore, meiotic DSB level is severely reduced in *pch2Δ spo11-HA* strains, whereas *pch2Δ SPO11-Flag* strains show wild-type levels of DSBs, as measured by Spo11-oligo complex labeling (Drew Thacker, personal communication). Subsequently, Spo11-oligos were deep-sequenced with Illumina Hiseq, and the reads were mapped to the *S. cerevisiae* genome.

Each Spo11-oligo map was first normalized to the millions of reads mapped (reads per million, RPM). At sub-kilobase scales, DSBs are clustered in hotspots, mostly in nucleosome-depleted promoters. This pattern was unaffected in *pch2* and *sir2* mutants, in that DSBs formed in the same hotspots (**Figure A.1**). *pch2* maps and *sir2* maps showed slightly decreasing correlation with wild-type data sets (Pearson's r = 0.89 when comparing *pch2* and wild-type maps, r = 0.90–0.91 when comparing *sir2* and wild-type maps) (**Figure A.1 and A.2**). Maps from biological replicate cultures of the same genotype agreed very well with each other (Pearson's r = 0.98–1.00; **Figure A.1 and A.2**) and thus were averaged into consensus maps for further analysis. The fold change of Spo11-oligo counts (mutant/wild type) in non-overlapping 5 kb bins on

Figure A.1 Spo11-oligo maps in wild type and mutants. (A) Reproducibility of Spo11-oligo maps. (B) DSBs form at the same hotspots in mutants as in wild type. Spo11 maps are normalized to reads per million (RPM) and smoothed with 201-bp Hann window.

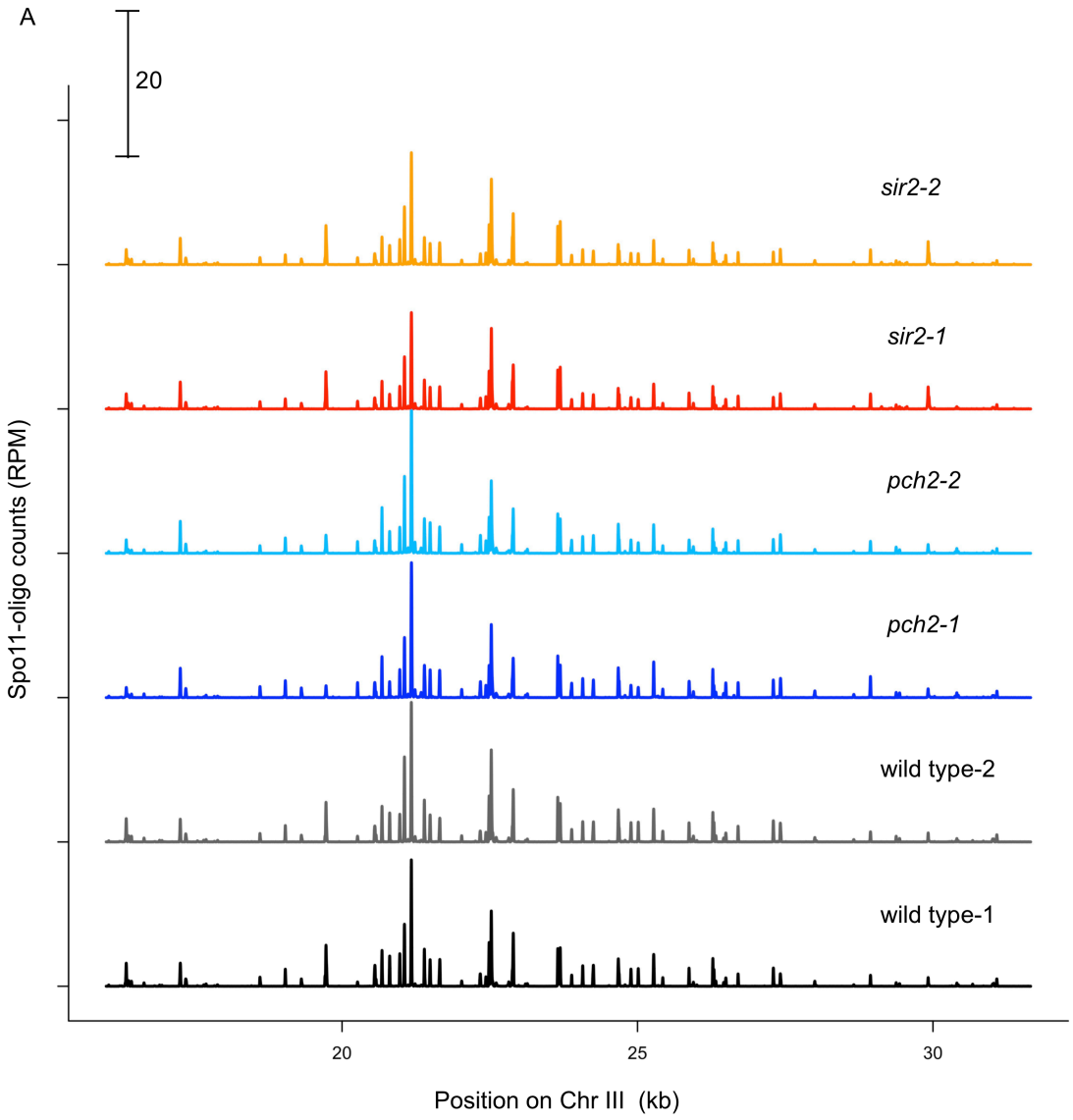
A
20
sir2-2
sir2-1
pch2-2
pch2-1
wild type-2
wild type-1
Spo11-oligo counts (RPM)
20
25
30
Position on Chr III (kb)

Figure A.1 (continued)

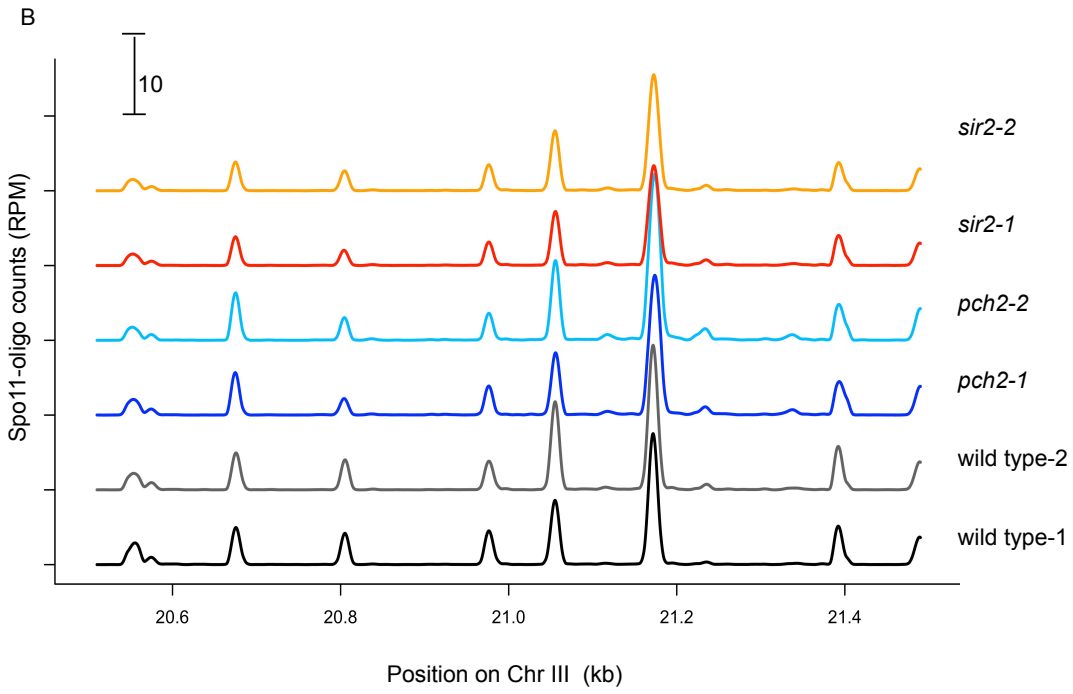

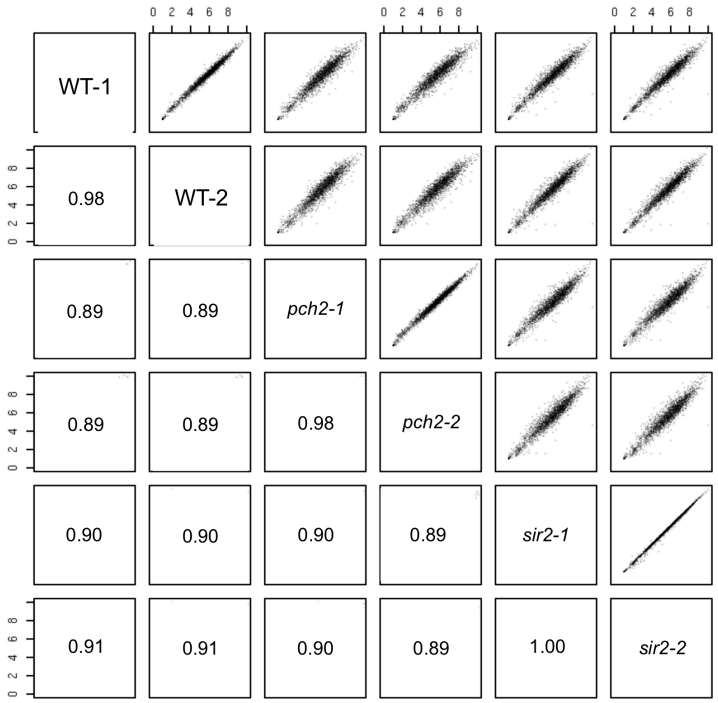

Figure A.2 Quantitative reproducibility of Spo11-oligo maps. Comparisons are shown for individual wild type (WT) or mutant datasets. Uniquely mapped Spo11 oligos were summed in non-overlapping 5-kb bins and expressed as reads per million (RPM) per kb (plotted on a log scale).Pairwise correlation coefficients are shown (Pearson's *r*).

all the chromosomes are shown in **Figure A.3 and A.4**. *pch2* and *sir2* mutants affected the genome-wide DSB landscape less severely than *set1* mutants (see **Chapter 4**). These affected DSB patterns are characterized in the following sections.

DSB activity around rDNA in pch2 and sir2 mutants. Recombination occurs 100-fold less frequently in the rDNA than in other regions, largely due to suppression of meiotic DSBs within rDNA, which is strongly dependent on Sir2-dependent heterochromatin formation (see **Chapter 1**) (Petes and Botstein 1977; Gottlieb and Esposito 1989; Mieczkowski *et al.* 2007). Furthermore, meiotic DSBs are also suppressed in regions flanking the rDNA array, which are the junctions between heterochromatin and euchromatin. *pch2* and *sir2* null mutants increased DSB frequency in the proximity of rDNA (**Figure A.3, A.4, A.5A–F**), consistent with published microarray-based DSB maps (Mieczkowski *et al.* 2007; Vader *et al.* 2011). Unlike *pch2*, which had a strong broad effect on both side of rDNA, *sir2* relieved DSB suppression predominantly on the left side of rDNA in a narrow region (**Figure A.3, A.4**).

Suppression of DSBs in subtelomeric regions in pch2 and sir2 mutants. Spo11-oligos are less frequent in the 20 kb closest to telomeres, consistent with the DSB suppression zones detected by ssDNA mapping (Blitzblau *et al.* 2007; Buhler *et al.* 2007; Pan *et al.* 2011). Deletion of *SIR2* showed more suppression of DSBs in regions beginning ~10–20 kb from the telomeres and extending ~120 kb toward the centromere (**Figure A.5G**), as suggested by Mieczkowski and colleagues (Mieczkowski *et al.* 2007). However, they also identified the elevation of DSB formation within ~ 10 kb of the chromosome ends in *sir2* mutants, which was not observed in my Spo11-oligo maps. This discrepancy is likely from strain background differences (their DSB maps were generated in the *rad50S* background). Thus, *rad50S* mutation may activate DSB formation within 20 kb from telomeres in *sir2* mutants.

Figure A.3 *pch2*/WT fold-change along 16 chromosomes. Both maps are normalized to reads per million before taking the ratio. Red lines show *pch2*/ WT ratios, which are calculated in 5 kb bins and smoothed by Lowess fit. Cyan points indicate centromere positions; green box illustrate the rDNA region (represented by two rDNA repeats) on chromosome XII. Dashed lines mark values assumed as 2-fold change.

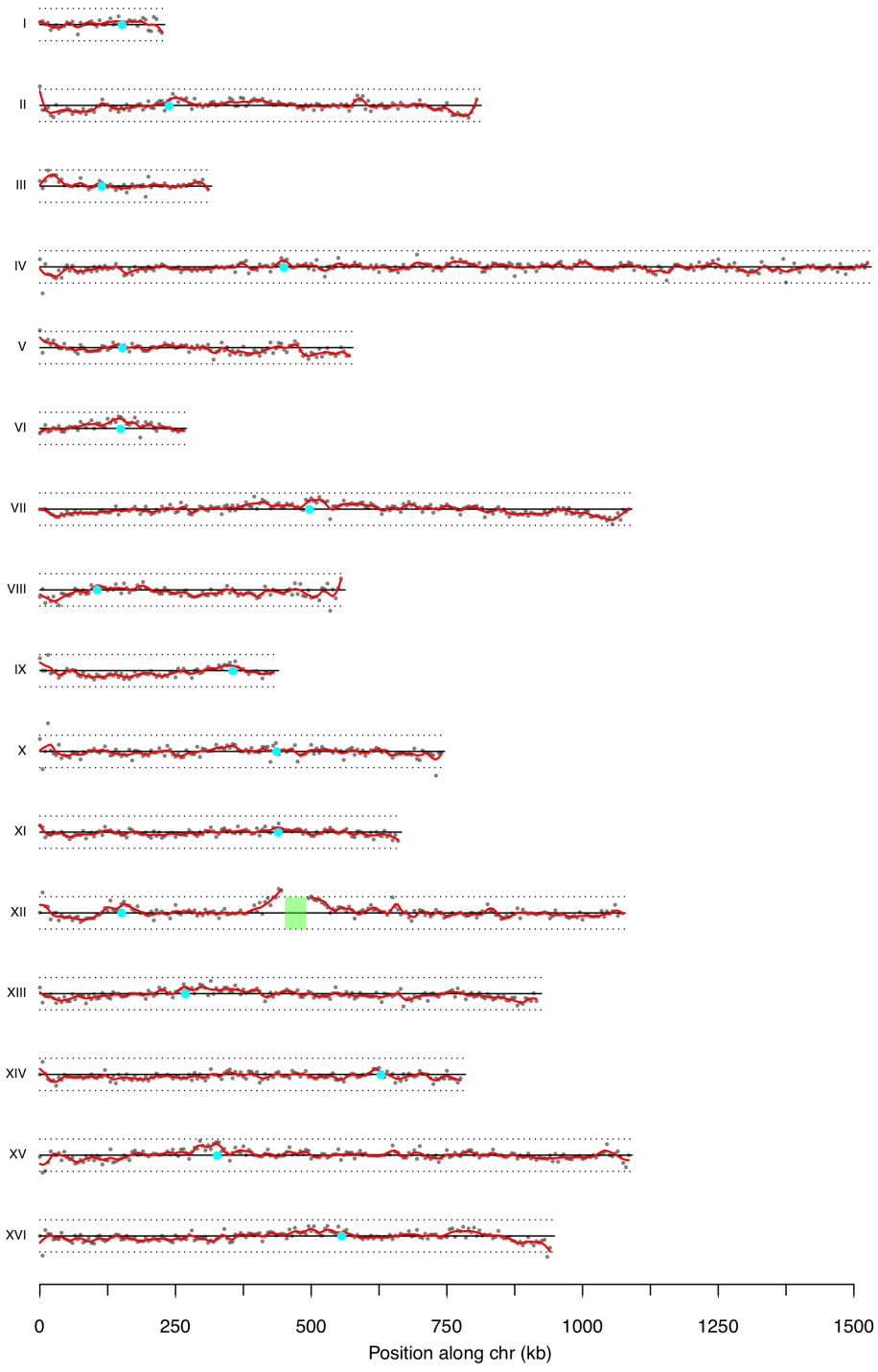
I
II
III
IV
V
VI
VII
VIII
IX
X
XI
XII
XIII
XIV
XV
XVI
0
250
500
750
1000
1250
1500
Position along chr (kb)

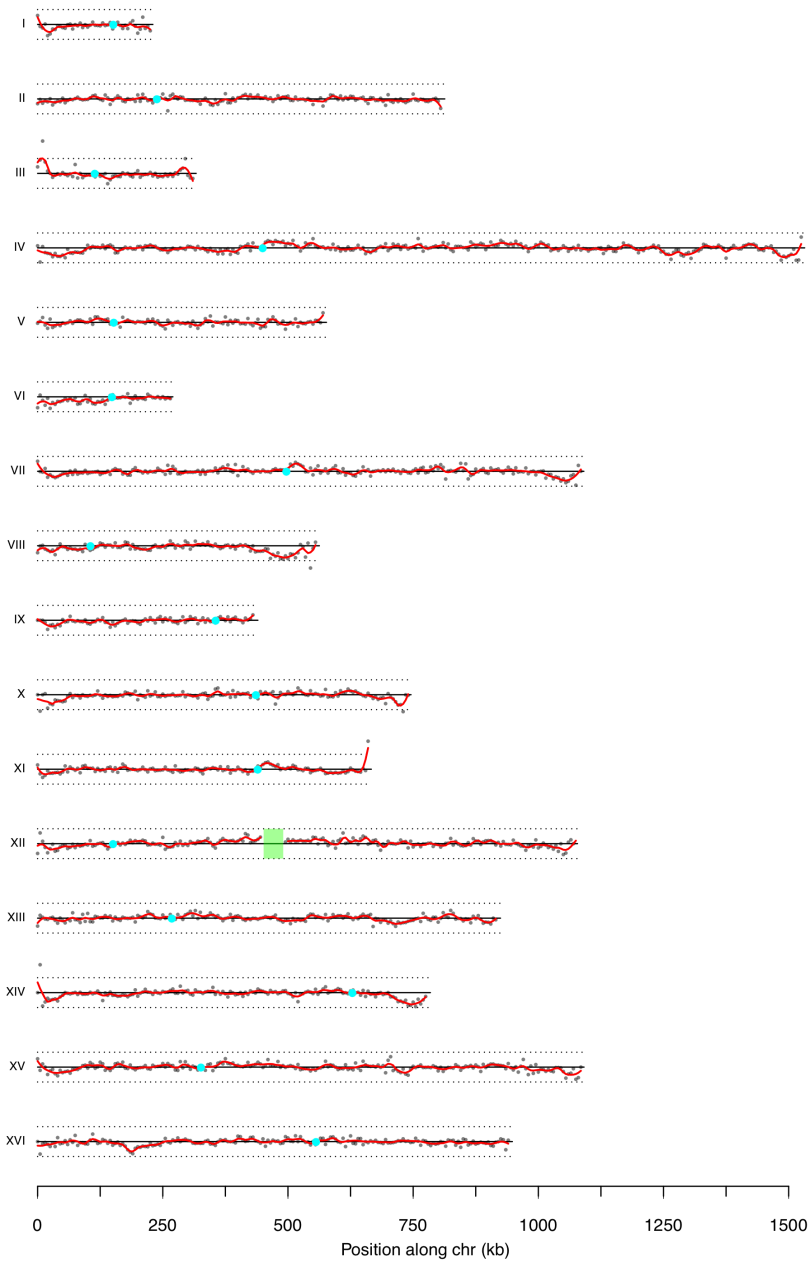

Figure A.4 *sir2*/WT fold-change along 16 chromosomes (labels as in Figure A. 3).

Figure A.5 Changes in the DSB landscape in *pch2* and *sir2* mutants. (A and C) Comparisons of Spo11-oligo counts in hotspots between wild type and mutant data sets. Subtelomeric, within 20 kb from telomeres; pericentric, within 10 kb from centromeres. Correlation coefficients are shown (Pearson's *r*). (B and D) Change in Spo11-oligo counts in hotspots grouped by chromosomal context. Red dashed lines mark values assumed as no change. Boxes indicate median and interquartile range; whiskers indicate the most extreme data points which are less than 1.5 times the interquartile range from the box; individual points are outliers. (E and F) Two wild-type biological replicate maps are compared as control. (G and H) *pch2* and *sir2* mutants suppress DSBs in 20–110 kb regions from telomeres, whereas DSBs are elevated within ~ 24 kb from centromeres. Oligo densities in 500 bp segments were averaged across all 32 chromosome arms and smoothed (Lowess). Dashed line shows genome average, and shading illustrates DSB suppression zones. These *sir2*- and *pch2*-specific phenotypes are not observed in transcription factor mutants *bas1* and *ino4*.

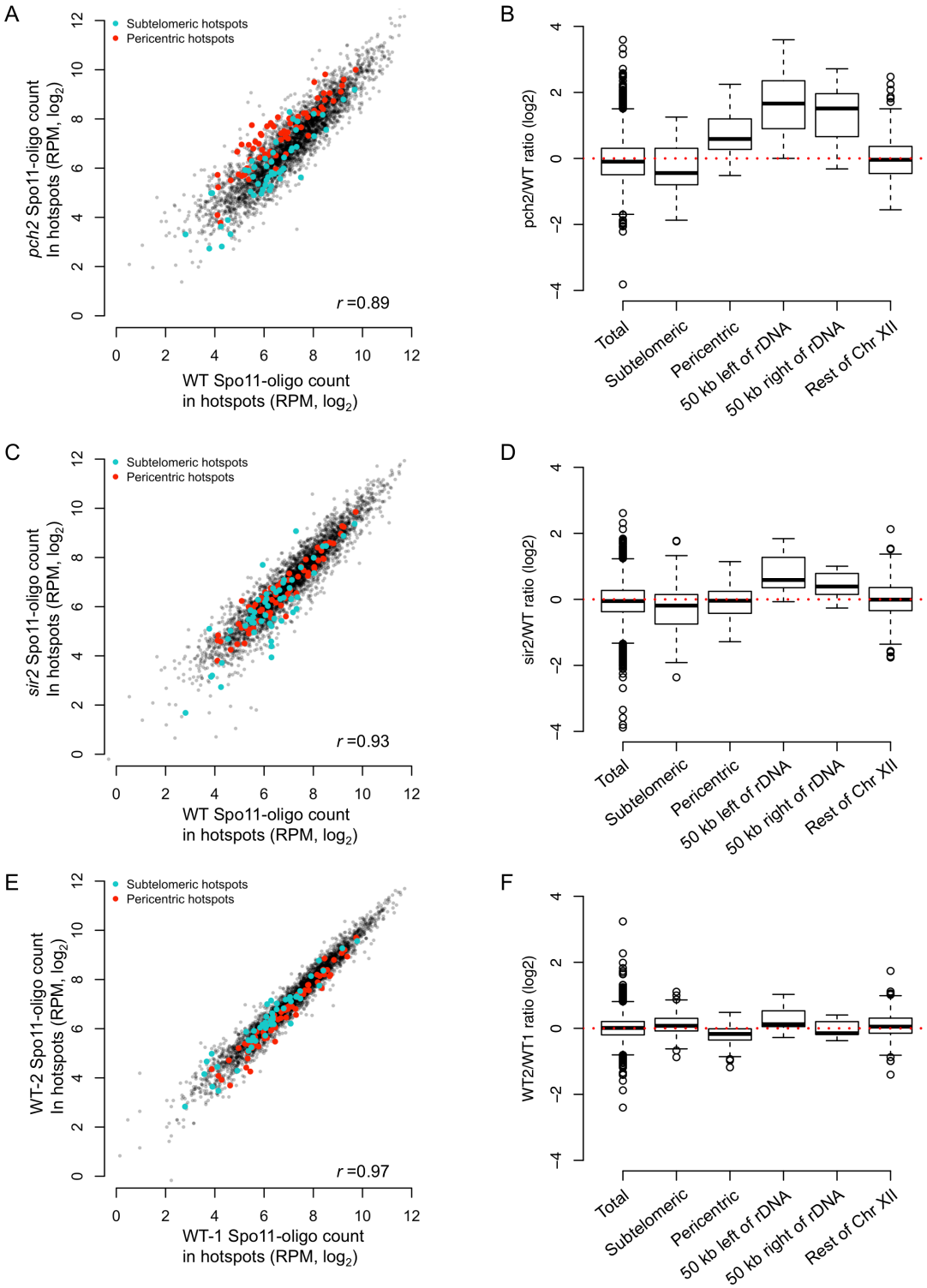
A
Subtelomeric hotspots
Pericentric hotspots
pch2 Spo11-oligo count
In hotspots (RPM, log2)
r =0.89
WT Spo11-oligo count
in hotspots (RPM, log2)
B
pch2/WT ratio (log2)
Total
Subtelomeric
Pericentric
50 kb left of rDNA
50 kb right of rDNA
Rest of Chr XII
C
Subtelomeric hotspots
Pericentric hotspots
sir2 Spo11-oligo count
In hotspots (RPM, log2)
r =0.93
WT Spo11-oligo count
in hotspots (RPM, log2)
D
sir2/WT ratio (log2)
Total
Subtelomeric
Pericentric
50 kb left of rDNA
50 kb right of rDNA
Rest of Chr XII
E
Subtelomeric hotspots
Pericentric hotspots
WT-2 Spo11-oligo count
In hotspots (RPM, log2)
r =0.97
WT-1 Spo11-oligo count
in hotspots (RPM, log2)
F
WT2/WT1 ratio (log2)
Total
Subtelomeric
Pericentric
50 kb left of rDNA
50 kb right of rDNA
Rest of Chr XII

Figure A.5 (continued)

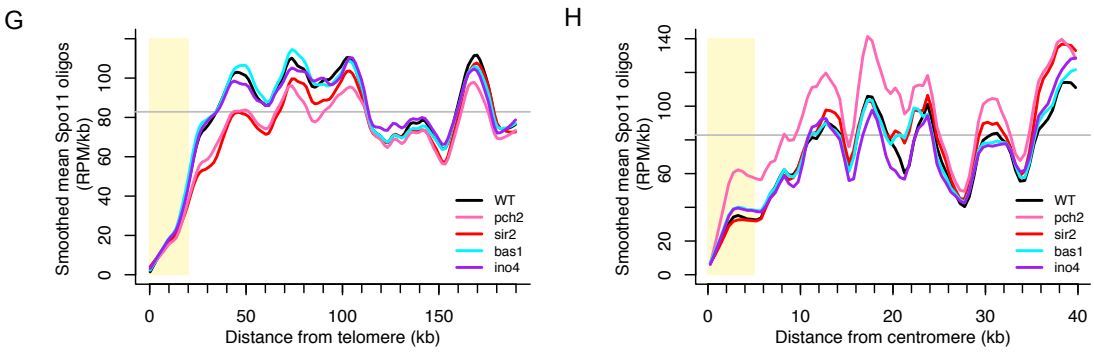

Unexpectedly, *pch2* mutants showed a similar extent of DSB suppression at ~20–120 kb regions from telomeres as *sir2* mutants (**Figure A.5G**). Pch2 and Sir2 may function in the same pathway affecting DSB formation in this region, since Sir2 binds to telomeres (Lieb *et al.* 2001) and has been shown to regulate Pch2 localization (San-Segundo and Roeder 1999). As controls, this phenotype was not seen in transcription factor mutants, *bas1* and *ino4*, which affect 13.1% and 29.7% of relatively hot hotspots (in which Spo11-oligo counts is more than 100 RPM), respectively (**Chapter 3**). Thus, like Sir2, Pch2 is evolved in shaping DSB landscape in subtelomeric regions, probably via the same pathway of Sir2.

Pericentric DSB suppression is affected in pch2 mutant. In *S. cerevisiae*, chromosomes consist of alternating domains of high and low recombination levels. In general, meiotic recombination is less frequent in the regions around centromeres. This repression of recombination is dependent on a functional centromere and at least partially due to a reduction in meiotic DSBs (Lambie and Roeder 1986; Lambie and Roeder 1988; Zenvirth *et al.* 1992; Baudat and Nicolas 1997). Prior studies show that the regions within ~5–10kb of centromeres have lower DSB frequency (Gerton *et al.* 2000; Buhler *et al.* 2007; Pan *et al.* 2011). Hotspot density is lower than the genome average within 10 kb of centromeres, and hotspot activity within 5 kb appears to be weaker (Pan *et al.* 2011). In *pch2* mutants, Spo11-oligo counts were elevated in pericentric hotspots (within 10 kb of centromeres) (**Figure A.5A–B**), and this phenotype was not observed when comparing the activity of these hotspots in *sir2* mutants to wild type (**Figure A.5C–D**), or between wild-type biological replicates (**Figure A.5E–F**). Furthermore, average DSB frequency was affected in *pch2* within ~25–35 kb from centromeres (**Figure A.5H**), but distance from centromeres and levels vary for different chromosomes (**Figure A.3**). The impact of such derepression events is discussed in **Chapter 5**.

REFERENCES

Abdullah, M. F., and R. H. Borts, 2001 Meiotic recombination frequencies are affected by nutritional states in *Saccharomyces cerevisiae*. Proc Natl Acad Sci U S A 98**:** 14524-14529.

Acquaviva, L., L. Szekvolgyi, B. Dichtl, B. S. Dichtl, C. de La Roche Saint Andre *et al*., 2013 The COMPASS subunit Spp1 links histone methylation to initiation of meiotic recombination. Science 339**:** 215-218.

Alani, E., R. Padmore and N. Kleckner, 1990 Analysis of wild-type and *rad50* mutants of yeast suggests an intimate relationship between meiotic chromosome synapsis and recombination. Cell 61**:** 419-436.

Arndt, K. T., C. Styles and G. R. Fink, 1987 Multiple global regulators control *HIS4* transcription in yeast. Science 237**:** 874-880.

Arnheim, N., P. Calabrese and I. Tiemann-Boege, 2007 Mammalian meiotic recombination hot spots. Annu Rev Genet 41**:** 369-399.

Bachhawat, N., Q. Ouyang and S. A. Henry, 1995 Functional characterization of an inositol-sensitive upstream activation sequence in yeast. A cis-regulatory element responsible for inositol-choline mediated regulation of phospholipid biosynthesis. J Biol Chem 270**:** 25087-25095.

Bailey, T. L., M. Boden, F. A. Buske, M. Frith, C. E. Grant *et al*., 2009 MEME SUITE: tools for motif discovery and searching. Nucleic Acids Res 37**:** W202-208.

Baudat, F., J. Buard, C. Grey, A. Fledel-Alon, C. Ober *et al*., 2010 PRDM9 is a major determinant of meiotic recombination hotspots in humans and mice. Science 327**:** 836-840.

Baudat, F., K. Manova, J. P. Yuen, M. Jasin and S. Keeney, 2000 Chromosome synapsis defects and sexually dimorphic meiotic progression in mice lacking Spo11. Mol Cell 6**:** 989-998.

Baudat, F., and A. Nicolas, 1997 Clustering of meiotic double-strand breaks on yeast chromosome III. Proc Natl Acad Sci U S A 94**:** 5213-5218.

Berchowitz, L. E., S. E. Hanlon, J. D. Lieb and G. P. Copenhaver, 2009 A positive but complex association between meiotic double-strand break hotspots and open chromatin in *Saccharomyces cerevisiae*. Genome Res 19**:** 2245-2257.

Bergerat, A., B. de Massy, D. Gadelle, P. C. Varoutas, A. Nicolas *et al*., 1997 An atypical topoisomerase II from *Archaea* with implications for meiotic recombination. Nature 386**:** 414-417.

Bhagat, R., E. A. Manheim, D. E. Sherizen and K. S. McKim, 2004 Studies on crossover-specific mutants and the distribution of crossing over in Drosophila females. Cytogenet Genome Res 107**:** 160-171.

Bhalla, N., and A. F. Dernburg, 2005 A conserved checkpoint monitors meiotic chromosome synapsis in *Caenorhabditis elegans*. Science 310**:** 1683-1686.

Bishop, D. K., D. Park, L. Xu and N. Kleckner, 1992 *DMC1*: A meiosis-specific yeast homolog of *E. coli recA* required for recombination, synaptonemal complex formation, and cell cycle progression. Cell 69**:** 439-456.

Blat, Y., and N. Kleckner, 1999 Cohesins bind to preferential sites along yeast chromosome III, with differential regulation along arms versus the centric region. Cell 98**:** 249-259.

Blat, Y., R. U. Protacio, N. Hunter and N. Kleckner, 2002 Physical and functional interactions among basic chromosome organizational features govern early steps of meiotic chiasma formation. Cell 111**:** 791-802.

Blitzblau, H. G., G. W. Bell, J. Rodriguez, S. P. Bell and A. Hochwagen, 2007 Mapping of meiotic single-stranded DNA reveals double-strand-break hotspots near centromeres and telomeres. Curr Biol 17**:** 2003-2012.

Borde, V., A. S. Goldman and M. Lichten, 2000 Direct coupling between meiotic DNA replication and recombination initiation. Science 290**:** 806-809.

Borde, V., W. Lin, E. Novikov, J. H. Petrini, M. Lichten *et al*., 2004 Association of Mre11p with double-strand break sites during yeast meiosis. Mol Cell 13**:** 389-401.

Borde, V., N. Robine, W. Lin, S. Bonfils, V. Geli *et al*., 2009 Histone H3 lysine 4 trimethylation marks meiotic recombination initiation sites. EMBO J 28**:** 99-111.

Borner, G. V., A. Barot and N. Kleckner, 2008 Yeast Pch2 promotes domainal axis organization, timely recombination progression, and arrest of defective recombinosomes during meiosis. Proc Natl Acad Sci U S A 105**:** 3327-3332.

Brick, K., F. Smagulova, P. Khil, R. D. Camerini-Otero and G. V. Petukhova, 2012 Genetic recombination is directed away from functional genomic elements in mice. Nature 485**:** 642-645.

Briggs, S. D., M. Bryk, B. D. Strahl, W. L. Cheung, J. K. Davie *et al*., 2001 Histone H3 lysine 4 methylation is mediated by Set1 and required for cell growth and rDNA silencing in Saccharomyces cerevisiae. Genes Dev 15**:** 3286-3295.

Buard, J., P. Barthès, C. Grey and B. de Massy, 2009 Distinct histone modifications define initiation and repair of meiotic recombination in the mouse. EMBO J 28**:** 2616-2624.

Buhler, C., V. Borde and M. Lichten, 2007 Mapping meiotic single-strand DNA reveals a new landscape of DNA double-strand breaks in *Saccharomyces cerevisiae*. PLoS Biol 5**:** e324.

Cao, L., E. Alani and N. Kleckner, 1990 A pathway for generation and processing of double-strand breaks during meiotic recombination in *S. cerevisiae*. Cell 61**:** 1089-1101.

Cervantes, M. D., J. A. Farah and G. R. Smith, 2000 Meiotic DNA breaks associated with recombination in *S. pombe*. Mol Cell 5**:** 883-888.

Chen, C., A. Jomaa, J. Ortega and E. E. Alani, 2014 Pch2 is a hexameric ring ATPase that remodels the chromosome axis protein Hop1. Proc Natl Acad Sci U S A 111**:** E44-53.

Chen, S. Y., T. Tsubouchi, B. Rockmill, J. S. Sandler, D. R. Richards *et al*., 2008a Global analysis of the meiotic crossover landscape. Dev Cell 15**:** 401-415.

Chen, Z., H. Yang and N. P. Pavletich, 2008b Mechanism of homologous recombination from the RecA-ssDNA/dsDNA structures. Nature 453**:** 489-484.

Cherry, J. M., C. Ball, S. Weng, G. Juvik, R. Schmidt *et al*., 1997 Genetic and physical maps of *Saccharomyces cerevisiae*. Nature 387**:** 67-73.

Cohn, M., G. Liti and D. Barton, 2005 Telomeres in fungi. Topics in Current Genetics 15**:** 101-130.

Cole, F., L. Kauppi, J. Lange, I. Roig, R. Wang *et al*., 2012 Homeostatic control of recombination is implemented progressively in mouse meiosis. Nat Cell Biol 14**:** 424-430.

Coop, G., X. Wen, C. Ober, J. K. Pritchard and M. Przeworski, 2008 High-resolution mapping of crossovers reveals extensive variation in fine-scale recombination patterns among humans. Science 319**:** 1395-1398.

Cotton, V. E., E. R. Hoffmann, M. F. Abdullah and R. H. Borts, 2009 Interaction of genetic and environmental factors in *Saccharomyces cerevisiae* meiosis: the devil is in the details. Methods Mol Biol 557**:** 3-20.

Cromie, G. A., R. W. Hyppa, H. P. Cam, J. A. Farah, S. I. Grewal *et al*., 2007 A discrete class of intergenic DNA dictates meiotic DNA break hotspots in fission yeast. PLoS Genet 3**:** e141.

Cromie, G. A., C. A. Rubio, R. W. Hyppa and G. R. Smith, 2005 A natural meiotic DNA break site in *Schizosaccharomyces pombe* is a hotspot of gene conversion, highly associated with crossing over. Genetics 169**:** 595-605.

Daignan-Fornier, B., and G. R. Fink, 1992 Coregulation of purine and histidine biosynthesis by the transcriptional activators BAS1 and BAS2. Proc Natl Acad Sci U S A 89**:** 6746-6750.

de Castro, E., I. Soriano, L. Marin, R. Serrano, L. Quintales *et al*., 2012 Nucleosomal organization of replication origins and meiotic recombination hotspots in fission yeast. EMBO J 31**:** 124-137.

de Massy, B., 2013a Initiation of meiotic recombination: how and where? Conservation and specificities among eukaryotes. Annu Rev Genet 47**:** 563-599.

de Massy, B., 2013b Spp1 links sites of meiotic DNA double-strand breaks to chromosome axes. Mol Cell 49**:** 3-5.

de Massy, B., V. Rocco and A. Nicolas, 1995 The nucleotide mapping of DNA double-strand breaks at the *CYS3* initiation site of meiotic recombination in *Saccharomyces cerevisiae*. Embo j 14**:** 4589-4598.

Denis, V., H. Boucherie, C. Monribot and B. Daignan-Fornier, 1998 Role of the myb-like protein bas1p in *Saccharomyces cerevisiae*: a proteome analysis. Mol Microbiol 30**:** 557-566.

Denis, V., and B. Daignan-Fornier, 1998 Synthesis of glutamine, glycine and 10-formyl tetrahydrofolate is coregulated with purine biosynthesis in *Saccharomyces cerevisiae*. Mol Gen Genet 259**:** 246-255.

Dernburg, A. F., K. McDonald, G. Moulder, R. Barstead, M. Dresser *et al*., 1998 Meiotic recombination in *C. elegans* initiates by a conserved mechanism and is dispensable for homologous chromosome synapsis. Cell 94**:** 387-398.

Diaz, R. L., A. D. Alcid, J. M. Berger and S. Keeney, 2002 Identification of residues in yeast Spo11p critical for meiotic DNA double-strand break formation. Mol Cell Biol 22**:** 1106-1115.

Dobin, A., C. A. Davis, F. Schlesinger, J. Drenkow, C. Zaleski *et al*., 2013 STAR: ultrafast universal RNA-seq aligner. Bioinformatics 29**:** 15-21.

Eickbush, T. H., and D. G. Eickbush, 2007 Finely orchestrated movements: evolution of the ribosomal RNA genes. Genetics 175**:** 477-485.

Fan, Q., F. Xu and T. D. Petes, 1995 Meiosis-specific double-strand DNA breaks at the *HIS4* recombination hot spot in the yeast *Saccharomyces cerevisiae*: control in cis and trans. Mol Cell Biol 15**:** 1679-1688.

Fan, Q. Q., and T. D. Petes, 1996 Relationship between nuclease-hypersensitive sites and meiotic recombination hot spot activity at the *HIS4* locus of *Saccharomyces cerevisiae*. Mol Cell Biol 16**:** 2037-2043.

Fan, Q. Q., F. Xu, M. A. White and T. D. Petes, 1997 Competition between adjacent meiotic recombination hotspots in the yeast *Saccharomyces cerevisiae*. Genetics 145**:** 661-670.

Farmer, S., E. J. Hong, W. K. Leung, B. Argunhan, Y. Terentyev *et al*., 2012 Budding yeast Pch2, a widely conserved meiotic protein, is involved in the initiation of meiotic recombination. PLoS One 7**:** e39724.

Fowler, K. R., S. Gutierrez-Velasco, C. Martin-Castellanos and G. R. Smith, 2013 Protein determinants of meiotic DNA break hot spots. Mol Cell 49**:** 983-996.

Fowler, K. R., M. Sasaki, N. Milman, S. Keeney and G. R. Smith, 2014 Evolutionarily diverse determinants of meiotic DNA break and recombination landscapes across the genome. Genome Res 24**:** 1650-1664.

Frazer, K. A., D. G. Ballinger, D. R. Cox, D. A. Hinds, L. L. Stuve *et al*., 2007 A second generation human haplotype map of over 3.1 million SNPs. Nature 449**:** 851-861.

Fukuda, T., K. Kugou, H. Sasanuma, T. Shibata and K. Ohta, 2008 Targeted induction of meiotic double-strand breaks reveals chromosomal domain-dependent regulation of Spo11 and interactions among potential sites of meiotic recombination. Nucleic Acids Res 36**:** 984-997.

Gelling, C. L., M. D. Piper, S. P. Hong, G. D. Kornfeld and I. W. Dawes, 2004 Identification of a novel one-carbon metabolism regulon in *Saccharomyces cerevisiae*. J Biol Chem 279**:** 7072-7081.

Gerton, J. L., J. DeRisi, R. Shroff, M. Lichten, P. O. Brown *et al*., 2000 Global mapping of meiotic recombination hotspots and coldspots in the yeast *Saccharomyces cerevisiae*. Proc Natl Acad Sci U S A 97**:** 11383-11390.

Gerton, J. L., and R. S. Hawley, 2005 Homologous chromosome interactions in meiosis: diversity amidst conservation. Nat Rev Genet 6**:** 477-487.

Glynn, E. F., P. C. Megee, H.-G. Yu, C. Mistrot, E. Unal *et al*., 2004 Genome-wide mapping of the cohesin complex in the yeast *Saccharomyces cerevisiae*. PLoS Biol 2**:** e259.

Goldfarb, T., and M. Lichten, 2010 Frequent and efficient use of the sister chromatid for DNA double-strand break repair during budding yeast meiosis. PLoS Biol 8**:** e1000520.

Gottlieb, S., and R. E. Esposito, 1989 A new role for a yeast transcriptional silencer gene, *SIR2*, in regulation of recombination in ribosomal DNA. Cell 56**:** 771-776.

Gray, S., R. M. Allison, V. Garcia, A. S. Goldman and M. J. Neale, 2013 Positive regulation of meiotic DNA double-strand break formation by activation of the DNA damage checkpoint kinase Mec1(ATR). Open Biol 3**:** 130019.

Grey, C., P. Barthes, G. Chauveau-Le Friec, F. Langa, F. Baudat *et al*., 2011 Mouse PRDM9 DNA-binding specificity determines sites of histone H3 lysine 4 trimethylation for initiation of meiotic recombination. PLoS Biol 9**:** e1001176.

Hayashi, K., K. Yoshida and Y. Matsui, 2005 A histone H3 methyltransferase controls epigenetic events required for meiotic prophase. Nature 438**:** 374-378.

Henzel, J. V., K. Nabeshima, M. Schvarzstein, B. E. Turner, A. M. Villeneuve *et al*., 2011 An asymmetric chromosome pair undergoes synaptic adjustment and crossover redistribution during *Caenorhabditis elegans* meiosis: implications for sex chromosome evolution. Genetics 187**:** 685-699.

Hirota, K., W. W. Steiner, T. Shibata and K. Ohta, 2007 Multiple modes of chromatin configuration at natural meiotic recombination hot spots in fission yeast. Eukaryot Cell 6**:** 2072-2080.

Ho, H. C., and S. M. Burgess, 2011 Pch2 acts through Xrs2 and Tel1/ATM to modulate interhomolog bias and checkpoint function during meiosis. PLoS Genet 7**:** e1002351.

Hochwagen, A., W.-H. Tham, G. A. Brar and A. Amon, 2005 The FK506 binding protein Fpr3 counteracts protein phosphatase 1 to maintain meiotic recombination checkpoint activity. Cell 122**:** 861-873.

Horowitz, H., P. Thorburn and J. E. Haber, 1984 Rearrangements of highly polymorphic regions near telomeres of Saccharomyces cerevisiae. Mol Cell Biol 4**:** 2509-2517.

Hovring, I., A. Bostad, E. Ording, A. H. Myrset and O. S. Gabrielsen, 1994 DNA-binding domain and recognition sequence of the yeast BAS1 protein, a divergent member of the Myb family of transcription factors. J Biol Chem 269**:** 17663-17669.

Hughes, T. R., and C. G. de Boer, 2013 Mapping yeast transcriptional networks. Genetics 195**:** 9-36.

Hunter, N., 2007 Meiotic Recombination, pp. 381-442 in *Molecular Genetics of Recombination*, edited by A. Aguilera and R. Rothstein. Springer-Verlag, Heidelberg.

Ide, S., T. Miyazaki, H. Maki and T. Kobayashi, 2010 Abundance of ribosomal RNA gene copies maintains genome integrity. Science 327**:** 693-696.

Ito, M., K. Kugou, J. A. Fawcett, S. Mura, S. Ikeda *et al*., 2014 Meiotic recombination cold spots in chromosomal cohesion sites. Genes Cells 19**:** 359-373.

Jessop, L., T. Allers and M. Lichten, 2005 Infrequent co-conversion of markers flanking a meiotic recombination initiation site in *Saccharomyces cerevisiae*. Genetics 169**:** 1353-1367.

Joshi, N., A. Barot, C. Jamison and G. V. Borner, 2009 Pch2 links chromosome axis remodeling at future crossover sites and crossover distribution during yeast meiosis. PLoS Genet 5**:** e1000557.

Joyce, E. F., and K. S. McKim, 2009 *Drosophila* PCH2 is required for a pachytene checkpoint that monitors double-strand-break-independent events leading to meiotic crossover formation. Genetics 181**:** 39-51.

Joyce, E. F., and K. S. McKim, 2010 Chromosome axis defects induce a checkpoint-mediated delay and interchromosomal effect on crossing over during Drosophila meiosis. PLoS Genet 6.

Joyce, E. F., M. Pedersen, S. Tiong, S. K. White-Brown, A. Paul *et al*., 2011 *Drosophila* ATM and ATR have distinct activities in the regulation of meiotic DNA damage and repair. J Cell Biol 195**:** 359-367.

Kaback, D. B., V. Guacci, D. Barber and J. W. Mahon, 1992 Chromosome size-dependent control of meiotic recombination. Science 256**:** 228-232.

Kaback, D. B., H. Y. Steensma and P. de Jonge, 1989 Enhanced meiotic recombination on the smallest chromosome of *Saccharomyces cerevisiae*. Proc Natl Acad Sci U S A 86**:** 3694-3698.

Kauppi, L., M. Barchi, J. Lange, F. Baudat, M. Jasin *et al*., 2013a Numerical constraints and feedback control of double-strand breaks in mouse meiosis. Genes Dev.

Kauppi, L., M. Jasin and S. Keeney, 2013b How much is enough? Control of DNA double-strand break numbers in mouse meiosis. Cell Cycle 12**:** 2719-2720.

Kauppi, L., A. J. Jeffreys and S. Keeney, 2004 Where the crossovers are: recombination distributions in mammals. Nat Rev Genet 5**:** 413-424.

Keeney, S., 2008 Spo11 and the Formation of DNA Double-Strand Breaks in Meiosis. Genome Dyn Stab 2**:** 81-123.

Keeney, S., C. N. Giroux and N. Kleckner, 1997 Meiosis-specific DNA double-strand breaks are catalyzed by Spo11, a member of a widely conserved protein family. Cell 88**:** 375-384.

Keeney, S., and N. Kleckner, 1995 Covalent protein-DNA complexes at the 5' strand termini of meiosis-specific double-strand breaks in yeast. Proc Natl Acad Sci U S A 92**:** 11274-11278.

Keeney, S., and N. Kleckner, 1996 Communication between homologous chromosomes: genetic alterations at a nuclease-hypersensitive site can alter mitotic chromatin structure at that site both in cis and in trans. Genes Cells 1**:** 475-489.

Keeney, S., J. Lange and N. Mohibullah, 2014 Self-organization of meiotic recombination initiation: general principles and molecular pathways. Annu Rev Genet 48**:** 187-214.

Khil, P. P., F. Smagulova, K. M. Brick, R. D. Camerini-Otero and G. V. Petukhova, 2012 Sensitive mapping of recombination hotspots using sequencing-based detection of ssDNA. Genome Res 22**:** 957-965.

Kimura, A., T. Umehara and M. Horikoshi, 2002 Chromosomal gradient of histone acetylation established by Sas2p and Sir2p functions as a shield against gene silencing. Nat Genet 32**:** 370-377.

Klapholz, S., C. S. Waddell and R. E. Esposito, 1985 The role of the *SPO11* gene in meiotic recombination in yeast. Genetics 110**:** 187-216.

Kleckner, N., 2006 Chiasma formation: Chromatin/axis interplay and the role(s) of the synaptonemal complex. Chromosoma 115**:** 175-194.

Klein, F., P. Mahr, M. Galova, S. B. Buonomo, C. Michaelis *et al*., 1999 A central role for cohesins in sister chromatid cohesion, formation of axial elements, and recombination during yeast meiosis. Cell 98**:** 91-103.

Kobayashi, T., 2011 How does genome instability affect lifespan?: roles of rDNA and telomeres. Genes Cells 16**:** 617-624.

Kon, N., M. D. Krawchuk, B. G. Warren, G. R. Smith and W. P. Wahls, 1997 Transcription factor Mts1/Mts2 (Atf1/Pcr1, Gad7/Pcr1) activates the *M26* meiotic recombination hotspot in *Schizosaccharomyces pombe*. Proc Natl Acad Sci U S A 94**:** 13765-13770.

Kong, A., G. Thorleifsson, D. F. Gudbjartsson, G. Masson, A. Sigurdsson *et al*., 2010 Fine-scale recombination rate differences between sexes, populations and individuals. Nature 467**:** 1099-1103.

Kugou, K., T. Fukuda, S. Yamada, M. Ito, H. Sasanuma *et al*., 2009 Rec8 guides canonical Spo11 distribution along yeast meiotic chromosomes. Mol Biol Cell 20**:** 3064-3076.

Kumar, R., H. M. Bourbon and B. de Massy, 2010 Functional conservation of Mei4 for meiotic DNA double-strand break formation from yeasts to mice. Genes Dev 24**:** 1266-1280.

Lam, I., and S. Keeney, 2014 Mechanism and Regulation of Meiotic Recombination Initiation. Cold Spring Harb Perspect Biol 7.

Lambie, E. J., and G. S. Roeder, 1986 Repression of meiotic crossing over by a centromere (*CEN3*) in *Saccharomyces cerevisiae*. Genetics 114**:** 769-789.

Lambie, E. J., and G. S. Roeder, 1988 A yeast centromere acts in cis to inhibit meiotic gene conversion of adjacent sequences. Cell 52**:** 863-873.

Lange, J., J. Pan, F. Cole, M. P. Thelen, M. Jasin *et al*., 2011 ATM controls meiotic double-strand-break formation. Nature 479**:** 237-240.

Lee, J. Y., A. Hayashi-Hagihara and T. L. Orr-Weaver, 2005 Roles and regulation of the *Drosophila* centromere cohesion protein MEI-S332 family. Philos Trans R Soc Lond B Biol Sci 360**:** 543-552.

Lengronne, A., Y. Katou, S. Mori, S. Yokobayashi, G. P. Kelly *et al*., 2004 Cohesin relocation from sites of chromosomal loading to places of convergent transcription. Nature 430**:** 573-578.

Li, X. C., and J. C. Schimenti, 2007 Mouse pachytene checkpoint 2 (trip13) is required for completing meiotic recombination but not synapsis. PLoS Genet 3**:** e130.

Lichten, M., 2008 Meiotic chromatin: The substrate for recombination initiation, pp. 165-193 in *Recombination and Meiosis*, edited by R. Egel and D. H. Lankenau. Springer-Verlag, Heidelberg.

Lichten, M., and B. de Massy, 2011 The impressionistic landscape of meiotic recombination. Cell 147**:** 267-270.

Lichten, M., and A. S. H. Goldman, 1995 Meiotic recombination hotspots. Annu Rev Genetics 29**:** 423-444.

Lieb, J. D., X. Liu, D. Botstein and P. O. Brown, 2001 Promoter-specific binding of Rap1 revealed by genome-wide maps of protein-DNA association. Nat Genet 28**:** 327-334.

Liu, J., T. C. Wu and M. Lichten, 1995 The location and structure of double-strand DNA breaks induced during yeast meiosis: evidence for a covalently linked DNA-protein intermediate. EMBO J 14**:** 4599-4608.

Liu, P., C. M. Carvalho, P. J. Hastings and J. R. Lupski, 2012 Mechanisms for recurrent and complex human genomic rearrangements. Curr Opin Genet Dev 22**:** 211-220.

Losada, A., and T. Hirano, 2005 Dynamic molecular linkers of the genome: the first decade of SMC proteins. Genes Dev 19**:** 1269-1287.

Louis, E. J., and J. E. Haber, 1992 The structure and evolution of subtelomeric Y' repeats in Saccharomyces cerevisiae. Genetics 131**:** 559-574.

Louis, E. J., E. S. Naumova, A. Lee, G. Naumov and J. E. Haber, 1994 The chromosome end in yeast: its mosaic nature and influence on recombinational dynamics. Genetics 136**:** 789-802.

Lu, S., C. Zong, W. Fan, M. Yang, J. Li *et al*., 2012 Probing meiotic recombination and aneuploidy of single sperm cells by whole-genome sequencing. Science 338**:** 1627-1630.

Lydall, D., Y. Nikolsky, D. K. Bishop and T. Weinert, 1996 A meiotic recombination checkpoint controlled by mitotic checkpoint genes. Nature 383**:** 840-843.

Lynn, A., R. Soucek and G. V. Borner, 2007 ZMM proteins during meiosis: crossover artists at work. Chromosome Res 15**:** 591-605.

Machanick, P., and T. L. Bailey, 2011 MEME-ChIP: motif analysis of large DNA datasets. Bioinformatics 27**:** 1696-1697.

MacIsaac, K. D., T. Wang, D. B. Gordon, D. K. Gifford, G. D. Stormo *et al*., 2006 An improved map of conserved regulatory sites for *Saccharomyces cerevisiae*. BMC Bioinformatics 7**:** 113.

MacQuarrie, K. L., A. P. Fong, R. H. Morse and S. J. Tapscott, 2011 Genome-wide transcription factor binding: beyond direct target regulation. Trends Genet 27**:** 141-148.

Mancera, E., R. Bourgon, A. Brozzi, W. Huber and L. M. Steinmetz, 2008 High-resolution mapping of meiotic crossovers and non-crossovers in yeast. Nature 454**:** 479-485.

Mao-Draayer, Y., A. M. Galbraith, D. L. Pittman, M. Cool and R. E. Malone, 1996 Analysis of meiotic recombination pathways in yeast *Saccharomyces cerevisiae*. Genetics 144**:** 71-86.

Martini, E., R. L. Diaz, N. Hunter and S. Keeney, 2006 Crossover homeostasis in yeast meiosis. Cell 126**:** 285-295.

McKim, K. S., and A. Hayashi-Hagihara, 1998 mei-W68 in *Drosophila melanogaster* encodes a Spo11 homolog: evidence that the mechanism for initiating meiotic recombination is conserved. Genes Dev 12**:** 2932-2942.

McVean, G. A., S. R. Myers, S. Hunt, P. Deloukas, D. R. Bentley *et al*., 2004 The fine-scale structure of recombination rate variation in the human genome. Science 304**:** 581-584.

Mieczkowski, P. A., M. Dominska, M. J. Buck, J. L. Gerton, J. D. Lieb *et al*., 2006 Global analysis of the relationship between the binding of the Bas1p transcription factor and meiosis-specific double-strand DNA breaks in *Saccharomyces cerevisiae*. Mol Cell Biol 26**:** 1014-1027.

Mieczkowski, P. A., M. Dominska, M. J. Buck, J. D. Lieb and T. D. Petes, 2007 Loss of a histone deacetylase dramatically alters the genomic distribution of Spo11p-catalyzed DNA breaks in *Saccharomyces cerevisiae*. Proc Natl Acad Sci U S A 104**:** 3955-3960.

Moens, P. B., and R. E. Pearlman, 1988 Chromatin organization at meiosis. Bioessays 9**:** 151-153.

Mortimer, R. K., D. Schild, C. R. Contopoulou and J. A. Kans, 1989 Genetic map of Saccharomyces cerevisiae, edition 10. Yeast 5**:** 321-403.

Murakami, H., V. Borde, A. Nicolas and S. Keeney, 2009 Gel electrophoresis assays for analyzing DNA double-strand breaks in *Saccharomyces cerevisiae* at various spatial resolutions. Methods Mol Biol 557**:** 117-142.

Murakami, H., V. Borde, T. Shibata, M. Lichten and K. Ohta, 2003 Correlation between premeiotic DNA replication and chromatin transition at yeast recombination initiation sites. Nucleic Acids Res 31**:** 4085-4090.

Murakami, H., and S. Keeney, 2008 Regulating the formation of DNA double-strand breaks in meiosis. Genes Dev 22**:** 286-292.

Murakami, H., and S. Keeney, 2014 Temporospatial coordination of meiotic DNA replication and recombination via DDK recruitment to replisomes. Cell 158**:** 861-873.

Myers, S., L. Bottolo, C. Freeman, G. McVean and P. Donnelly, 2005 A fine-scale map of recombination rates and hotspots across the human genome. Science 310**:** 321-324.

Myers, S., R. Bowden, A. Tumian, R. E. Bontrop, C. Freeman *et al*., 2010 Drive against hotspot motifs in primates implicates the PRDM9 gene in meiotic recombination. Science 327**:** 876-879.

Nagaoka, S. I., T. J. Hassold and P. A. Hunt, 2012 Human aneuploidy: mechanisms and new insights into an age-old problem. Nat Rev Genet 13**:** 493-504.

Nasmyth, K., and C. H. Haering, 2005 The structure and function of SMC and kleisin complexes. Annu Rev Biochem 74**:** 595-648.

Neale, M. J., and S. Keeney, 2009 End-labeling and analysis of Spo11-oligonucleotide complexes in Saccharomyces cerevisiae. Methods Mol Biol 557**:** 183-195.

Neale, M. J., J. Pan and S. Keeney, 2005 Endonucleolytic processing of covalent protein-linked DNA double-strand breaks. Nature 436**:** 1053-1057.

Nichols, M. D., K. DeAngelis, J. L. Keck and J. M. Berger, 1999 Structure and function of an archaeal topoisomerase VI subunit with homology to the meiotic recombination factor Spo11. EMBO J 18**:** 6177-6188.

Ohta, K., T. Shibata and A. Nicolas, 1994 Changes in chromatin structure at recombination initiation sites during yeast meiosis. Embo j 13**:** 5754-5763.

Ohta, K., T. C. Wu, M. Lichten and T. Shibata, 1999 Competitive inactivation of a double-strand DNA break site involves parallel suppression of meiosis-induced changes in chromatin configuration. Nucleic Acids Res 27**:** 2175-2180.

Padmore, R., L. Cao and N. Kleckner, 1991 Temporal comparison of recombination and synaptonemal complex formation during meiosis in *S. cerevisiae*. Cell 66**:** 1239-1256.

Page, S. L., and R. S. Hawley, 2004 The genetics and molecular biology of the synaptonemal complex. Annu Rev Cell Dev Biol 20**:** 525-558.

Pan, J., M. Sasaki, R. Kniewel, H. Murakami, H. G. Blitzblau *et al*., 2011 A hierarchical combination of factors shapes the genome-wide topography of yeast meiotic recombination initiation. Cell 144**:** 719-731.

Panizza, S., M. A. Mendoza, M. Berlinger, L. Huang, A. Nicolas *et al*., 2011 Spo11-accessory proteins link double-strand break sites to the chromosome axis in early meiotic recombination. Cell 146**:** 372-383.

Parvanov, E. D., P. M. Petkov and K. Paigen, 2010 Prdm9 controls activation of mammalian recombination hotspots. Science 327**:** 835.

Petes, T. D., 2001 Meiotic recombination hot spots and cold spots. Nat Rev Genet 2**:** 360-369.

Petes, T. D., and D. Botstein, 1977 Simple Mendelian inheritance of the reiterated ribosomal DNA of yeast. Proc Natl Acad Sci U S A 74**:** 5091-5095.

Petukhova, G. V., P. J. Romanienko and R. D. Camerini-Otero, 2003 The Hop2 protein has a direct role in promoting interhomolog interactions during mouse meiosis. Dev Cell 5**:** 927-936.

Plug, A. W., J. Xu, G. Reddy, E. I. Golub and T. Ashley, 1996 Presynaptic association of Rad51 protein with selected sites in meiotic chromatin. Proc Natl Acad Sci U S A 93**:** 5920-5924.

Pokholok, D. K., C. T. Harbison, S. Levine, M. Cole, N. M. Hannett *et al*., 2005 Genome-wide map of nucleosome acetylation and methylation in yeast. Cell 122**:** 517-527.

Ponticelli, A. S., E. P. Sena and G. R. Smith, 1988 Genetic and physical analysis of the *M26* recombination hotspot of *Schizosaccharomyces pombe*. Genetics 119**:** 491-497.

Ponticelli, A. S., and G. R. Smith, 1992 Chromosomal context dependence of a eukaryotic recombinational hot spot. Proc Natl Acad Sci U S A 89**:** 227-231.

Pratto, F., K. Brick, P. Khil, F. Smagulova, G. V. Petukhova *et al*., 2014 DNA recombination. Recombination initiation maps of individual human genomes. Science 346**:** 1256442.

Prieler, S., A. Penkner, V. Borde and F. Klein, 2005 The control of Spo11's interaction with meiotic recombination hotspots. Genes Dev 19**:** 255-269.

Riles, L., J. E. Dutchik, A. Baktha, B. K. McCauley, E. C. Thayer *et al*., 1993 Physical maps of the six smallest chromosomes of *Saccharomyces cerevisiae* at a resolution of 2.6 kilobase pairs. Genetics 134**:** 81-150.

Robine, N., N. Uematsu, F. Amiot, X. Gidrol, E. Barillot *et al*., 2007 Genome-wide redistribution of meiotic double-strand breaks in *Saccharomyces cerevisiae*. Mol Cell Biol 27**:** 1868-1880.

Rocco, V., and A. Nicolas, 1996 Sensing of DNA non-homology lowers the initiation of meiotic recombination in yeast. Genes Cells 1**:** 645-661.

Rockmill, B., and G. S. Roeder, 1991 A meiosis-specific protein kinase homolog required for chromosome synapsis and recombination. Genes Dev 5**:** 2392-2404.

Rockmill, B., K. Voelkel-Meiman and G. S. Roeder, 2006 Centromere-proximal crossovers are associated with precocious separation of sister chromatids during meiosis in *Saccharomyces cerevisiae*. Genetics 174**:** 1745-1754.

Roguev, A., D. Schaft, A. Shevchenko, W. W. Pijnappel, M. Wilm *et al*., 2001 The Saccharomyces cerevisiae Set1 complex includes an Ash2 homologue and methylates histone 3 lysine 4. EMBO J 20**:** 7137-7148.

Roig, I., J. A. Dowdle, A. Toth, D. G. de Rooij, M. Jasin *et al*., 2010 Mouse TRIP13/PCH2 is required for recombination and normal higher-order chromosome structure during meiosis. PLoS Genet 6.

Rusche, L. N., A. L. Kirchmaier and J. Rine, 2003 The establishment, inheritance, and function of silenced chromatin in *Saccharomyces cerevisiae*. Annu Rev Biochem 72**:** 481-516.

San Filippo, J., P. Sung and H. Klein, 2008 Mechanism of eukaryotic homologous recombination. Annu Rev Biochem 77**:** 229-257.

San-Segundo, P. A., and G. S. Roeder, 1999 Pch2 links chromatin silencing to meiotic checkpoint control. Cell 97**:** 313-324.

San-Segundo, P. A., and G. S. Roeder, 2000 Role for the silencing protein Dot1 in meiotic checkpoint control. Mol Biol Cell 11**:** 3601-3615.

Santiago, T. C., and C. B. Mamoun, 2003 Genome expression analysis in yeast reveals novel transcriptional regulation by inositol and choline and new regulatory functions for Opi1p, Ino2p, and Ino4p. J Biol Chem 278**:** 38723-38730.

Sasaki, M., J. Lange and S. Keeney, 2010 Genome destabilization by homologous recombination in the germ line. Nature 11**:** 182-195.

Sasaki, M., S. E. Tischfield, M. van Overbeek and S. Keeney, 2013 Meiotic recombination initiation in and around retrotransposable elements in *Saccharomyces cerevisiae*. PLoS Genet 9**:** e1003732.

Sauve, A. A., C. Wolberger, V. L. Schramm and J. D. Boeke, 2006 The biochemistry of sirtuins. Annu Rev Biochem 75**:** 435-465.

Schuchert, P., M. Langsford, E. Kaslin and J. Kohli, 1991 A specific DNA sequence is required for high frequency of recombination in the *ade6* gene of fission yeast. Embo j 10**:** 2157-2163.

Schwacha, A., and N. Kleckner, 1994 Identification of joint molecules that form frequently between homologs but rarely between sister chromatids during yeast meiosis. Cell 76**:** 51-63.

Schwaiger, M., H. Kohler, E. J. Oakeley, M. B. Stadler and D. Schubeler, 2010 Heterochromatin protein 1 (HP1) modulates replication timing of the *Drosophila* genome. Genome Res 20**:** 771-780.

Schwank, S., R. Ebbert, K. Rautenstrauss, E. Schweizer and H. J. Schuller, 1995 Yeast transcriptional activator *INO2* interacts as an Ino2p/Ino4p basic helix-loop-helix heteromeric complex with the inositol/choline-responsive element necessary for expression of phospholipid biosynthetic genes in *Saccharomyces cerevisiae*. Nucleic Acids Res 23**:** 230-237.

Serrentino, M.-E., and V. Borde, 2012 The spatial regulation of meiotic recombination hotspots: Are all DSB hotspots crossover hotspots? Exp Cell Res 318**:** 1347-1352.

Shilatifard, A., 2012 The COMPASS family of histone H3K4 methylases: mechanisms of regulation in development and disease pathogenesis. Annu Rev Biochem 81**:** 65-95.

Smagulova, F., I. V. Gregoretti, K. Brick, P. Khil, R. D. Camerini-Otero *et al*., 2011 Genome-wide analysis reveals novel molecular features of mouse recombination hotspots. Nature 472**:** 375-378.

Sollier, J., W. Lin, C. Soustelle, K. Suhre, A. Nicolas *et al*., 2004 Set1 is required for meiotic S-phase onset, double-strand break formation and middle gene expression. Embo j 23**:** 1957-1967.

Sommermeyer, V., C. Beneut, E. Chaplais, M. E. Serrentino and V. Borde, 2013 Spp1, a member of the Set1 Complex, promotes meiotic DSB formation in promoters by tethering histone H3K4 methylation sites to chromosome axes. Mol Cell 49**:** 43-54.

Stankiewicz, P., and J. R. Lupski, 2010 Structural variation in the human genome and its role in disease. Annu Rev Med 61**:** 437-455.

Stapleton, A., and T. D. Petes, 1991 The Tn3 beta-lactamase gene acts as a hotspot for meiotic recombination in yeast. Genetics 127**:** 39-51.

Steiner, W. W., R. W. Schreckhise and G. R. Smith, 2002 Meiotic DNA breaks at the *S. pombe* recombination hot spot *M26*. Mol Cell 9**:** 847-855.

Steiner, W. W., E. M. Steiner, A. R. Girvin and L. E. Plewik, 2009 Novel nucleotide sequence motifs that produce hotspots of meiotic recombination in *Schizosaccharomyces pombe*. Genetics 182**:** 459-469.

Suka, N., K. Luo and M. Grunstein, 2002 Sir2p and Sas2p opposingly regulate acetylation of yeast histone H4 lysine16 and spreading of heterochromatin. Nat Genet 32**:** 378-383.

Sun, H., D. Treco and J. W. Szostak, 1991 Extensive 3'-overhanging, single-stranded DNA associated with the meiosis-specific double-strand breaks at the *ARG4* recombination initiation site. Cell 64**:** 1155-1161.

Thacker, D., N. Mohibullah, X. Zhu and S. Keeney, 2014 Homologue engagement controls meiotic DNA break number and distribution. Nature 510**:** 241-246.

Tischfield, S. E., and S. Keeney, 2012 Scale matters: the spatial correlation of yeast meiotic DNA breaks with histone H3 trimethylation is driven largely by independent colocalization at promoters. Cell Cycle 11**:** 1496-1503.

Trapnell, C., B. A. Williams, G. Pertea, A. Mortazavi, G. Kwan *et al*., 2010 Transcript assembly and quantification by RNA-Seq reveals unannotated transcripts and isoform switching during cell differentiation. Nat Biotechnol 28**:** 511-515.

Vader, G., H. G. Blitzblau, M. A. Tame, J. E. Falk, L. Curtin *et al*., 2011 Protection of repetitive DNA borders from self-induced meiotic instability. Nature 477**:** 115-119.

Wagstaff, J. E., S. Klapholz, C. S. Waddell, L. Jensen and R. E. Esposito, 1985 Meiotic exchange within and between chromosomes requires a common Rec function in *Saccharomyces cerevisiae*. Mol Cell Biol 5**:** 3532-3544.

Wahls, W. P., and M. K. Davidson, 2010 Discrete DNA sites regulate global distribution of meiotic recombination. Trends Genet 26**:** 202-208.

Wahls, W. P., and G. R. Smith, 1994 A heteromeric protein that binds to a meiotic homologous recombination hot spot: correlation of binding and hot spot activity. Genes Dev 8**:** 1693-1702.

Watanabe, Y., 2005 Shugoshin: guardian spirit at the centromere. Curr Opin Cell Biol 17**:** 590-595.

Watanabe, Y., and P. Nurse, 1999 Cohesin Rec8 is required for reductional chromosome segregation at meiosis. Nature 400**:** 461-464.

Weiner, B. M., and N. Kleckner, 1994 Chromosome pairing via multiple interstitial interactions before and during meiosis in yeast. Cell 77**:** 977-991.

White, M. A., P. Detloff, M. Strand and T. D. Petes, 1992 A promoter deletion reduces the rate of mitotic, but not meiotic, recombination at the *HIS4* locus in yeast. Curr Genet 21**:** 109-116.

White, M. A., M. Dominska and T. D. Petes, 1993 Transcription factors are required for the meiotic recombination hotspot at the *HIS4* locus in Saccharomyces cerevisiae. Proc Natl Acad Sci U S A 90**:** 6621-6625.

White, M. A., M. Wierdl, P. Detloff and T. D. Petes, 1991 DNA-binding protein RAP1 stimulates meiotic recombination at the *HIS4* locus in yeast. Proc Natl Acad Sci U S A 88**:** 9755-9759.

Wojtasz, L., K. Daniel, I. Roig, E. Bolcun-Filas, H. Xu *et al*., 2009 Mouse HORMAD1 and HORMAD2, two conserved meiotic chromosomal proteins, are depleted from synapsed chromosome axes with the help of TRIP13 AAA-ATPase. PLoS Genet 5**:** e1000702.

Woltering, D., B. Baumgartner, S. Bagchi, B. Larkin, J. Loidl *et al*., 2000 Meiotic segregation, synapsis, and recombination checkpoint functions require physical interaction between the chromosomal proteins Red1p and Hop1p. Mol Cel Biol 20**:** 6646-6658.

Wu, H. Y., and S. M. Burgess, 2006 Two distinct surveillance mechanisms monitor meiotic chromosome metabolism in budding yeast. Curr Biol 16**:** 2473-2479.

Wu, P. Y., and P. Nurse, 2014 Replication origin selection regulates the distribution of meiotic recombination. Mol Cell 53**:** 655-662.

Wu, T.-C., and M. Lichten, 1994 Meiosis-induced double-strand break sites determined by yeast chromatin structure Science 263**:** 515-518.

Wu, T. C., and M. Lichten, 1995 Factors that affect the location and frequency of meiosis-induced double-strand breaks in *Saccharomyces cerevisiae*. Genetics 140**:** 55-66.

Xu, L., and N. Kleckner, 1995 Sequence non-specific double-strand breaks and interhomolog interactions prior to double-strand break formation at a meiotic recombination hot spot in yeast. EMBO J 14**:** 5115-5128.

Yamashita, K., M. Shinohara and A. Shinohara, 2004 Rad6-Bre1-mediated histone H2B ubiquitylation modulates the formation of double-strand breaks during meiosis. Proc Natl Acad Sci U S A 101**:** 11380-11385.

Zakharyevich, K., Y. Ma, S. Tang, P. Y.-H. Hwang, S. Boiteux *et al*., 2010 Temporally and biochemically distinct activities of Exo1 during meiosis: Double-strand break resection and resolution of double Holliday junctions. Mol Cell 40**:** 1001-1015.

Zanders, S., and E. Alani, 2009 The *pch2Delta* mutation in baker's yeast alters meiotic crossover levels and confers a defect in crossover interference. PLoS Genet 5**:** e1000571.

Zanders, S., M. Sonntag Brown, C. Chen and E. Alani, 2011 Pch2 modulates chromatid partner choice during meiotic double-strand break repair in *Saccharomyces cerevisiae*. Genetics 188**:** 511-521.

Zenvirth, D., T. Arbel, A. Sherman, M. Goldway, S. Klein *et al*., 1992 Multiple sites for double-strand breaks in whole meiotic chromosomes of *Saccharomyces cerevisiae*. Embo j 11**:** 3441-3447.

Zhang, L., K. P. Kim, N. E. Kleckner and A. Storlazzi, 2011a Meiotic double-strand breaks occur once per pair of (sister) chromatids and, via Mec1/ATR and Tel1/ATM, once per quartet of chromatids. Proc Natl Acad Sci U S A 108**:** 20036-20041.

Zhang, L., H. Ma and B. F. Pugh, 2011b Stable and dynamic nucleosome states during a meiotic developmental process. Genome Res 21**:** 875-884.

Zhu, C., K. J. Byers, R. P. McCord, Z. Shi, M. F. Berger *et al*., 2009 High-resolution DNA-binding specificity analysis of yeast transcription factors. Genome Res 19**:** 556-566.

Zhu, X., and S. Keeney, 2014 Zip it up to shut it down. Cell Cycle 13**:** 2157-2158.

Zickler, D., and N. Kleckner, 1999 Meiotic chromosomes: Integrating structure and function. Annu Rev Genet 33**:** 603-754.